Fractional Order Current Mode Circuits

Thesis Submitted to the Delhi Technological University
for the award of the degree of

DOCTOR OF PHILOSOPHY

in

Electronics & Communication Engineering

by

Rakesh Verma
(Enrollment No.: 2K14/Ph.D/EC/12)

Under the Supervision of

Prof. Neeta Pandey
&
Prof. Rajeshwari Pandey

Department of Electronics & Communication Engineering
Delhi Technological University, Delhi - 110042

Department of Electronics & Communication Engineering
Delhi Technological University
Delhi-110042, India.

December 2019

Delhi Technological University

Formerly Delhi College of engineering

Shahbad Daulatpur, Bawana Road, Delhi-110042

CERTIFICATE

This is to certify that the thesis entitled **"Fractional Order Current Mode Circuits"** submitted by **Rakesh Verma** (2K/14/PHD/EC/12) to the **Department of Electronics and Communication Engineering, Delhi Technological University** for the award of the degree of **Doctor of Philosophy** is based on the original research work carried out him under our guidance and supervision. In our opinion, the thesis has reached the standard fulfilling the requirements of the regulations relating to the degree. It is further certified that the work presented in this thesis is not submitted to any other university or institution for the award of any degree or diploma.

Prof. Rajeshwari Pandey

Supervisor
Department of ECE
Delhi Technological University
Delhi-110042
India

Prof. Neeta Pandey

Supervisor
Department of ECE
Delhi Technological University
Delhi-110042
India

Prof. N. S. Raghava
Head of Department
Department of ECE
Delhi Technological University
Delhi-110042
India

CANDIDATE'S DECLARATION

I hereby certify that the research work, which is being presented in the thesis, entitled, **"Fractional Order Current Mode Circuits"** in fulfillment of requirements of the award of the degree of Doctor of Philosophy, is an authentic record of my research work carried under the supervision of **Prof. Neeta Pandey** and **Prof. Rajeshwari Pandey**. The matter presented in this work has not been submitted elsewhere in part or fully to any other University or Institution for the award of any degree or diploma.

Rakesh Verma

(2K14/PHD/EC/12)
Department of ECE
Delhi Technological University
Delhi - 110042, India

ACKNOWLEDGEMENT

I would like to express my deep and sincere gratitude to my thesis supervisors **Dr. Neeta Pandey** and **Dr. Rajeshwari Pandey, Professors** at **Department of Electronics and Communication Engineering, DTU, Delhi** for giving constant encouragement and valued constructive criticism. I am very glad and indebted for their kindness and spent valuable time to drive my work into a noval research area and complete my work successfully.

I wish to express my heartfelt thanks to **Prof. N. S. Raghava, Head of Department** and **Prof. S. Indu Former Head of Department** at **Department of Electronics and Communication Engineering, DTU, Delhi** for their valuable support and encouragement.

I am thankful to **Dr. D. R. Bhaskar, Professors** at **Department of Electronics and Communication Engineering, DTU, Delhi** and my supervisor of M.Tech Thesis **Dr. Pragati Kumar, Professor** at **Department of Electrical Engineering, DTU, Delhi** for rejuvenating my spirits and keeping my motivation at level high.

I would also like to thank to **all faculty members** of **Department of Electronics and Communication Engineering, DTU, Delhi** for their contributions in one or the other ways to keep my research work in right direction.

I express my deep sense of gratitude to **Mr. Baljeet Singh** and my Ph.D batch mates and other research scholars especially, **K. Gurumurthy, Praveen Rani, Priyanka Gupta** for the help of arranging important components in EDC laboratory for the experimental works.

Although for financial help, I owe to **my family** and **my mother-in-law** but my deep sense of gratitude for their support and patience. I also thank to **Department of Electronics and Communication Engineering, DTU, Delhi** and **Department of Electronics and Communication Engineering, NSIT, Delhi** for appointing me as Guest/ Part-Time Faculty.

I would never forget the deepest concern of **my grandmother** and **my wife Tanuja Verma** for their forever love, care and beliefs during the overall journey of PhD research work.

Finally I would like to thank almighty God for his blessings without which nothing is possible in this world.

(Rakesh Verma)

LIST OF FIGURES

LIST OF TABLES

LIST OF SYMBOLS

S.No.	Symbols	Descriptions
1	FO	Fractional-Order
2	FOE	Fractional Order Element
3	CFE	Continued Fraction Expansion
4	FBD	Functional Block Diagram
5	FC	Fractional Order Capacitor
6	CFOA	Current Feedback Operational Amplifier
7	OTA	Operational Transconductance Amplifier
8	FLTI	Fractional-Order Linear Time Invariant
9	GIC	Generalized Impedance Converter
10	NIC	Negative Impedance Converter
11	C-Multiplier	Capacitance Multiplier
12	PLL	Phase-Locked Loop
13	FLF	Follow The Ladder Feedback
14	IFLF	Inverse Follow The Ladder Feedback
15	IIMC	Inverted Impedance Multiplier Circuit
16	FOF	Fractional Order Filter
17	IIC	Impedance Inverter Circuit
18	FI	Fractional Order Inductor
19	CMOS	Complementary Metal Oxide Semiconductor
20	PRB	Parallel Resonator Block
21	FLPF	Fractional Order (Step) Low Pass Filter/
22	FHPF	Fractional Order (Step) High Pass Filter
23	FBPF	Fractional Order Band Pass Filter
24	FBSF	Fractional Order Band Stop Filter

25	FAPF	Fractional Order All Pass Filter
26	GSA	Gravitational Search Algorithm
27	RGA	Real Coded Genetic Algorithm
28	PSO	Particle Swarm Optimization
29	FSF	Fractional Step Filter
30	LP	Low Pass
31	HP	High Pass
32	BP	Band Pass
33	AP	All Pass

ABSTRACT

Fractional calculus, i.e., fractional-order differentiation or integration, is a part of mathematics dealing with derivatives of arbitrary order. The fractional calculus is more than 300 years old topic and gaining research interest in recent past. It has become a powerful and widely used tool to demonstrate the characteristics of many systems in the real world.

The fractional order dynamic system offers extra degree of freedom to control the phenomena of system. Fractional approach has been used in modeling of various physical processes such as anomalous diffusion, flow of fluid in porous media, heat conduction in a semi infinite slab, voltage-current relation in a semi-infinite transmission line, the charging and discharging of lossy capacitors etc.

The fractional-order circuits and systems incorporate fractional calculus concepts and have immense potential in the field of signal processing, control systems, biomedical instrumentation, and many more. Thus the aim of this thesis is to generalize the narrow integer-order circuits to more general fractional-order counterparts. In this work design of current mode circuits has been investigated from fractional-order perspective and is briefly presented below.

The capacitance scaling in integer and fractional order capacitors is addressed first and a novel Current Feedback Operational Amplifier based capacitance multiplier is proposed. It provides high multiplication factor with low component spread. This circuit is generalized in fractional domain along with three other

capacitance multipliers. An application based on parallel RLC resonator is included to show its usefulness.

The concept of Operational Transconductance Amplifier based impedance inverted is used to present a novel Inverted Impedance Multiplier Circuit which is further generalized to fractional domain. The proposal is illustrated through implementation of fractional higher order filter.

Further two topologies for electronically tunable fractional order filters based on Operational Transconductance Amplifier are presented. The first is multi input single output structure which provides all pass and low pass responses. The second topology provides low pass and band pass responses simultaneously.

The next objective of this work is proposition of higher fractional order filters which are realized by cascading filters of order ($1+\alpha$) with higher integer order filters. The proposed filters are designed by approximating the fractional Laplacian operator by an appropriate integer order transfer function. Subsequently, functional block diagram approach is used for Current Feedback Operational Amplifier based realization of low and high filters of order ($1+\alpha$). The concept is illustrated through Current Feedback Operational Amplifier based low pass filter of order ($5+\alpha$) as obtained by cascading low pass filter of order ($1+\alpha$) with proposed leapfrog realization of 4^{th} order low pass filter. The work is extended to Current Feedback Operational Amplifier based high pass filter of order ($5+\alpha$).

The functionality of all the propositions is verified through SPICE simulations. The Current Feedback Operational Amplifier based circuits are simulated using its macro model whereas 0.18 μm TSMC CMOS process parameters are used for Operational Transconductance Amplifier based circuits. Some of the circuits are also verified experimentally. Mathematical formulation for sensitivity of filters is included and examined through MATLAB simulations. The stability of proposed structures is also investigated.

CONTENTS

CHAPTER 1

INTRODUCTION

1.1Background

The processes in nature and real objects can be modeled more precisely by using fractional calculus than classical integer order methods [1-3]. The voltage-current relation in a semi-infinite transmission line [1], flow of fluid in a porous media and conduction of heat in a semi-infinite slab [2] are some of the illustrations where the governing equations can be modeled more accurately by fractional order differential or integral operators. Similarly the charging and discharging of lossy capacitors inherently follow fractional order dynamics [4].

The classical integer order models have primarily been used due to the absence of solution methods for fractional differential equations. Currently, a number of approximations for fractional differential and integral calculus are available in the literature and are being applied to control systems [3, 5-7], biomedical instrumentation [8, 9], circuit theory and signal processing [4, 10] applications. The emphasis is also being given on generalizing fundamentals of conventional circuit theory and stability techniques into the FO-domain for their analysis [11, 12]. It is shown that the higher order integer order circuits can be replaced by lower order FO-circuits [13].

A fractional order Laplacian operator is used to represent FO circuit and systems. The Laplace transformation method of fractional order operator can easily be simplified into integer approximation form where it is made physically realizable with fractional order element (FOE) whose impedance can be represented as $Z(s) = as^{\alpha}$ [14] (α- fractional order of FOE). The FOE with positive fraction represents fractional inductor (FI) while those with negative fraction correspond to fractional capacitor (FC). Research on hardware realization of FOE [15 – 25] is still in nascent stage and variety of approximations [24, 26-28] are available in literature to emulate the behavior of FOE which differ in the frequency range of operation and relative percentage errors when compared with ideal one [21].

Over the last few decades current mode (CM) processing has emerged as an alternative design technique for signal processing [29, 30]. The CM circuits are low impedance node networks; hence result in low time constant. This improves system performance in terms of speed and slew rate. Current- mode signal processing has resulted in emergence of numerous analog building blocks (ABB) as mentioned in [29] and references cited therein which are used for realization of various signal processing and generation circuits. The development of CM FO circuits and systems has recently gained momentum due to inherent advantageous features namely wider bandwidth, higher slew rate, lower power consumption and simpler circuitry. A variety of applications such as active and passive filters [15, 16, 18, 20, 31 - 71], analog controllers [3, 5-7, 21, 72 - 82], oscillators [83 - 90], multivibrators [91] etc., have emerged as a natural outcome of this momentum.

1.2 Literature Survey

Though the fractional calculus is more than 300 years old topic [3], the circuit design in fractional domain has recently gained significant research interest. There is a vast scope in designing of fractional order circuits and the candidate has focused on FOE and fraction order filter. The available literature in these two areas has been reviewed and is described below.

Fractional order elements (FOE)

Fractional order element [6, 14, 16, 17, 19, 21, 92 - 113], also known as constant phase element (CPE) is a fundamental component for designing the fractional order analog circuits. Attempts have been made to develop off-shelf fractional capacitor (FC) and make it available in market just like normal capacitor with reliable performance and specified tolerances both for the order and value of the FC. The fabrication of packaged half-order FC by using photolithographic fractal structures on silicon is presented in [16] and by coating a copper plated epoxy glass with a porous film of poly-methyl-methacrylate (PMMA) is given in [17, 92]. Besides this, Liquid electrode [93 - 97], CMOS emulator [98, 99], graphene-percolated polymer composite [100], dielectric of poly (vinylidene fluoride) [101], and CNT-polymer nanocomposite [102] are also used. However, these implementations are bulky and non-reconfigurable. In literature, various rational approximations are available to implement FOE. Some of these approximations are: Oustaloup Recursive approximation [26], Carlson approximation [26], Matsuda approximation [26], Chareff approximation [26] and Continued Fraction Expansion (CFE) [26], Modified Oustaloup [27] and El-Khazali reduced order approximation [28]. It is found in literature that CFE approximation is widely used for FOE realization. The impedance function obtained through FOE approximation can be realized using various RC networks such as RC tree [14, 21, 24], cross RC ladder [6], domino ladder [6] etc. The computation of component values of RC tree network depends on the magnitude and order of the FOE. To introduce flexibility, researchers have also explored FOE implementations by using MOS transistors [104, 105], current mirrors [106, 107] and operational transconductance amplifier (OTA) [19, 98, 99, 110 - 114]. The MOS based emulators use active inductor [104] and low/ high pass filter sections [105]. MOS capacitors are employed in current mirror based integrators/ differentiators [106, 107, 114] emulators. Operational transconductance amplifier (OTA) based emulators are reported in [19, 98, 99, 109-114] which use either functional block diagram approach [19, 98, 99,110]/ bilinear immittances [112, 113] to realize approximated function or replace resistor by OTA in RC ladder network. The order of FOE may be adjusted by appropriate selection of bias currents in OTA based circuits. The magnitude scaling is achieved by adjusting bias currents of all OTAs [16, 98, 99, 110 - 114] or connecting FOE in series, parallel or series parallel combination [19].

The concept of the mutual inductance in the fractional-order domain is generalized thereby fractional mutual inductance (FMI) is realized with the help of differential voltage current-controlled conveyor transconductance amplifiers (DVCCCTA) based Fractional order Mutual Coupled Circuit (FMCC) based on fractional order inductor [115]. Two applications of FMCC namely double-tuned filter and impedance matching circuits are also presented. Apart from these immittance simulators are also proposed using GIC [15, 31 - 33], FDNR [31] and mutator [116] which are subsequently used for FOF realizations.

It is clear from above discussion that limited literature is available on magnitude scaling of FOE. Further, the order of FOE ($\alpha < 1$) is manipulated by varying bias current but the work on order of FOEs higher than two is not available in open literature. Keeping these points in view, scheme for magnitude scaling and FOE order alteration may be investigated.

Fractional order filters (FOF)

A wide range of fractional order analog filters [15, 16, 18, 20, 31 - 71, 117] are developed using various ABBs such as Op-Amp [15, 16, 18, 31 - 36, 38 - 40, 43, 49, 54 - 56], Operational Transconductance Amplifier (OTA) with Current Feedback Operational Amplifier (CFOA) [20], Second generation Current Conveyor (CCII) [37, 41, 42, 44, 53, 116], DVCC and voltage buffers [45], Current Differencing Buffered Amplifier [46], OTA [50, 117], Multi-Output Transconductance Amplifier (MOTA) with Adjustable Current Amplifier (ACA) [51], Operational Transconductance Amplifier (OTA) with ACA [52], OTA with ACA and Current Follower (CF) [56 - 59]; Universal Voltage Conveyor (UVC) [60]; Differential Difference Current Conveyor (DDCC) [61]; CFOA [62]; ACA with CF [63 – 65]; OTA with ACA [66]; Balanced-Output Transconductance Amplifier (BOTA) with ACA and CF [67]. In fractional domain, low pass, high pass, band pass, band stop and all pass filters responses are abbreviated as FLPF, FHPF, FBPF, FBSF and FAPF. Two design approaches are primarily used to develop FOFs and are discussed below:

The first approach uses approximated function of integer order *m* to emulate the behaviour of fractional order element (FOE). Larger is the value of *m* better would be the matching between ideal and approximated responses. Any one of Least–squares method [26], Chareff [26], Oustaloup [21, 26, 118], Matsuda [21, 26], Carlson [21, 26], Continued Fraction Expansion (CFE) [21, 26], Valsa [119] or Laguerre [120] based approximations may be used for this purpose. The FOE structure so obtained is then substituted in place of integer order element in existing circuits [16, 34 – 46] to obtain fractional order response. Some of the popular second order filters circuits investigated are Sallen-Key [38 - 40], Kerwin-Huelsman-Newcomb (KHN) biquad [18, 37 - 43], Tow-Thomas (TT) biquad [16, 34, 35, 41] and $RL_{\beta}C_{\alpha}$ [12, 32, 33, 48] filters. This approach has also been used to derive FOFs from first [45, 47, 50, 53] and third order [46] filters. The FOFs with Chebyshev, Inverse Chebyshev and Butterworth characteristics are reported in [35], [36] and [34, 39, 48, 54 - 67] respectively. Apart from these immittance simulators are also proposed using GIC [15, 31 - 33], FDNR [31, 44] and mutator [116] which are subsequently used for FOF realizations. The filters based on this approach are implemented using various ABBs [15, 16, 18, 20, 31 - 46, 49 - 53] and are summarized in Table 1.1. It may be noted that limited literature is available on electronically tunable FOFs and there is scope of developing FOFs inheriting electronic tunability.

Table 1.1: Summary of active FOFs using first approach

Ref.	ABB used	Filter Response	Conventional Circuit Used	Order of Filter	No. of elements				Type of FOE used	Electronic Tunability
					ABBs	R	C	C_α		
[15]	Op-Amp	FBPF, FBSF	Parallel RLC Resonator using GIC based inductor simulation	(1+α +β)	2	6	1	2	PMMA coated FC	No
[16]	Op-Amp	FLPF, FBPF	Tow-Thomas Biquad	(1+α)	3	6	1	1	Domino ladder RC network	No
[18]	Op-Amp	FLPF, FBPF	KHN Biquad	(α+β)	3	6	0	2	PMMA coated FC	No
[20]	OTA, CFOA	FLPF	Multiple Loop Feedback Topology	(1+α)	1, 1	2	1	1	Net-grid type $s^{0.5}$ order FOE	Yes
[33]	Op-Amp	FBPF	Multiple Amplifier Biquad (MAB) using FDNR	2α	2, 4	4-5, 6/ 8	3	2/ 3	Domino ladder RC network	No
[34]	Op-Amp	FLPF, FHPF, FBPF, FBSF	Series RLC using GIC based inductor simulation	(α+β)	2	5	0	2	Domino ladder RC network	No
[35]	Op-Amp	FBPF	Series RLC using GIC based inductor simulation	(α+β)	2	5	0	2	PMMA coated FC	No
[36]	Op-Amp	FO Butterworth LP Filter	Multifeedback, Tow Thomas	(1+α)	2, 3	3. 6	1,1	1,1	Domino ladder RC network	No
[37]	Op-Amp	FO Chebyshev LP Filter	Tow Thomas	(1+α)	3	6	1	1	Domino ladder RC network	No
[38]	Op-Amp	FO-Inverse Chebyshev LP Filter	Multiple Input Biquad	(1+α)	3	8	1	1	Domino ladder RC network	No
[39]	CCII	FLPF, FHPF, FBPF	KHN Biquad	(α+β)	5	6	0	2	Domino RC ladder network	No
[40]	Op-Amp	FLPF,FHPF, FBPF	KHN and Sallen-Key Biquads	2α	3, 1	6, 4-5	0	2	Self similar RC tree	No

[41]	Op-Amp	FLPF	KHN and Sallen-Key Biquads	(α+β)	3, 1	6, 4	0	2	Self similar RC tree	No
[42]	Op-Amp	FLPF	KHN and Sallen-Key Biquads	(α+β)	3, 1	6, 4	0	2, 2	Self similar RC tree	No
[43]	CCII	FLPF	KHN, Tow Thomas Biquads	(α+β)	5, 3	6, 4	0	2	Self similar RC tree	No
[44]	CCII	FLPF, FHPF, FBPF	KHN Biquad	(α+β)	5	7	0	2	Self similar RC tree	No
[45]	Op-Amp	FLPF	KHN Biquad	(α+β)	3	6	0	2	Self similar RC tree	No
[46]	CCII	FLPF	FDNR	2α	1	2	0	2	PMMA coated FC	No
[47]	DVCC, voltage buffer	FAPF	APF	α	1, 2	1	0	1	Foster II RC network	No
[48]	CDBA	FLPF, FHPF, FBPF	Third order multifunctionalFilter	(α+β +ϒ)	1	5	0	5	Domino ladder RC network	No
[51]	Op-Amp	FO Inverse Filters: FLPF, FHPF, FBPF	Second order Inverse Filter	2α	1	3, 2, 3	0	2, 3, 2	Domino ladder RC network	No
[52]	OTA	FAPF	First Order Filter	α	2	0	0	1	Domino ladder RC network	Yes
[53]	MOTA, ACA	FLPF, FBPF	Fully Differential Second order Filter	(1+α)	2, 1	0	1	1	Domino ladder RC network	Yes
[54]	OTA, ACA	FLPF, FHPF, FBPF, FBSF	Multifunctional FOF	(1+α)	2, 4	0	1	1	Domino ladder RC network	Yes
[55]	CCII	FLPF, FHPF, FBPF, FAPF	Generalized Two Port Network	α , (α+β)	1-2	1-6	0	1-2	RC ladder network	No
[116]	CCII	FLPF	Mutator	(α+β)	3	4	0	2	Self similar RC tree	No

In second approach, an integer (m) order approximation for fractional order Laplacian operator ($0<\alpha<1$) is used which modifies FOF of order ($1+\alpha$) to integer order function of (m + 1) order [54 - 70]. The transfer function (TF) of ($1+\alpha$) order modifies to third order integer order TF. Cascading of first and second order filter sections are used to realize this TF in [54, 70]; and functional block diagram (FBD) of follow the leader feedback (FLF) and inverse follow the leader feedback (IFLF) topologies are used in [56, 59, 60, 62 - 66, 69] and [57, 58, 61] respectively. The realizations based on ABBs, MOS transistors, and Field Programmable Analog Arrays (FPAAs) are available in [56, 60, 61 - 67], [69] and [70] respectively. A summary of previously reported ABB based FOFs using second approach is given in Table 1.2. It is clear from Table 1.2 that higher order FOFs ($n+\alpha$ order) are realized by FBD approach. These may be realized either by cascading of FBD based ($1+\alpha$) order filter with integer order filter of (n-1) order or through FBD of ($n+\alpha$) order FOF. There is a lean presence of higher order FOFs in literature. Therefore, design of higher order FOFs may be explored using existing methods of realizing higher integer order filters.

1.3 Objectives and Contribution

Based on literature survey and research gaps following objectives are set:

1. To develop capacitance scaling scheme for FC.
2. To explore FOE order alteration scheme.
3. To develop electronically tunable FOF.
4. To realize higher order FOFs.

The candidates' contribution towards these objectives is as follows:

- A capacitance multiplier is developed and is generalized in fractional domain
- Inverted impedance multiplier circuit is developed followed by its generalization

- Design of two electronically tunable filters
- Higher order FOF realization by cascading of (1+α) order filter with integer order filter of (n-1) order based of leapfrog method.

Table 1.2: Summary of active FOFs using second approach

Ref.	**ABB(s)**	**(1+α) order Filter**					**Higher (n+α) order filter tested**	**Electronic Tunability**	**Hardware implementation**
		Filter Response	**Design Method**	**No. of elements**					
				ABBs	**R**	**C**			
[54]	Op-amp	FLPF	Cascade of first and second order filter sections	2	10	3	Yes	No	Yes
[55]	Op-amp	FLPF	GSA	7	17	3	Yes	No	No
[56]	OTA, DO-CF, ACA	FHPF	FLF	6	0	3	No	Yes	No
[57]	OTA, MO/FD-CF, ACA	SE-FLPF, FD-FLPF	IFLF	6	0	3, 6	No	Yes	No
[58]	OTA, ACA, MO-CF	FLPF	IFLF	6	0	3	No	Yes	Yes
[59]	OTA, ACA, CF	FLPF, FHPF	FLF	7	0	3	No	Yes	Yes
[60]	UVC	FLPF, FHPF	FLF	4, 4-5	10, 11-12	3	No	No	Yes
[61]	DDCC	FLPF	IFLF	5	7	3	Yes	No	Yes
[62]	CFOA	FLPF	FLF	4	10	3	No	No	Yes
[63]	ACA, MO-CF	FLPF	FLF	3/ 8	3	3	No	Yes	No
[64]	ACA, FD-CF	SE-FLPF, FD-FLPF	FLF	8	6	6	No	Yes	No
[65]	DO/ MO-CF, ACA	FLPF	FLF	3/ 8	3	3	No	Yes	Yes
[66]	OTA, ACA	FLPF	FLF	6	0	3	No	Yes	No
[67]	BOTA, ACA, FD-CF	FD-FLPF, FD-FHPF, FD-FBPF, FD-FBSF	IFLF	3, 4, 2	0	6	No	Yes	No

-

1.4 Thesis Layout

Based on the work on each objective the thesis work can be presented as mentioned below:

Chapter 1

This chapter describes the background and motivation of the work carried out in the thesis. Literature review of available analog FO circuits is put forward followed by identification of research gaps and the objectives set for the work. The thesis organization is briefly described.

Chapter 2

This chapter gives a brief description of FOE realization using CFE approximation and stability of fractional order circuit. It also includes characterization of active blocks (CFOA and OTA) used to develop different circuits in the thesis.

Chapter 3

This chapter first presents a new capacitance multiplier (C-multiplier) circuit based on CFOA. The performance of the proposed circuit is examined for non-ideal effects of CFOA and a compensation scheme is suggested. The functionality is verified through simulations and experimentation where the FC is modeled using domino RC ladder network. The proposed circuit along with three other CFOA C-multiplier circuits is generalized in fractional domain. The behavior of the proposed circuits is examined using MATLAB simulations and SPICE simulations. The circuit applications of proposed C-multiplier circuits are also included in this chapter.

Chapter 4

A higher order fractional element using the concept of impedance inverter circuit based on OTA is put forward in this chapter. Firstly, the concept of OTA impedance inverter is generalized in fractional domain which is followed by presentation of novel OTA based IIMC and its generalization. Effect of OTA parasites on performance of proposed IIMC is also presented. The usefulness of the proposal is illustrated through implementation of FOF of higher order using IIMC. Stability and non-ideal effects of higher order filter are also examined. The functional verification of all proposed circuits is done through SPICE simulations and hardware prototyping using LM 13600N dual OTAs IC.

Chapter 5

This chapter is devoted to electronically tunable filters based on OTA. Two OTA based topologies are generalized in fractional domain. The first topology is multiple input single output FOF and provides FAPF and FLPF responses. The second topology provides FLPF and FBPF responses simultaneously and is a single input multiple output FOF. The critical frequencies, sensitivity and stability conditions are mathematically formulated. SPICE simulation results are included for functional verification and to show electronic tunability of filter parameters.

Chapter 6

This chapter puts forward a new proposal for Current Feedback Operational Amplifier (CFOA) based Low pass (LP) and High Pass (HP) FOFs. The proposed filters are designed by approximating the fractional Laplacian operator by second integer order transfer function. Subsequently, FBD approach is used for CFOA based realization of LP and HP FOFs of order ($1+\alpha$). Higher order FOFs are realized by cascading FOF of order ($1+\alpha$) with higher integer order filters. To illustrate this, CFOA based LP (HP) FOFs of order ($5+\alpha$) are obtained by cascading LP (HP) FOFs of order ($1+\alpha$) with proposed leapfrog realization of 4^{th} order LP (HP) filter. The proposal is verified through SPICE simulations and experimentation. Stability, sensitivity and non-ideal analyses are also included.

Chapter 7

This chapter summarizes the work presented in the thesis and identifies the future scope.

CHAPTER 2

BASIC CONCEPTS OF FRACTIONAL ORDER CIRCUITS

2.1 Introduction

Factional order circuit design has gained significant research attention due to extra degree of freedom provided by fractional order elements in recent past. This has created huge opportunity to investigate design flexibility which is not possible in narrow and finite subset of conventional integer order circuits.

As discussed in Chapter 1, FO circuits use FOE(s) which are realized through physical implementation [92 - 97, 100 - 102] or hardware emulators based on various structures [19, 98, 99, 104-113] such as passive resistor-capacitor (RC) elements arranged in the form of RC tree [14, 21], cross RC ladder [6], domino ladder [6] etc. The passive RC networks are obtained on the basis of different approximations such as Oustaloup Recursive approximation [26], Carlson approximation [26], Matsuda approximation [26], Chareff approximation [26], Continued Fraction Expansion (CFE) [26], Modified Oustaloup [27] and El-Khazali reduced order approximations [28]. Another FOE realization scheme is based on obtaining a suitable integer order transfer function first for the system to be realized and its active realization is then carried out using FBD approach.

The CFE approximation method is used widely to develop FO circuits in the literature and has been adopted in this work too, to develop various FO circuits. The CFE approximation and its use for emulating FC are detailed in this chapter for making this thesis more comprehensive. A brief description of stability is given next which is followed by the characterization of active blocks CFOA and OTA which are used to verify proposed circuits. The FBD approach has been detailed in chapter 6.

2.2 FOE based on CFE method

In this section the CFE approximation method for emulating the behavior of FOE is described briefly. The CFE method uses series expansion of $(1+x)^{\alpha}$ [26] as given by (2.1)

$$(1+x)^{\alpha} = \frac{1}{1-}\frac{\alpha x}{1+}\frac{(1+\alpha)x}{2+}\frac{(1-\alpha)x}{3+}\frac{(2+\alpha)x}{2+}\frac{(2-\alpha)x}{5+\cdots}$$

Or,

$$\cfrac{1}{1-\cfrac{\alpha x}{1+\cfrac{(1+\alpha)x}{2+\cfrac{(1-\alpha)x}{3+\cfrac{(2+\alpha)x}{2+\cfrac{5}{(2-\alpha)x}}}}}} \tag{2.1}$$

On the substitution of x = s-1, integer order approximation form with infinite terms for fractional order Laplacian operator s^{α} is obtained. Depending upon the accuracy requirement we may retain finite number of terms for representing s^{α}. The order of CFE approximation of s^{α} depends upon the power of s in the integer order approximation forms. If terms up to s^n are retained it is termed as n^th^ order approximation. Using this method 1st, 2nd, 3rd and 4th order transfer functions [26] are presented by (2.2) – (2.5) respectively for the ease of comprehension.

$$\frac{(1+\alpha)s+(1-\alpha)}{(1-\alpha)s+(1+\alpha)} \tag{2.2}$$

$$\frac{(\alpha^2+3\alpha+2)s^2+(-2\alpha^2+8)s+(\alpha^2-3\alpha+2)}{(\alpha^2-3\alpha+2)s^2+(-2\alpha^2+8)s+(\alpha^2+3\alpha+2)} \tag{2.3}$$

$$\frac{(\alpha^3+6\alpha^2+11\alpha+6)s^3+(-3\alpha^3-6\alpha^2+27\alpha+54)s^2+(3\alpha^3-6\alpha^2-27\alpha+54)s \\ +(-\alpha^3+6\alpha^2-11\alpha+6)}{(-\alpha^3+6\alpha^2-11\alpha+6)s^3+(3\alpha^3-6\alpha^2-27\alpha+54)s^2+(-3\alpha^3-6\alpha^2+27\alpha+54)s \\ +(\alpha^3+6\alpha^2+11\alpha+6)} \quad (2.4)$$

$$\frac{(\alpha^4+10\alpha^3+35\alpha^2+50\alpha+24)s^4+(-4\alpha^4-20\alpha^3+40\alpha^2+320\alpha+384)s^3 \\ +(6\alpha^4-150\alpha^3+864)s^2+(-4\alpha^4+20\alpha^3+40\alpha^2-320\alpha+384)s \\ +(\alpha^4-10\alpha^3+35\alpha^2-50\alpha+24)}{(\alpha^4-10\alpha^3+35\alpha^2-50\alpha+24)s^4+(-4\alpha^4+20\alpha^3+40\alpha^2-320\alpha+384)s^3 \\ +(6\alpha^4-150\alpha^3+864)s^2+(-4\alpha^4-20\alpha^3+40\alpha^2+320\alpha+384)s \\ +(\alpha^4+10\alpha^3+35\alpha^2+50\alpha+24)} \quad (2.5)$$

In general any nth order CFE approximation function represents an impedance function and may be physically implemented with RC ladder network using partial fraction method. Thus CFE approximated FC can be obtained by using reciprocal of respective nth order function. The realization of a 4th order CFE approximated form for FC is explained below.

The impedance function of FC is obtained by reciprocal of (2.5) and can be approximated by domino RC ladder network of Fig. 2.1. The impedance function of Fig. 2.1 is given by (2.6).

$$Z_{C_\alpha}=R_a+\frac{1/C_b}{s+\frac{1}{R_bC_b}}+\frac{1/C_c}{s+\frac{1}{R_cC_c}}+\frac{1/C_d}{s+\frac{1}{R_dC_d}}+\frac{1/C_e}{s+\frac{1}{R_eC_e}} \quad (2.6)$$

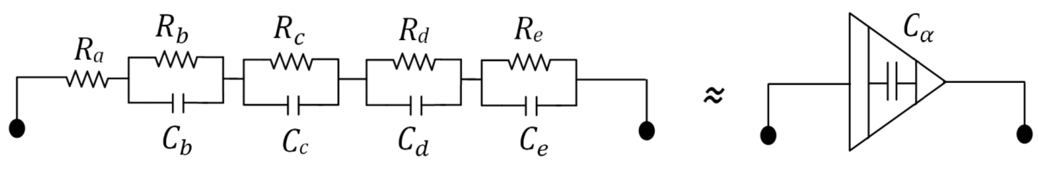

Fig. 2.1: A 4th order domino RC ladder circuit [32]

The values of components used in (2.6) may be obtained by carrying out partial fraction of (2.5) which may be expressed as [24].

$$Z(s) = k + \sum_{i=1}^{i=4} \frac{r_i}{s + p_i} \tag{2.7}$$

where k and r_i are constant terms. The p_i are poles of the impedance; The values of components may be found by

$$\begin{aligned} &R_a = k, \\ &C_b = 1/r_1, \qquad R_b = 1/C_b|p_1| \\ &C_c = 1/r_2, \qquad R_c = 1/C_c|p_2| \\ &C_d = 1/r_3, \qquad R_d = 1/C_d|p_3| \\ &C_e = 1/r_3, \qquad R_e = 1/C_e|p_4| \end{aligned} \tag{2.8}$$

The desired value of FC having scaled frequency ω_c can be determined with the help of magnitude (k_m) and frequency (k_f) scaling factors giving the following relationships between unscaled and scaled component values

$$R_s = k_m . R;$$

and

$$C_s = \frac{C}{k_f k_m} \tag{2.9}$$

where (R, C) and (R_s, C_s) are unscaled and scaled component values respectively. The scaling factors k_m and k_f are given by (2.10)

$$k_m = \frac{1}{C_\alpha \omega_c^\alpha} \;, \qquad k_f = \omega_c \tag{2.10}$$

Using (2.10), the desired scaling impedance function can be written as

$$Z_{C_\alpha}|_s = R_1 + \frac{1/C_2}{s+\frac{1}{R_2C_2}} + \frac{1/C_3}{s+\frac{1}{R_3C_3}} + \frac{1/C_4}{s+\frac{1}{R_4C_4}} + \frac{1/C_5}{s+\frac{1}{R_5C_5}}$$

(2.11)

Comparing (2.6) and (2.11), the scaled components are expressed as

$$\begin{aligned} &R_a = R_1.k_m, && \\ &R_b = R_2.k_m, && C_b = C_2/k_f k_m \\ &R_c = R_3.k_m, && C_c = C_3/k_f k_m \\ &R_d = R_4.k_m, && C_d = C_4/k_f k_m \\ &R_e = R_5.k_m, && C_e = C_5/k_f k_m \end{aligned}$$

(2.12)

The magnitude and phase of FC impedance function are $1/(\omega^\alpha C_\alpha)$ and $-\alpha\pi/2$ respectively. Therefore, the magnitude response of FC of order α would show a negative slope of $(-20\alpha\log_{10}\omega)$ while its phase remains constant. SPICE simulations have been carried out for examining behavior of FCs of order 0.1, 0.5 and 0.9 with a center frequency of 1 kHz using the component settings of Table 2.1. The corresponding theoretical and simulated magnitude and phase responses are shown in Fig. 2.2. A deviation of ±1.5 dB is observed between simulated and theoretical magnitude responses of FCs of orders 0.1, 0.5 and 0.9 in the frequency ranges of (2.7 Hz - 365 kHz), (9 Hz - 105 kHz) and (4 Hz - 230 kHz) respectively. The simulated phase deviates from theoretical phase by ±0.30° for FCs of orders 0.1, 0.5 and 0.9 in the frequency ranges of (170 Hz - 6.8 kHz), (180 Hz - 5.5 kHz) and (150 Hz - 7.5 kHz) respectively.

Table 2.1: Component setting of FC

Order	$R_a(\Omega)$	$R_b(\Omega)$	$R_c(\Omega)$	$R_d(\Omega)$	R_e (Ω)	C_b(nF)	C_c(μF)	C_d(μF)	C_e(μF)
0.1	274.7k	81.9k	56.1k	66.3k	154.1k	0.165	0.0015	0.0052	0.015
0.5	1.402k	3.17k	4.78k	11.2k	92.9k	6.64	0.023	0.043	0.055
0.9	2.6	16.5	49.9	255.9	55789.8	1846	2.97	2.69	0.544

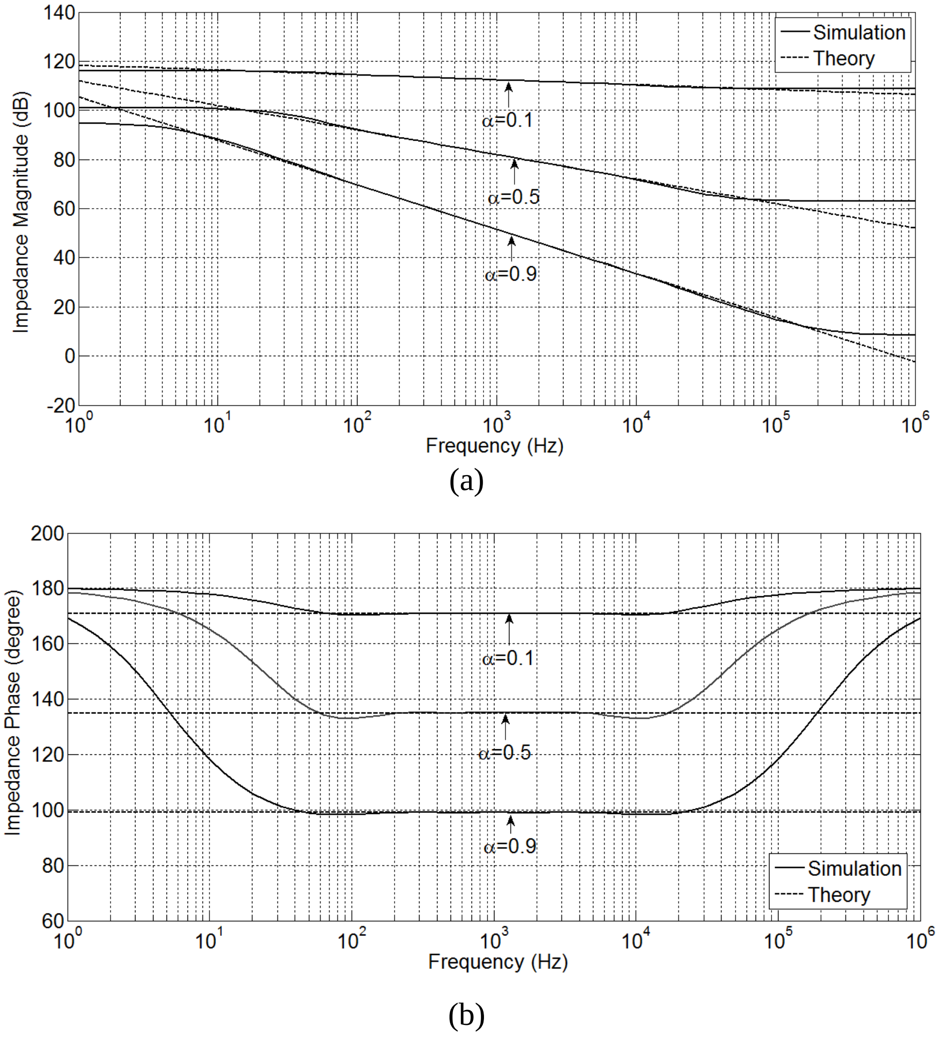

Fig. 2.2: Frequency responses for FC **(a)** magnitude and **(b)** phase

2.3 Stability Analysis

The section describes the stability analysis of fractional order circuits. It is well known that for a linear time invariant (LTI) system to be stable, all the roots of the characteristic equation should be on the left half of complex plane. However, this constraint is relaxed in FO systems and roots may exist on the right half of complex plane. The stability analysis of FO domain is well explained in [11] and has been adapted in the present work. The stability of fractional-order linear time invariant (FLTI) systems can be examined by converting s-plane to F-plane which is defined as $F = s^{\alpha}$. The physical s-plane is transformed from $\pm \pi$ to $\pm\alpha\pi$ for F-plane. The unstable region is defined up to $\pm \pi/2$ in s-plane and is transformed to region up to $\pm\alpha\pi/2$ in F-plane.

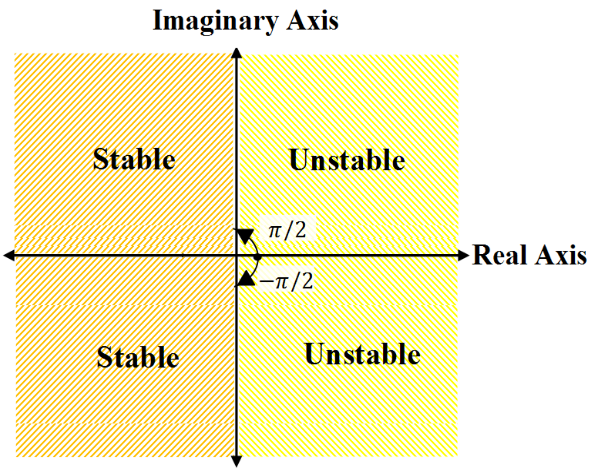

(a)

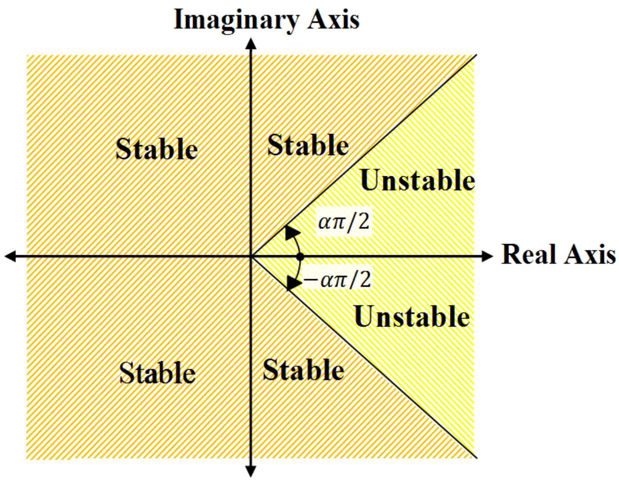

(b)

Fig. 2.3: Stability Region in Complex **(a)** s-plane and **(b)** F-plane

In another method the s-plane is transformed into a W-plane defined as $W = s^{1/m}$ and is applicable only if α can be represented as a ratio of two positive integers such that $\alpha = n/m$. The transformation from s plane into W plane remains independent of n.

In this work, stability analysis is carried out using root locus technique for FO linear system. The location of poles is determined from the characteristic equation of FLTI system. The stability of FLTI system is verified by checking whether the roots fall in stable region or not.

2.4 Active Blocks Used in this work

In this work, the FO circuits based on active blocks CFOA and OTA are proposed. This section briefly describes these active blocks.

2.4.1 CFOA: Port Relation and Their Characterization

The circuit symbol of CFOA is given in Fig. 2.4 (a) and corresponding port relationships is given by (2.13).

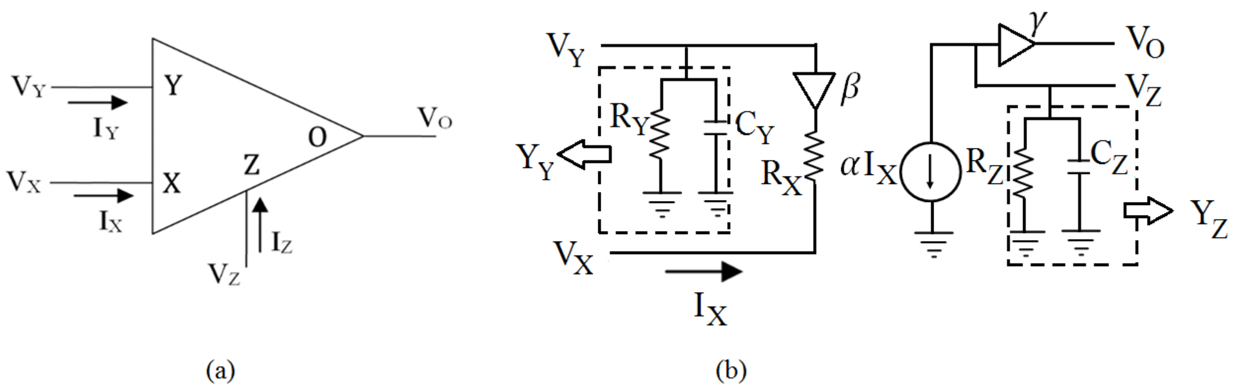

Fig. 2.4: (a) CFOA symbol and **(b)** its equivalent circuit with non-idealities

$$\begin{bmatrix} I_Y \\ V_X \\ I_Z \\ V_O \end{bmatrix} = \begin{bmatrix} 0 & 0 & 0 & 0 \\ 1 & 0 & 0 & 0 \\ 0 & 1 & 0 & 0 \\ 0 & 0 & 1 & 0 \end{bmatrix} \begin{bmatrix} V_Y \\ I_X \\ V_Z \\ I_O \end{bmatrix} \tag{2.13}$$

In practice, the port relation may deviate from (2.13). Figure 2.4 (b) shows equivalent circuit with CFOA non-idealities. The (R_Y, C_Y) and (R_Z, C_Z)

correspond to parasitic resistor and capacitor at Y and Z terminals while R_X represent parasitic resistor at X terminal. There are two voltage buffers between Y and X-terminals; and O and Z-terminals; and one current follower between Z and X-terminals where α represents current transfer gain; and β, γ correspond to voltage transfer gains due to tracking errors of CFOA. Considering the non-idealities outlined above, (2.13) modifies to (2.14).

$$\begin{bmatrix} I_Y \\ V_X \\ I_Z \\ V_O \end{bmatrix} = \begin{bmatrix} 0 & 0 & 0 & 0 \\ \beta & 0 & 0 & 0 \\ 0 & \alpha & 0 & 0 \\ 0 & 0 & \gamma & 0 \end{bmatrix} \begin{bmatrix} V_Y \\ I_X \\ V_Z \\ I_O \end{bmatrix} \tag{2.14}$$

Ideally these values are $G_{Y1} = G_{Z1} = G_{Z2} = R_{X1} = R_{X2} = C_{Y1} = C_{Z1} = C_{Z2} = 0$ and $\alpha = \beta = \gamma = 1$.

The functionality of CFOA is verified using macro model of CFOA IC [121] (AD844AN) using through SPICE simulations with corresponding supply voltages of ±10 V. The DC responses of CFOA are shown in Fig. 2.5. The variation of V_X with respect to V_Y is shown in Fig. 2.5 (a). It is observed that V_X closely follows V_Y in voltage range ± 6.69 V with tracking error of 0.2 V. The I_Z variation with I_X is depicted in Fig. 2.5 (b) whereas Fig. 2.5 (c) shows variation of V_O with V_Z. It may be seen from the characteristics that I_X follows I_Z closely in current range ±3.38 mA with tracking error of 0.2 mA and similarly V_O follows V_Z in the voltage range ± 7.1V with tracking error of 0.06 V. From DC simulations values of current and voltage transfer ratios due to tracking errors are obtained as: α = 0.9997, β = 0.9756, γ = 0.9999.

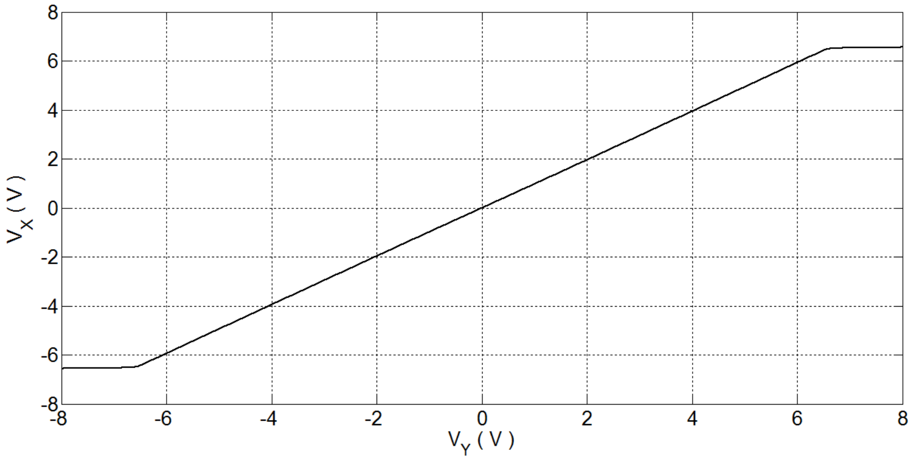

(a)

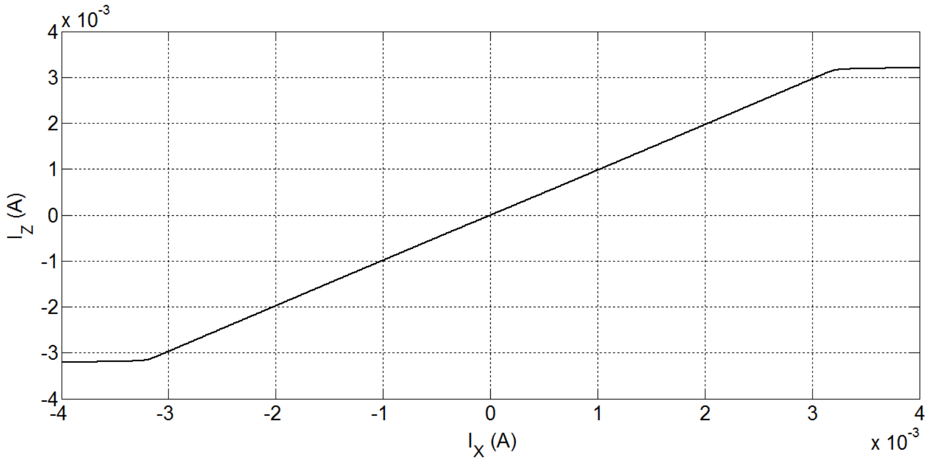

(b)

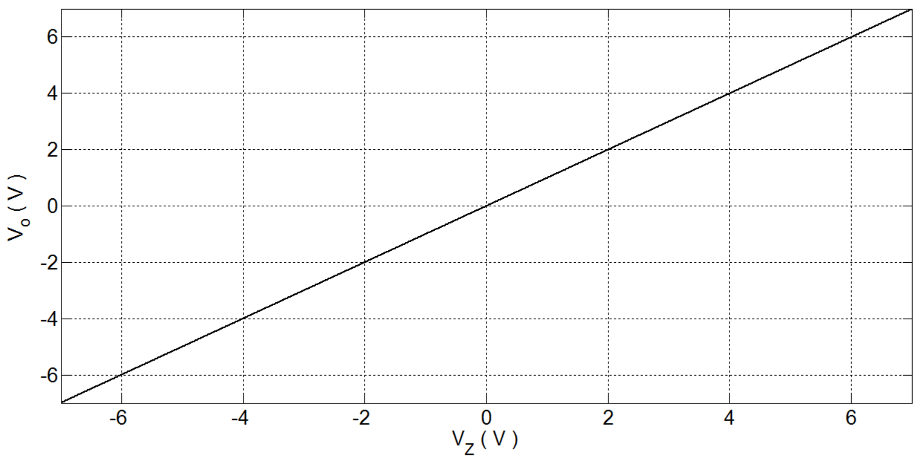

(c)

Fig. 2.5: DC response for **(a)** V_X vs. V_Y, **(b)** I_Z vs I_X and **(c)** V_O vs V_Z

The frequency responses for voltage and current transfers are depicted in Fig 2.6. The voltage transfers at X and O terminals are shown in Figs 2.6 (a) and (b) respectively with their corresponding 3 dB frequencies are 419 MHz and 12.56

MHz. The frequency response of current transfer at Z terminal is presented in Fig. 2.6 (c) and 3 dB frequency is recorded as 10.28 MHz. The CFOA parasitics are obtained through simulations are given as $R_X = 50\ \Omega$, $R_Y = 2\ M\Omega$, $C_Y = 2$ pF, $R_Z = 3\ M\Omega$, $C_Z = 4.5$ pF.

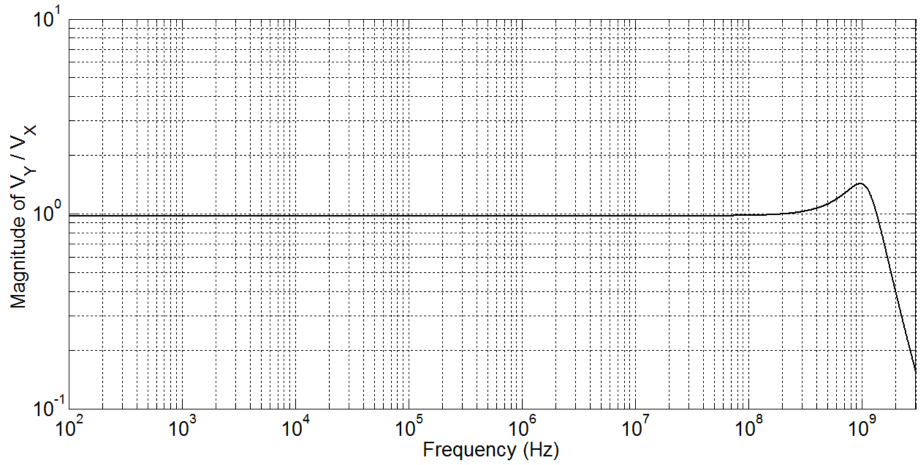

(a)

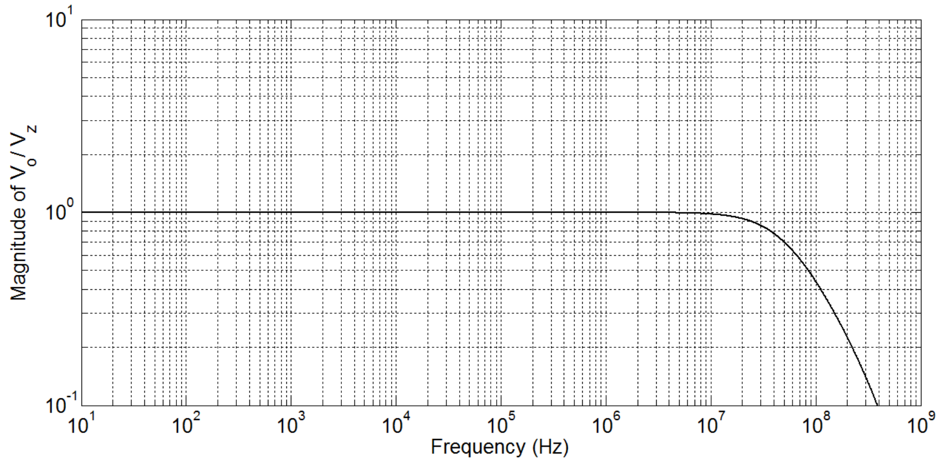

(b)

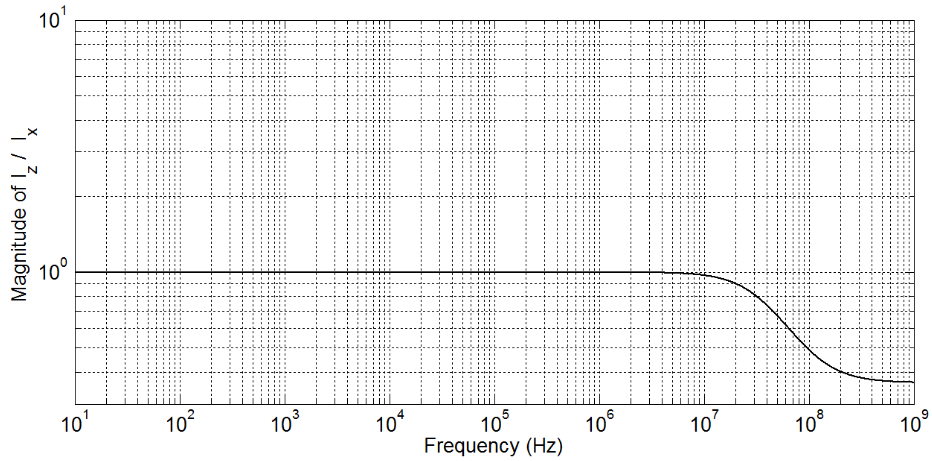

(c)

Fig. 2.6: Frequency responses of **(a)** V_Y/V_X **(b)** V_O / V_Z **(c)** I_Z / I_X

2.4.2 OTA: Port Relations and Their Characterization

The OTA processes differential voltage and provides output current. Its circuit symbol of OTA and CMOS schematic are given in Fig. 2.7. The port relationship of OTS is given by (2.15).

$$I_{O\pm} = \pm g_m (V_+ - V_-) \tag{2.15}$$

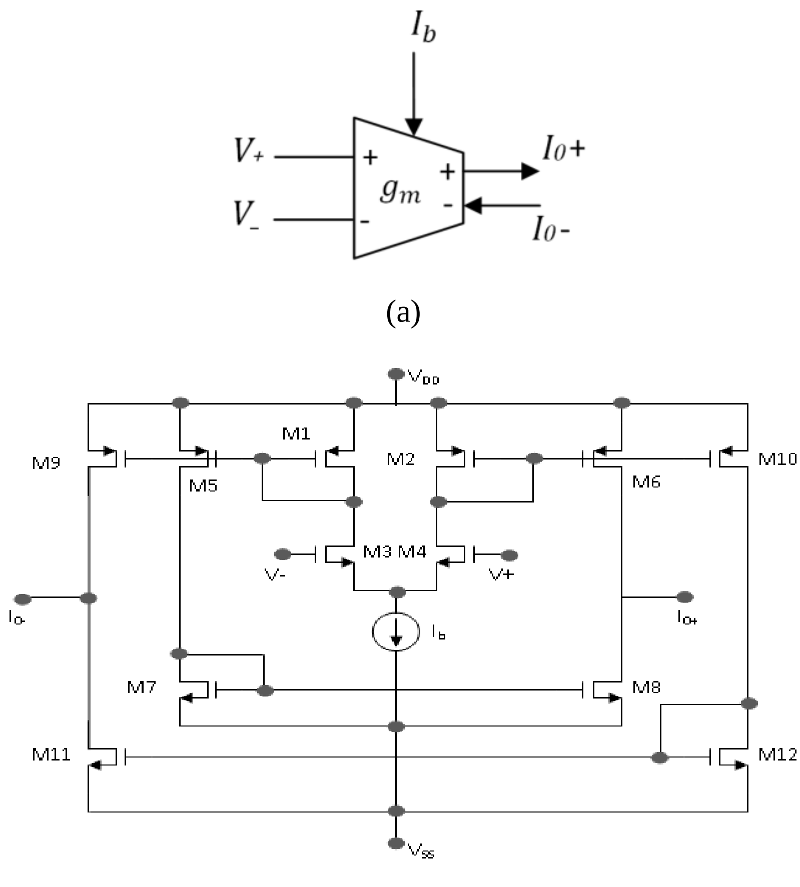

(b)

Fig. 2.7: OTA **(a)** Circuit Symbol and its **(b)** CMOS realization [122]

Here the transconductance gain (g_m) of OTA and it is related to bias current *(I_b)* through (2.16).

$$g_m = \sqrt{\left(\mu_n C_{ox} \frac{W}{L} I_b\right)} \tag{2.16}$$

The symbols μ_n, C_{ox} and W/L respectively represent electron mobility, gate oxide capacitance per unit area and aspect ratio of differential pair (M_3, M_4) respectively. The dependence of g_m on bias current (I_b) may be used to add electronic tunability of the circuit parameters.

2.4.3 Simulation Results of OTA

The OTA of Fig. 2.7 was simulated using 0.18 μm CMOS process parameter and the supply voltage of ±1.8 V is taken. The aspect ratios of the transistors $M_{3–4}$, $M_{1–2, 5–6, 9–10}$ and $M_{7–8, 11–12}$ are taken as (5.76 μm/0.72 μm), (2.16 μm/0.72 μm) and (1.44 μm/0.72 μm) respectively. The DC response plotted for a bias current of 15 μA is shown in Fig. 2.8 (a) and the transconductance gain is obtained as 150 μA/V. The electronic tunability of transconductance gain is depicted in Fig. 2.8 (b) and the maximum transconductance gain of 564 μA/V is obtained at a bias current of 300 μA. The frequency response for same simulation settings is presented in Fig. 2.8 (c). The 3 dB frequency of OTA is measures to be 201 MHz. Furthermore, the simulated value of the parasitic capacitance at output terminal is observed to be 5.39 pF.

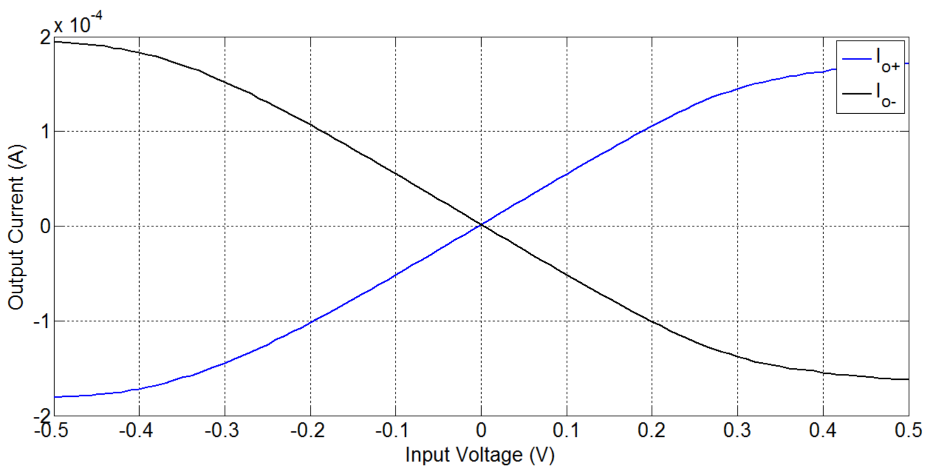

(a)

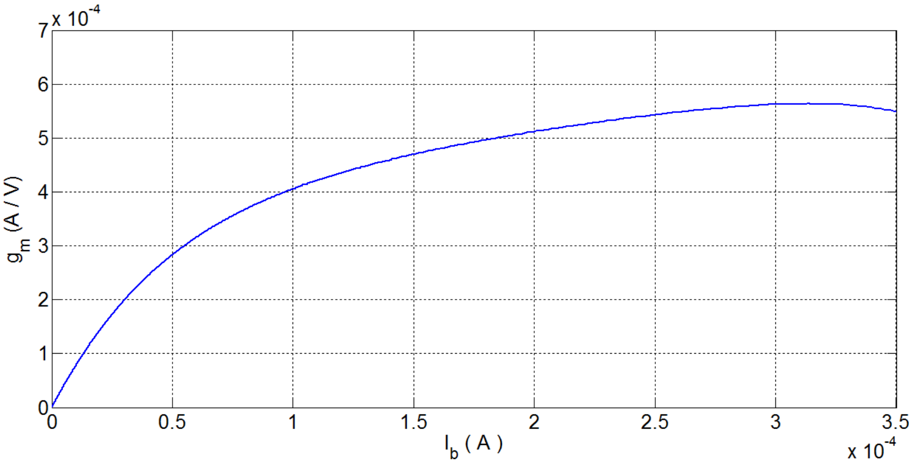

(b)

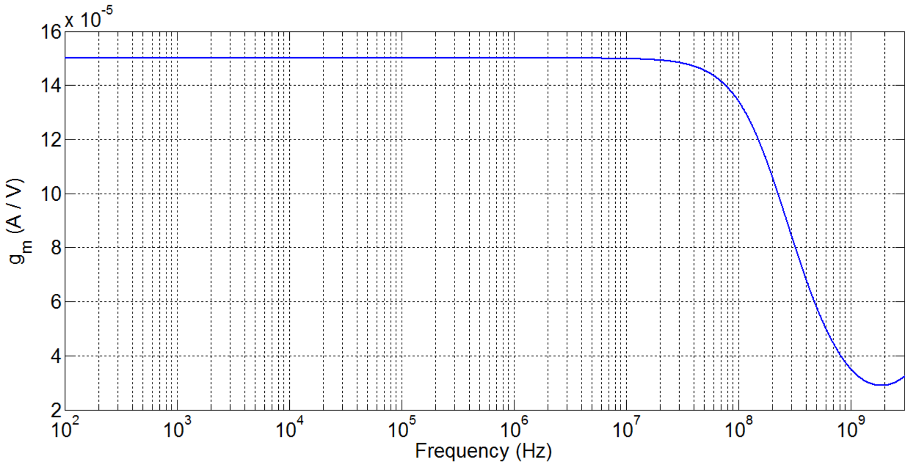

(c)

Fig. 2.8: (a) DC response, **(b)** transconductance variation with I_b **(c)** AC responses of OTA

2.5 Conclusion

In this chapter, a brief review of CFE approximation method for realizing FOE is given. The circuit realization of 4th order CFE approximation form is discussed thereafter. A method for checking stability of fractional order circuits and systems is also presented. Preliminary discussion on active blocks CFOA and OTA is also given as these blocks are used for verifying various propositions. SPICE simulations are included to comprehend the presentation.

CHAPTER 3

INTEGER AND FRACTIONAL ORDER CAPACITANCE MULTIPLIER CIRCUITS

The contents and results of the following papers have been reported in this chapter:

[1] **R. Verma,** N. Pandey, R. Pandey, “Novel CFOA based capacitance multiplier and its application”, AEU- International Journal of Electronics and Communications, vol. 107, pp. 192-198, 2019. (Elsevier) **Indexing: SCI, SCIE, SCOPUS; IF: 2.115**

[2] **R. Verma**, N. Pandey, R. Pandey, “Capacitance characteristics behavior of 0.5 order FC USING CFOA BASED FC MULTIPLIER", Advances in Electrical and Electronic Engineering **(Communicated)**

3.1 Introduction

Monolithic integration of circuits and systems has witnessed a tremendous boost due to continuous downsizing of device dimensions. Low frequency applications such as sensing and subsequent processing of biomedical signals and integration of loop filter used in PLL could not be benefited from this as these require large value capacitors. Researchers, therefore, look forward for alternate schemes for placing a small capacitor on-chip and use a multiplier circuit. The schemes of impedance transformation such as gyrator, generalized impedance converter (GIC) and negative impedance converter (NIC) etc. have been reported in the literature that offer tuning of capacitance multiplier (C-multiplier) circuit. Such C-multiplier circuits have been deployed for appropriate tuning of filters [123 - 135], oscillators [136], phase-locked loops (PLLs) [137] and series resonators [138]. Commercially available active elements such as operational transconductance amplifier (OTA) [139 - 141], Op-amp [123, 137] and AD 844 (CFOA) [142 - 145] based C-multiplier circuits are reported in the literature.

This chapter first presents a new C-multiplier circuit based on CFOA. Four CFOA based C-multiplier circuits are generalized in fractional domain. The performance of the proposed circuits is examined for nonideal effects of CFOA and a compensation scheme is suggested. The functionality of the realized multipliers is verified using SPICE simulations where the FC is modeled using domino RC ladder network. The circuit applications of proposed C-multiplier circuits are also included in this chapter.

3.2 Proposed CFOA based capacitance multiplier

The study of CFOA based C-multiplier circuit [142 - 148] shows that the multiplication factor (K) of capacitance (C) can be expressed in the form of (i) 1+P [143, 145], (ii) 1-P [145] and (iii) 1/(1+P) [143, 145] where P represents resistor ratio. The structures of type (ii) may be used to realize a C-multiplier circuit presenting a negative capacitance value if P is greater than unity and a positive value for P less than unity. The C-multiplier circuit may be obtained by adaptation of CFOA based gyrator [149 - 151]/ GIC [152] which provide multiplication factor of P/ P^2. Other characteristics are summarized below:

- [143, 146] provide lossy capacitance whereas lossless capacitance is obtained in [142, 144 - 152]
- [142, 145, 146, 148 - 151] realize grounded capacitance while floating grounded capacitance realization are found in [143, 144, 147, 152]
- [143, 145, 150, 151] can emulate both positive and negative C-multiplier circuit while positive C occurs in [142, 143, 145, 149, 152] and negative C in [143, 145, 148]
- The multiplication factor of C-multiplier circuits of type (iii) and type (ii) with P >1 is less than unity. So, the effective value of capacitor decreases which may be used multiplication factor capacitor which is not available otherwise.
- Larger component spread (resistance ratio) is needed to achieve higher multiplication factor [143, 145, 149 - 152].

A new type of C-multiplier circuit with multiplication factor of K=1/(1-P) is presented here. This type of circuit can provide very high multiplication factor by selecting P close to unity. The closer is P to unity, higher would be the multiplication factor resulting in smaller component spread.

The schematic of proposed C-multiplier circuit is shown in Fig. 3.1. It uses two CFOAs, two resistors and a capacitor (for non-compensating circuit). The proposed circuit uses floating capacitor which may be realized using Metal-insulator-metal (MIM) or metal-oxide-metal (MOM) double poly (poly1-poly2) capacitor processes [153].

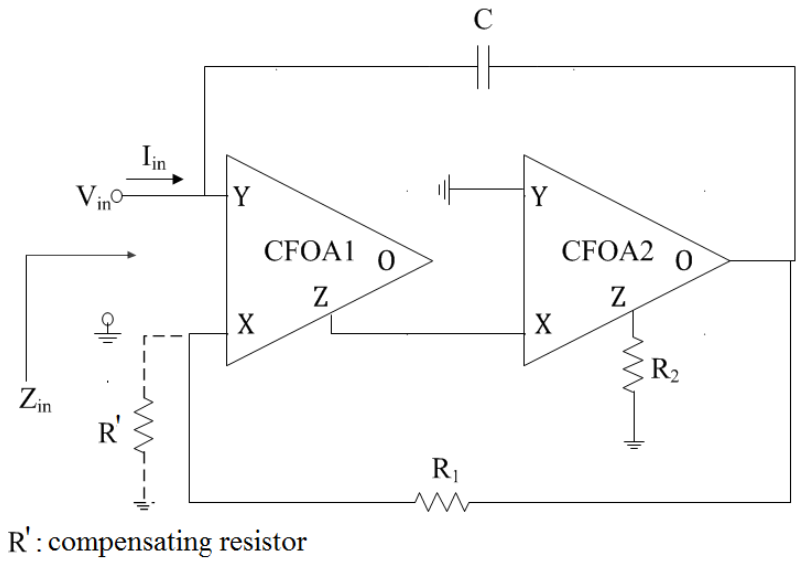

Fig. 3.1: Proposed CFOA based C-multiplier circuit

Considering port relation of CFOA, the input impedance of the proposed circuit is computed as

$$Z_{in}(s) = \frac{1}{sC_{eff}} = \frac{1}{s(KC)} = \frac{1 - R_2/R_1}{sC} \tag{3.1}$$

where $K = 1/(1 - R_2/R_1)$ It is clear from (3.1) that the smaller is the component spread larger will be the multiplication factor (K) e. g. $R_2 = 0.9\ R_1$

gives K = 10. The sensitivity of the (K) with respect to R_2/R_1 is $S^K_{R_2/R_1} = \frac{R_2/R_1}{1-R_2/R_1}$. Therefore, the advantage comes at the cost of higher sensitivity of K.

3.2.1 Non-Ideal Analysis

To analyze the proposed circuit's behavior in presence of CFOA non-idealities, the input impedance is recomputed as

$$Z_{in}(s)|_n = \frac{1}{sC + G_{Y1} + sC_{Y1} + \frac{(\alpha^2\beta\gamma)sC}{(G_2 + G_{Z2} + sC_{Z2})(R_1 + R_{X1})(1 + R_{X2}G_{Z1} + sR_{X2}C_{Z1}) - \alpha^2\gamma}} \tag{3.2}$$

where G_{Y1}, C_{Y1}, G_{Z1}, C_{Z1}, R_{X1}; and G_{Z2}, C_{Z2}, R_{X2} are parasitics of CFOA1; and CFOA2 respectively.

Considering $R_{X2}G_{Z1} \ll 1$ operating frequency $\omega < min\left(\frac{1}{R_{Y1}(C_{Y1}+C)}, \frac{1}{R_{Z2}C_{Z2}}, \frac{1}{R_{X2}C_{Z1}},\right)$, (3.2) reduces to

$$Z_{in}(s)|_n \approx \frac{1}{sC + \frac{(\alpha^2\beta\gamma)sC}{(G_2 + G_{Z2})(R_1 + R_{X1}) - \alpha^2\gamma}} \tag{3.3}$$

which gives multiplication factor as

$$K_n = 1 + \frac{\alpha^2\beta\gamma}{(G_2 + G_{Z2})(R_1 + R_{X1}) - \alpha^2\gamma} \tag{3.4}$$

3.2.2 The Proposed Compensation Method

It may be observed from (3.4) that multiplication factor (K_n) drastically decreases for $\alpha, \beta, \gamma < 1$. To compensate this, a grounded resistor R' at X-terminal of CFOA1 may be placed (as shown in Fig. 3.1) which modifies (3.2) to

$$Z_{in}^{'}(s)|_n = \frac{1}{sC + G_{Y1} + sC_{Y1} + \frac{(\alpha^2\beta\gamma)sC}{R_{X1}(G_2 + G_{Z2} + sC_{Z2})(1 + R_{X2}G_{Z1} + sR_{X2}C_{Z1}) - \alpha^2\gamma\left(\frac{R'}{R_1 + R'}\right)}}$$

(3.5)

Considering $R_{X2}G_{Z1} \ll 1$, operating frequency $\omega < min\left(\frac{1}{R_{Z2}C_{Z2}}, \frac{1}{R_{X2}C_{Z1}},\right)$ and neglecting parasitic effect at Y-terminal, (3.5) reduces to

$$Z_{in}^{'}(s)|_n \approx \frac{1}{sC + \frac{(\alpha^2\beta\gamma)sC}{R_{X1}(G_2 + G_{Z2})(1 + R_{X2}G_{Z1}) - \alpha^2\gamma\left(\frac{R^{'}}{R_1 + R^{'}}\right)}}$$

(3.6)

To find the value of R’, (3.1) may be rewritten as

$$Z_{in}(s) = \frac{1}{sC + \frac{sC}{G_2R_1 - 1}}$$

(3.7)

The relation between R_1 and R' is obtained by comparing (3.6) and (3.7) as

$$R^{'} = \frac{P}{1 - P}R_1$$

(3.8)

where

$$P = \beta\left(\frac{R_{X1}(G_2 + G_{Z2})(1 + R_{X2}G_{Z1})}{\alpha^2\beta\gamma} - \frac{R_1}{R_2} + 1\right)$$

(3.9)

3.2.3 Simulation Results

The behavior of proposed C-multiplier circuit is examined under (i) ideal, (ii) non-ideal and (iii) compensated conditions. The simulation responses are depicted in Fig. 3.2 for factor K=100 where R_1= 20.02 kΩ R_2= 20 kΩ, R'= 32.16Ω C = 1nF. It may be noted that the impedance of the proposed compensated C-multiplier circuit closely follows the ideal one.

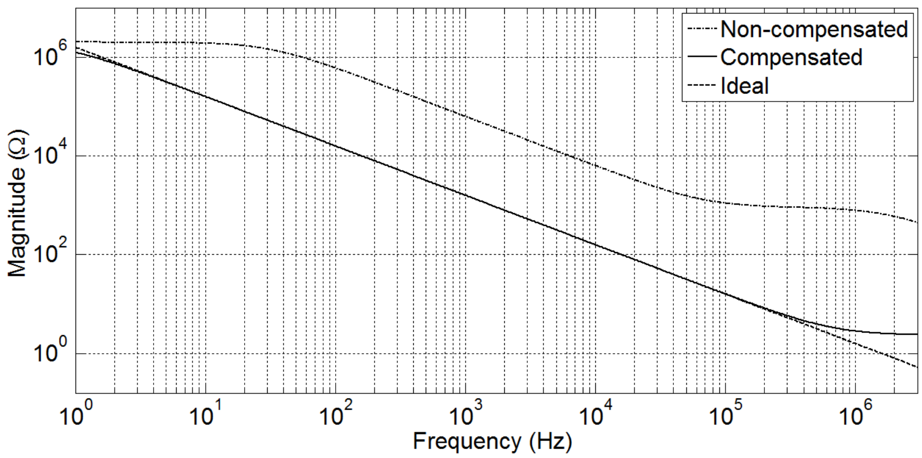

Fig. 3.2: Simulated magnitude responses of proposed CFOA based C-multiplier circuit

The functionality of the proposed capacitance multiplier is also examined using the following simulations conditions:

(i) K is fixed and varying C;

(ii) C is fixed and varying K; and

which are designated as case 1 and case 2 respectively; and detailed simulation settings are placed in Table 3.1. Simulated and theoretical frequency responses are plotted in Figs. 3.3(a) and 3.3(b) respectively for cases 1 and 2. The effective value of capacitance and frequency range is also listed in Table 3.1.

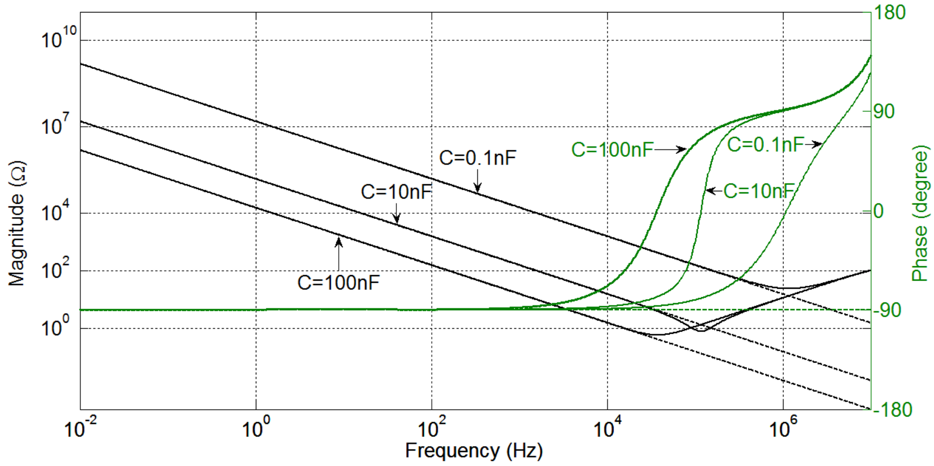

(a)

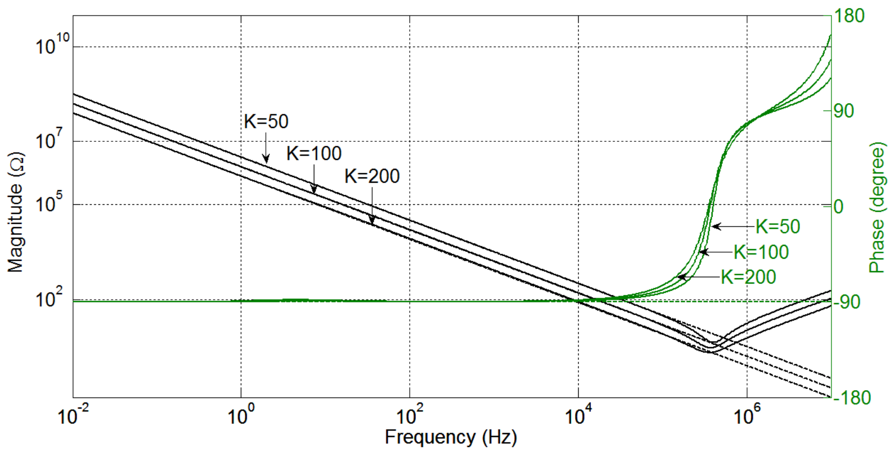

(b)

Fig. 3.3: Simulation (solid lines) and ideal (dashed lines) magnitude (in black) and phase (in green) responses of the proposed circuit for **(a)** case 1**(b)** case 2

Table 3.1: Detailed simulation settings and summary of observations

Case	**Components tuning**					**Realized C_{eff} (F)**	**Frequency response**	
	C (nF)	**K tuning**					**Magnitude response within 7% error**	**Phase response within 6^0 phase error**
		K	**R_1 (kΩ)**	**R_2 (kΩ)**	**R' (kΩ)**			
1	0.1	100	20.202	20	4.4	10n	upto 390 kHz	upto 67.6 kHz
	10					1µ	upto 43.6 kHz	upto 20.5 kHz
	100					10µ	upto 25.1 kHz	upto 2.89 kHz
2	1	50	20.408	20	9.1	50n	upto 141 kHz	upto 75.8 kHz
		100	20.202	20	4.4	100n	upto 144.5 kHz	upto 55 kHz
		200	20.1	20	2.23	200n	upto 190 kHz	upto 40.7 kHz

3.2.4 Experimental Results

The functionality of the proposed circuit is examined using CFOA IC AD844AN. The capacitance C is taken as 1 nF and the proposed circuit is bread-boarded for K = 5 by choosing R_1 = 25 kΩ and R_2 = 20 kΩ. Power supplies of ±10 V are taken. An input sinusoid of $V_{peak\text{-}peak}$ = 2 V is applied and the magnitude of proposed C-multiplier is measured. Figure 3.4 shows the ideal, simulated and experimental magnitude responses for proposed circuit. The experimental magnitude response of proposed multiplier follows the ideal response in the frequency range of 20 Hz- 2.8 kHz with 10% deviations.

It is emphasized here that high multiplication factor requires passive components with great precision. Therefore, it is difficult to achieve very high multiplication factor. In integrated circuit realization, such precision may be achieved by using electronically tunable resistors.

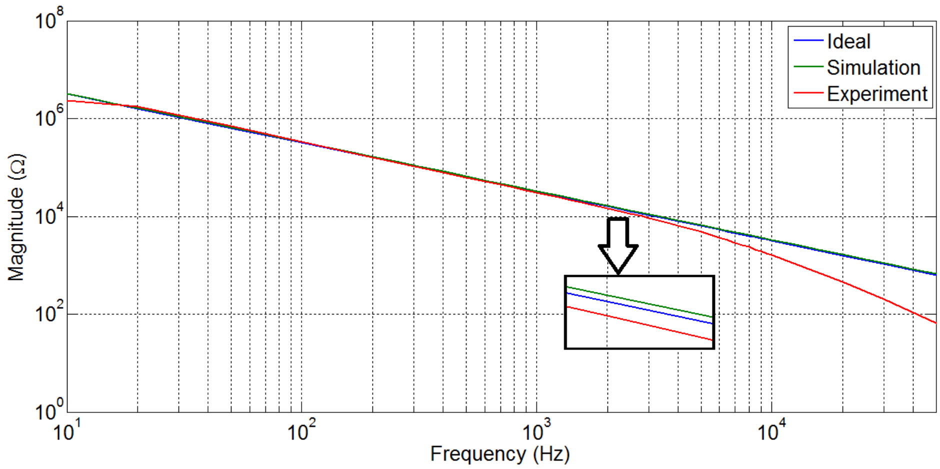

Fig. 3.4: Ideal, simulated and experimental magnitude responses for proposed circuit

3.2.5 Application of the proposed C Multiplier

In this section, the proposed circuit is employed for reconfiguration of a parallel resonator block (PRB) given in Fig. 3.5 (a) where R_{eff}, L_{eff} and C_{eff} represent effective values of resistor, inductor and capacitor respectively. Figure 3.1 is used to realize C_{eff}. The parallel RL combination is replaced by CFOA based implementation shown in Fig. 3.5 (b) [154]. The values of R_{eff} and L_{eff} are given by

$$R_{eff} = \frac{R_1' R_2'}{R_1' + R_2'} \ , \qquad L_{eff} = C_{eff}' R_1' R_2'$$

(3.10)

where C_{eff}' is obtained from circuit of Fig. 3.1.

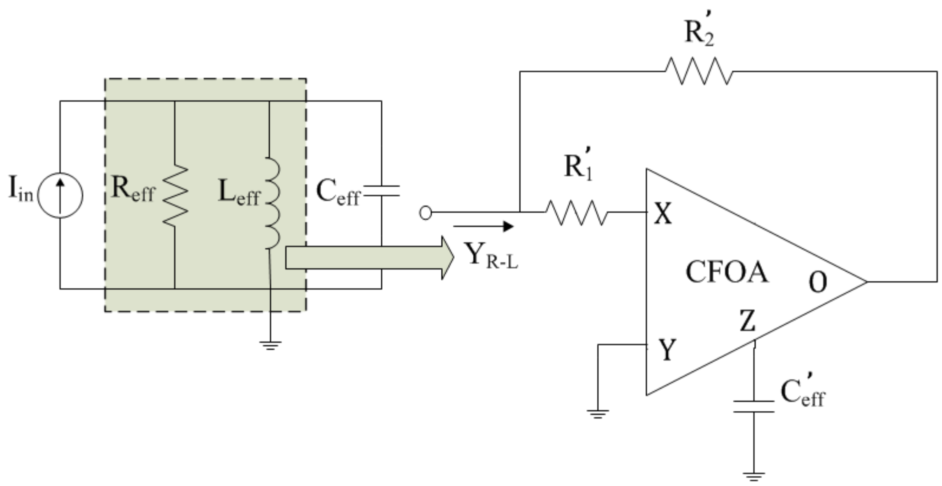

(a) **(b)**

Fig. 3.5: (a) Reconfiguration of PRB **(b)** CFOA based active simulation of parallel RL combination

The impedance function of the reconfigured PRB is given as

$$Z_{in} = \frac{1}{Y_{in}} = \frac{1}{\frac{1}{R_{eff}} + \frac{1}{sL_{eff}} + sC_{eff}}$$

(3.11)

and its performance parameters resonant frequency (ω_0), quality-factor (Q) and peak impedance at resonant frequency ($Z_{in}|_{\omega_0}$) are evaluated as

$$\omega_0 = \sqrt{\frac{1}{L_{eff} C_{eff}}}$$

$$Q = R_{eff}.\sqrt{\frac{C_{eff}}{L_{eff}}}$$

$$Z_{in}|_{\omega_0} = R_{eff} \tag{3.12}$$

Assuming K_1 and K_2 as multiplication factors for C_{eff} and C'_{eff} i. e. $C_{eff} = K_1C$, and $C'_{eff} = K_2C'$ the performance parameters of (3.12) can be rearranged as

$$\omega_0 = \sqrt{\frac{1}{K_2C'R'_1R'_2}.\frac{1}{K_1C}}$$

$$Q = \frac{\sqrt{R'_1R'_2}}{R'_1 + R'_2}.\sqrt{\frac{K_1C}{K_2C'}}$$

$$Z_{in}|_{\omega_0} = \frac{R'_1R'_2}{R'_1 + R'_2} \tag{3.13}$$

The performance parameters of the reconfigured resonator can be tuned by controlling the effective values of components (C_{eff}, L_{eff}, R_{eff}) of the reconfigured resonator.

3.2.5.1 Simulation Results

The performance of proposed circuit is examined under following test cases:

Case 1: Tuning R'_1 and R'_2 while maintaining $R'_1 = R'_2$ and keeping K_1 and K_2 constant

Case 2: Tuning K_1 and K_2 while maintaining $K_1 = K_2$

Case 3: Tuning K_1 and K_2 while retaining their product ($K_1.K_2$) constant

Case 1 affects the performance parameters ω$_0$ and $Z_{in}|_{\omega_0}$ and is thus useful when these parameters need be changed for the fixed value of Q-factor. Case 2 is useful for changing ω$_0$ while retaining the Q-factor and $Z_{in}|_{\omega_0}$ constant. Case 3 is appropriate for varying Q-factor and keeping ω$_0$ and $Z_{in}|_{\omega_0}$ constant. Simulations for all the three cases are carried out with test conditions listed in Table 3.2 and the input impedance under the test conditions are plotted in Fig. 3.6. The performance parameters are also listed in Table 3.2.

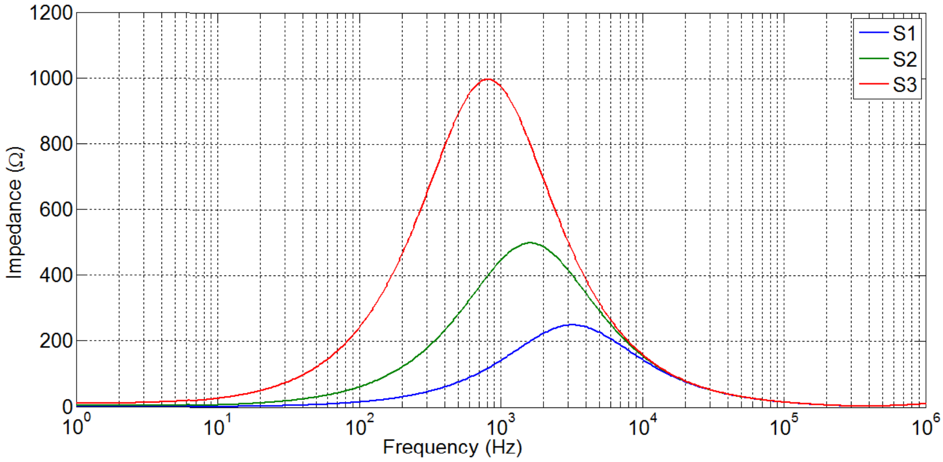

(a)

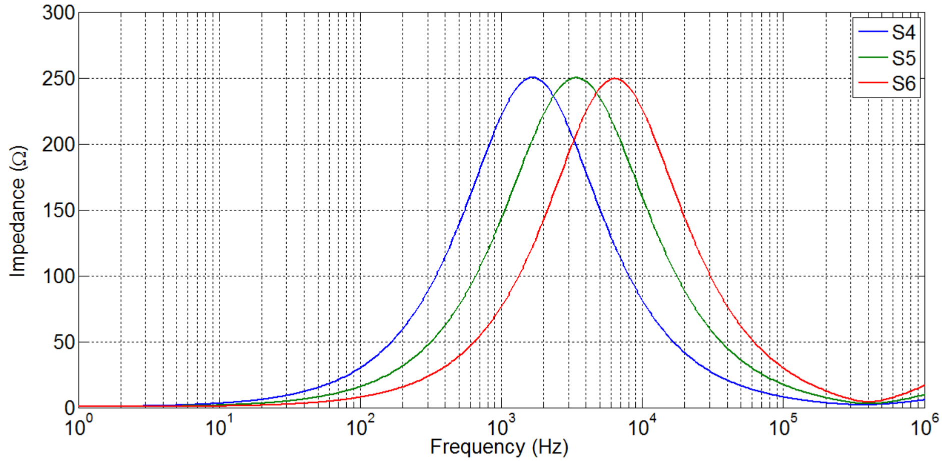

(b)

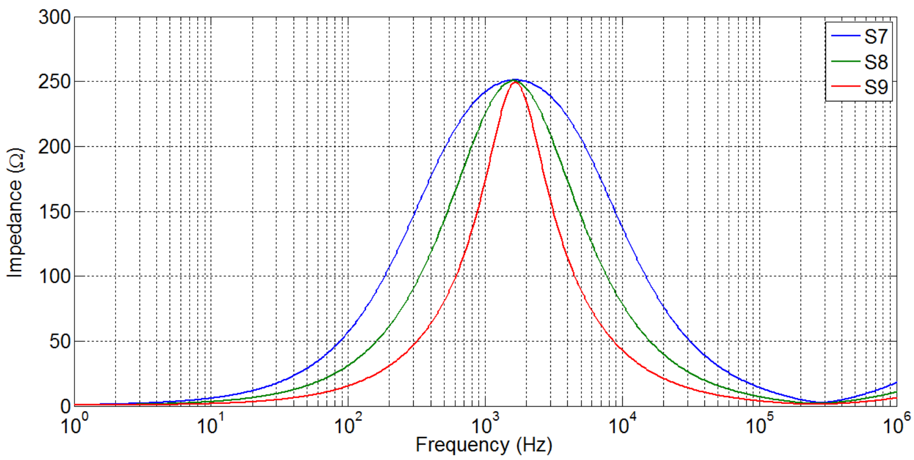

Fig. 3.6: Simulation outputs for input impedance of reconfigured PRB (Fig. 3.5) for **(a)** Case 1, **(b)** Case 2 and **(c)** Case 3

Table 3.2: Component setting and performance parameters of reconfigured PRB

Case	Case Test no.	R_{eff}		C_{eff}			L_{eff}			ω_0 (krad/s)	Q	$Z_{in}\|_{\omega_0}$ (kΩ)
		$R'_1 = R'_2$ (kΩ)	R_{eff} (kΩ)	K_1	C (nF)	C_{eff} (nF)	K_2	C' (nF)	L_{eff} (H)			
	S1	0.5	0.25						0.025	20		0.25
1	S2	1	0.5	100	1	100	100	1	0.1	10	0.5	0.5
	S3	2	1						0.4	5		1
	S4			200		200	200		0.05	10		
2	S5	0.5	0.25	100	1	100	100	1	0.025	20	0.5	0.25
	S6			50		50	50		0.0125	40		
	S7			50		100	200		0.1		0.25	
3	S8	0.5	0.25	100	2	200	100	2	0.05	10	0.5	0.25
	S9			200		400	50		0.025		1	

A close observation of Table 3.2 suggests following:

- Case1: different desirable impedance peaks (= 0.25 kΩ, 0.5 kΩ, 1 kΩ) and fixed Q (= 0.5) at different ω_0 (= 20 krad/s, 10 krad/s, 5 krad/s)
- Case2: ω_0 tuning (= 10 krad/s, 20 krad/s, 40 krad/s) with constant impedance peaks (= 0.25 kΩ) and Q (=0.5)
- Case3: Q tuning (= 0.25, 0.5, 1) with constant impedance peaks (= 0.25 kΩ) and ω_0 (= 10 krad/s).

3.3 CFOA based FC Multiplier Circuit

In this section capacitance scaling of FC using CFOA based C multiplier circuits is presented. Figure 3.7 shows proposed CFOA based FC multiplier circuits. The topologies of Fig. 3.7 (a) – (c) are realized by generalizing C multipliers reported in [145] while topology of Fig. 3.7 (d) is obtained using topology reported in section 3.2. Routine analysis of the circuits of Figs. 3.7 (a), (b), (c) and (d) yields in the following impedance functions

$$Z_{in\alpha_1}(s) = \frac{1}{\omega^\alpha (1 - R_2/R_1) C_\alpha} \tag{3.14}$$

$$Z_{in\alpha_2}(s) = \frac{(1 + R_2/R_1)}{\omega^\alpha C_\alpha} \tag{3.15}$$

$$Z_{in\alpha_3}(s) = \frac{1}{\omega^\alpha (1 + R_2/R_1) C_\alpha} \tag{3.16}$$

$$Z_{in\alpha_4}(s) = \frac{(1 - R_2/R_1)}{\omega^\alpha C_\alpha} \tag{3.17}$$

Equations (3.14) – (3.17) show that FC is scaled by factors K_i (i = 1,..,4) where $K_1 = (1 - R_2/R_1)$, $K_2 = 1/(1 + R_2/R_1)$, $K_3 = (1 + R_2/R_1)$, and $K_4 = 1/(1 - R_2/R_1)$.

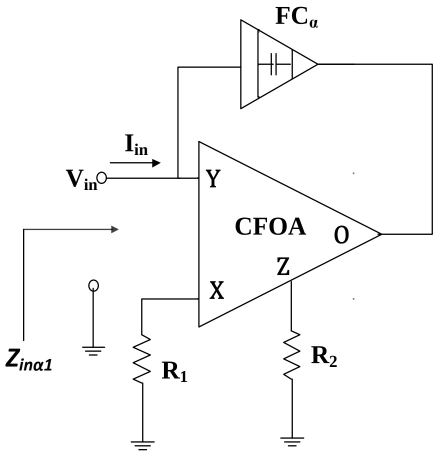

(a)

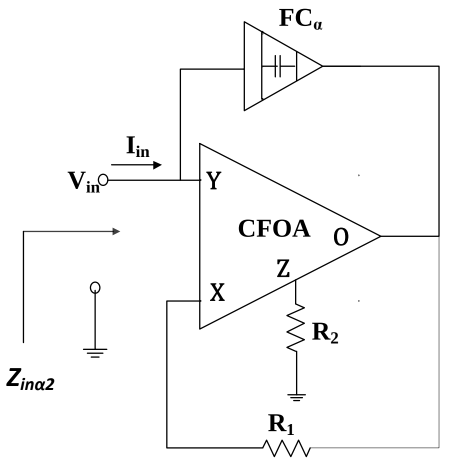

(b)

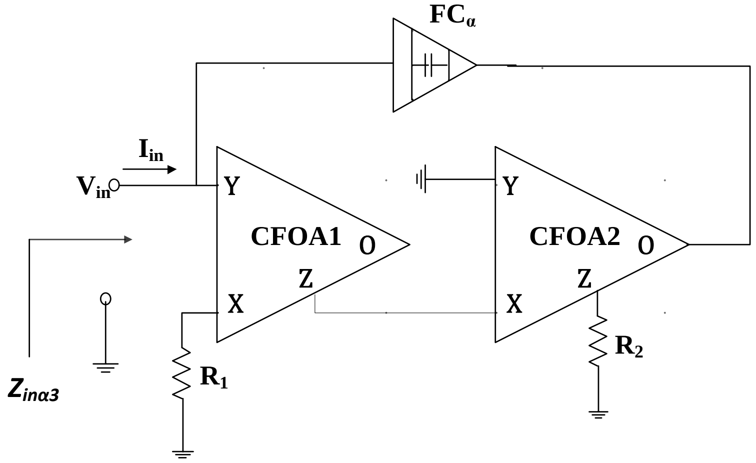

(c)

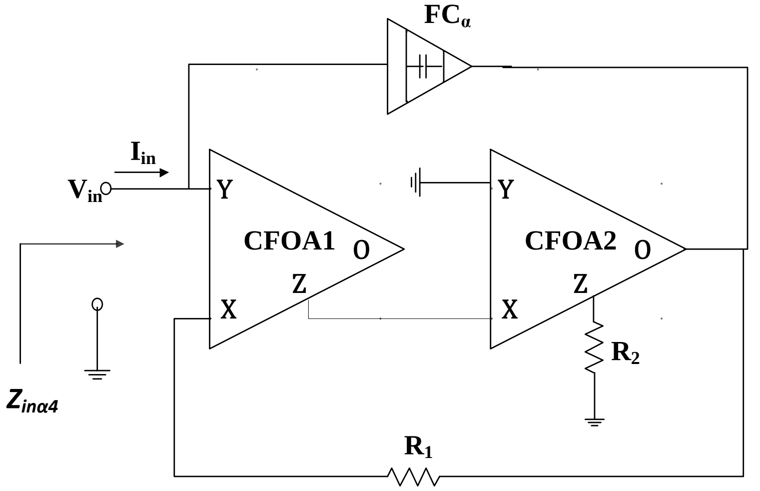

(d)

Fig. 3.7: CFOA based FC multiplier circuits

3.3.1 Impedance Characteristics

It may be observed that the impedance functions of realized multipliers are majorly influenced by two factors (i) α, and (ii) R_2/ R_1. To achieve higher multiplier factor, larger resistor ratio (R_2/R_1) is needed for topologies of Figs. 3.7(a) and 3.7(c) whereas similar results may be obtained by selecting R_2/R_1 closer to unity for topology of Fig. 3.7 (d). Further, all the topologies show an increasing trend in impedance for decreasing α (α < 1) for fixed resistor ratio.

To examine the effect of combined variation of α and R_2/ R_1, MATLAB simulations for change in impedance magnitude with respect to α and R_2/ R_1 for circuits of Figs. 3.7 (a) – (d) are plotted in Figs. 3.8 (a) – (d). The simulation results corroborate with the theoretical results. It may be noted that smaller α values have larger impact on impedance magnitude for a resistor ratio (R_2 / R_1) close to unity for Fig. 3.8(a)/ much larger than unity for Fig. 3.7(b)/ negligible for Figs. 3.7 (c) - (d).

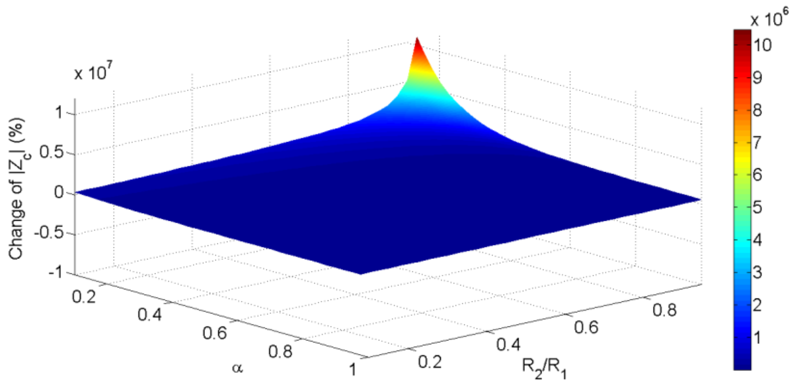

(a)

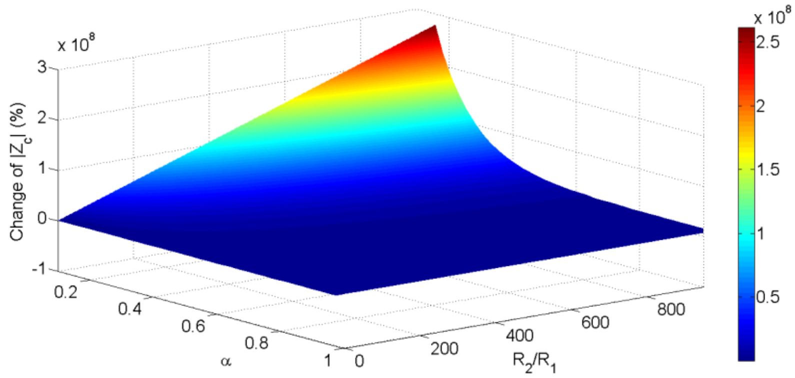

(b)

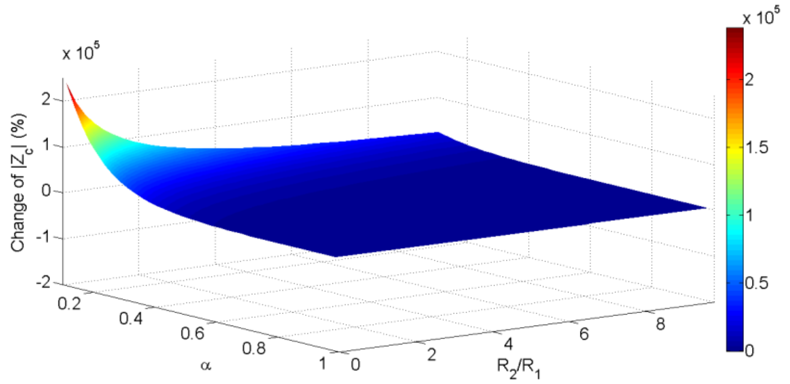

(c)

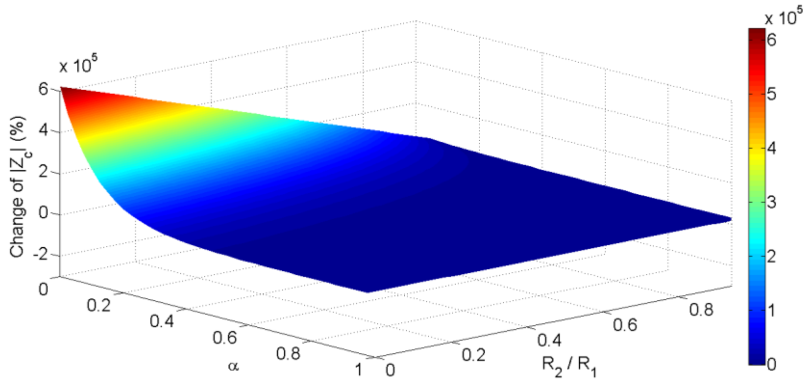

(d)

Fig. 3.8: Percent change in impedance magnitude with respect to α and R_2/ R_1

3.3.2 Non-Ideal Analysis

To analyze the behavior of proposed circuits in presence of CFOA non-idealities, the input impedance functions of topologies of Fig. 3.7 are recomputed as

$$Z_{in\alpha_1}(s)|_n = \frac{1}{Y_Y + s^{\alpha}C_{\alpha}\left[1 - \frac{\alpha_c\beta_v}{(R_1 + R_X)(G_2 + Y_Z)}\right]} \tag{3.18}$$

$$Z_{in\alpha_2}(s)|_n = \frac{1}{Y_Y + s^{\alpha}C_{\alpha}\left[1 - \frac{\alpha_c\beta_v\gamma_v}{(R_1 + R_X)(G_2 + Y_Z) + \alpha_c\gamma_v}\right]} \tag{3.19}$$

$$Z_{in\alpha_3}(s)|_n = \frac{1}{Y_{Y1} + s^{\alpha}C_{\alpha}\left[1 + \frac{\alpha_{c1}\alpha_{c2}\beta_{v1}}{(R_1 + R_{X1})(1 + R_{X2}Y_{Z1})(G_2 + Y_{Z2})}\right]} \tag{3.20}$$

$$Z_{in\alpha_4}(s)|_n = \frac{1}{Y_{Y1} + s^{\alpha}C_{\alpha}\left[1 + \frac{\alpha_{c1}\alpha_{c2}\beta_{v1}\gamma_{v2}}{(R_1 + R_{X1})(1 + R_{X2}Y_{Z1})(G_2 + Y_{Z2}) - \alpha_{c1}\alpha_{c2}\gamma_{v2}}\right]} \tag{3.21}$$

where subscript n corresponds to nonideal; and subscripts 1 and 2 with current transfer gain (α_c), voltage transfer gains (β_v, γ_v); and parasitics, Y_Y, R_X, Y_Z correspond to CFOA1 and CFOA2.

It may be noted from Figs. 3.7 (a-d) that Y-terminal of CFOA/ CFOAs is either connected to input or to ground, therefore the performance remains unaltered due to parasitic associated with this terminal. The parasitic at X terminal of CFOA may be accommodated by adjusting the value of external resistor connected to it. The overall impact of CFOA parasitics on FC multiplier behavior may be ignored by considering the frequency of operation much below than parasitic pole ($1/(R_Z C_Z)$) associated with Z terminal. In view of above facts, the multiplier factors (K_i, i =1, 2, 3, 4) for topologies of Figs. 3.7(a)-(d) modify to

$$K_1|_n = 1 - \alpha_c \beta_v \frac{R_2}{R_1} \tag{3.22}$$

$$K_2|_n = \frac{1 + (\alpha_c \gamma_v - \alpha_c \beta_v \gamma_v) R_2/R_1}{1 + \alpha_c \gamma_v R_2/R_1} \tag{3.23}$$

$$K_3|_n = 1 + \alpha_{c1} \alpha_{c2} \beta_{v1} \frac{R_2}{R_1} \tag{3.24}$$

$$K_4|_n = \frac{1 - (\alpha_{c1} \alpha_{c2} \gamma_{v2} - \alpha_{c1} \alpha_{c2} \beta_{v1} \gamma_{v2}) R_2/R_1}{1 - \alpha_{c1} \alpha_{c2} \gamma_{v2} R_2/R_1} \tag{3.25}$$

respectively.

3.3.3 Simulation Results

The functionality of the realized multipliers is verified using SPICE simulations using CFOA model [155]. The FC is implemented using infinite order domino RC ladder network truncated to 12 numbers of blocks [25] as shown in Fig. 3.9. The component values of FC model having α=0.5 and C_α=3.75μF are R_0 = 330kΩ, R_1 = 82kΩ, R_2 = 33kΩ, R_3=12kΩ, R_4 = 4.7kΩ, R_5 = 2kΩ, R_6 = 736Ω, R_7 = 270 Ω, R_8 = 120Ω, R_9 = 47Ω, R_{10} = 8.2 Ω, R_{11} = 18.2 Ω, C_0 = 4.7 μF, C_1 = 3.1 μF,

$C_2 = 1\ \mu F$, $C_3 = 470nF$, $C_4 = 168nF$, $C_5 = 68nF$, $C_6 = 27nF$, $C_7 = 10nF$, $C_8 = 4.7nF$, $C_9 = 1nF$, $C_{10} = 2.2nF$.

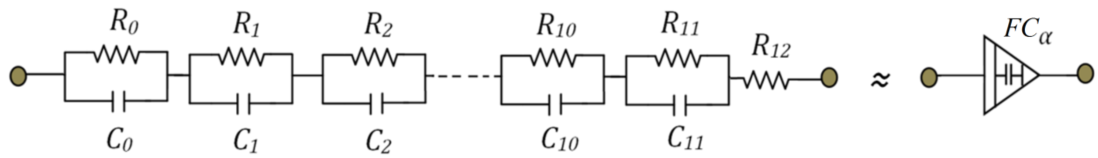

Fig. 3.9: Truncated RC domino ladder network realizing FC [25]

Simulations are performed for different scaling factors for topologies of Fig. 3.7 for examining impedance magnitude and phase response and corresponding results are placed as Fig. 3.10. Table 3.3 enlists simulation setting for capacitance scaling factors and component settings used therein; and performance of circuits. In the view of non-ideal effects of CFOA on the realized circuits, it may be observed that Fig. 3.7 (b) and (c) have more linearity than Fig. 3.7 (a) and (d). In Fig. 3.7 (a), (d); it increases the range of operation for lesser value of R_2 / R_1.

Table 3.3: The components values and performance of FC multipliers

Components Setting and Performance Evaluation	**Fig. 3.7 (a)**			**Fig. 3.7 (b)**			**Fig. 3.7 (c)**			**Fig. 3.7 (d)**		
Multiplication Factor	0.02	0.1	0.5	0.02	0.1	0.5	2	10	50	2	10	50
R_1 (kΩ)	1	1	1	1	1	1	1	1	1	1	1	1
R_2 (kΩ)	0.98	0.9	0.5	49	9	1	1	9	49	0.5	0.9	0.98
$(C_\alpha)_{eff}$ F(℧/s^α)	75n	0.375μ	1.875μ	75n	0.375μ	1.875μ	7.5μ	37.5μ	187.5μ	7.5μ	37.5μ	187.5μ
Frequency range of magnitude response (Hz) (within 1.5dB deviation)	0.05-50.1k	0.04-330k	0.042-588k	0.046-392k	0.042-1Meg	0.042-935k	0.04-625k	0.04-676k	0.04-741k	0.042-970k	0.052-218k	1.4-14.8k
Frequency range of phase response (Hz) (within 2.5° deviation)	13.3-6k	0.44-53k	0.43-426k	0.57-44k	0.45-107k	0.42-525k	0.4-202k	0.4-154k	0.4-120k	0.44-28k	4.6-14.5k	19.5-3k

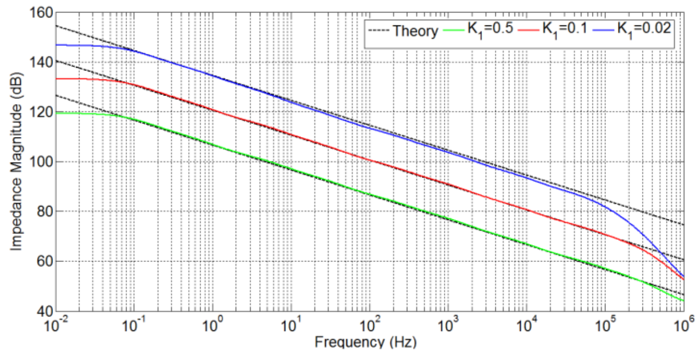
Theory
K_1=0.5
K_1=0.1
K_1=0.02
Impedance Magnitude (dB)
Frequency (Hz)

(a)

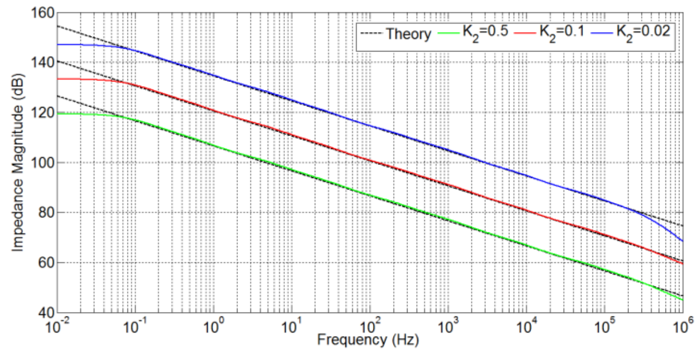
Theory
K_2=0.5
K_2=0.1
K_2=0.02
Impedance Magnitude (dB)
Frequency (Hz)

(b)

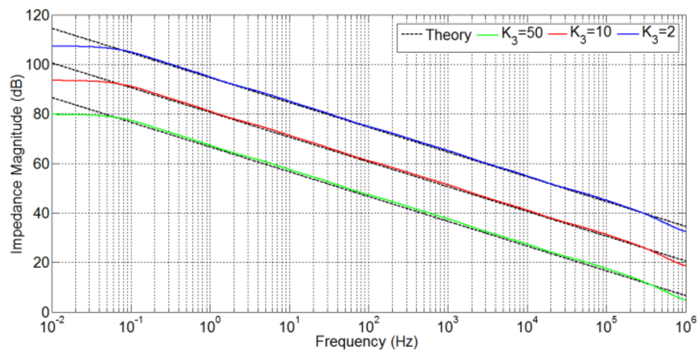
Theory
K_3=50
K_3=10
K_3=2
Impedance Magnitude (dB)
Frequency (Hz)

(c)

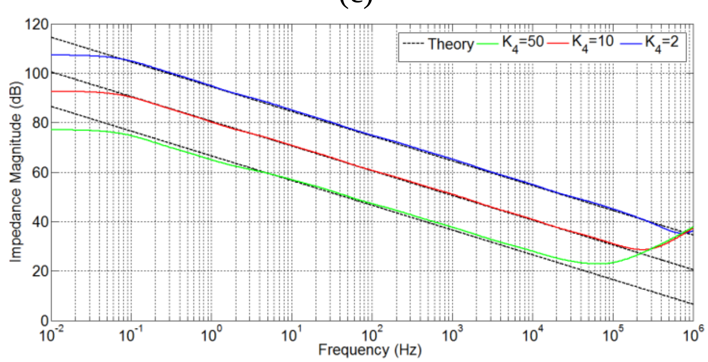
Theory
K_4=50
K_4=10
K_4=2
Impedance Magnitude (dB)
Frequency (Hz)

(d)

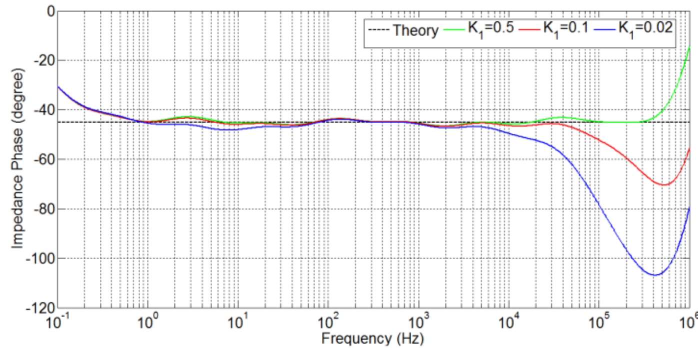

(e)

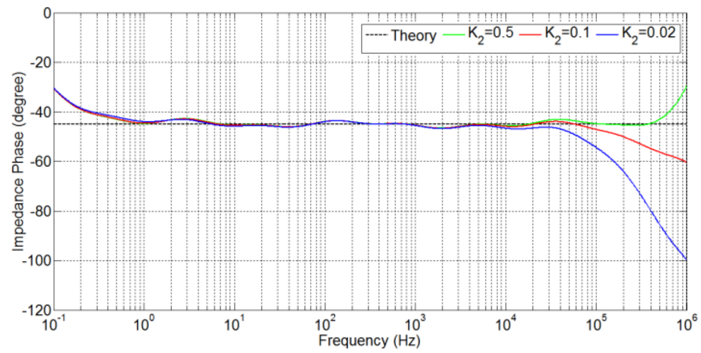

(f)

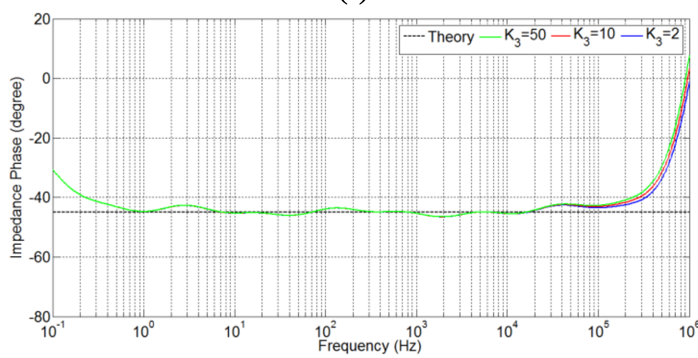

(g)

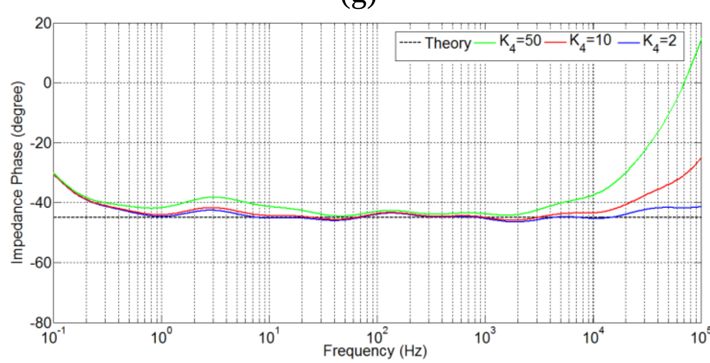

(h)

Fig. 3.10: Simulated impedance magnitude **(a) - (d)** and phase **(e) – (h)** responses for circuits of Figs. 3.7 (a) - (d)

3.3.4 Application

To illustrate the use of proposed multiplier, CFOA based lossy/ lossless integrator circuit is constructed as shown in Fig. 3.11. The notation $(FC_\alpha)_{eff}$ indicates the effective capacitance value of FC (that is $C_{\alpha eff} = K_i.C_\alpha$). The transfer functions of lossy and lossless fractional integrators can be expressed as follows

$$T(s)^{\alpha}_{lossy} = \frac{V_O(s)}{V_{in}(s)} = -\frac{R_2}{R_1}.\frac{1}{1 + s^{\alpha} R_2 C_{\alpha eff}}$$

$$T(s)^{\alpha}_{lossless} = \frac{V_O(s)}{V_{in}(s)} = -\frac{1}{s^{\alpha} R_1 C_{\alpha eff}} \tag{3.26}$$

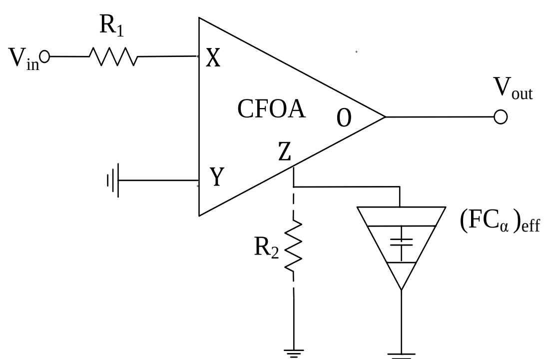

Fig. 3.11: CFOA based fractional lossy/ lossless integrator

The simulated magnitude and phase responses of fractional order lossy/ lossless integrators using 0.5 order FC multiplier with multiplier factors of (2, 10, 50) are depicted in Figs. 3.12(a) - (b) and 3.12(c) - (d) respectively. It may be observed that the simulated magnitude responses for lossy and lossless integrators follow theoretical values with deviations of (0.45 dB, 0.7 dB, 1.5 dB) and (0.6 dB, 0.8 dB, 1.5 dB) up to frequencies (380 kHz, 457 kHz, 1.7 MHz) and (410 kHz, 483 kHz, 1.7 MHz) respectively. Further, phase deviations are well within 2.5° for frequencies up to (370 kHz, 280 kHz, 215 kHz) for lossy integrator and that for lossless integrator in the frequency range of (5.6 Hz-343 kHz, 3.3 Hz-278 kHz, 0.43 Hz-214 kHz).

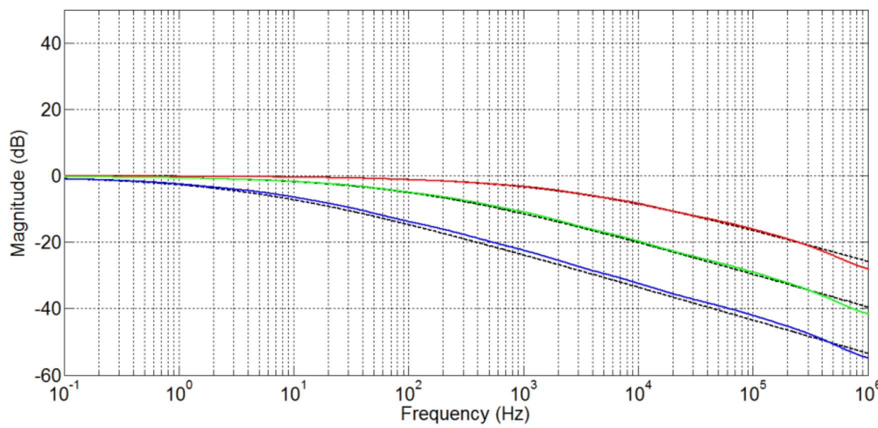

(a)

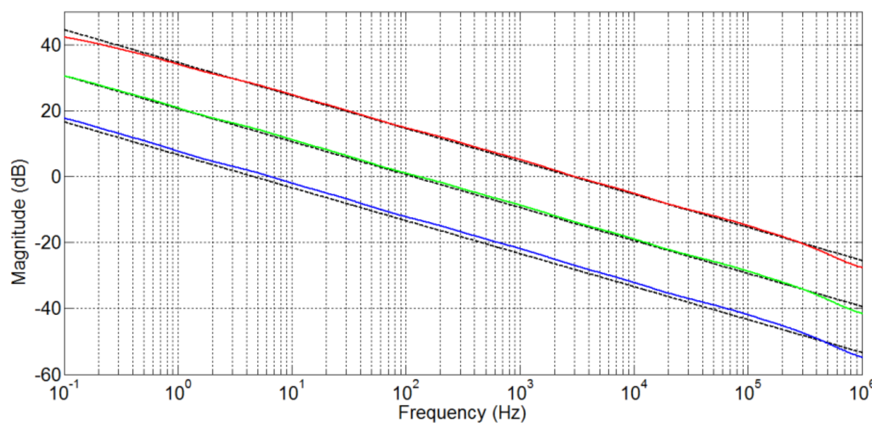

(b)

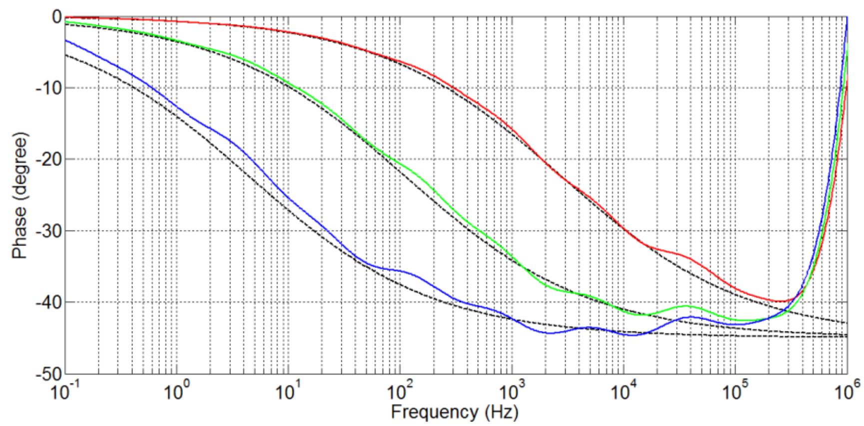

(c)

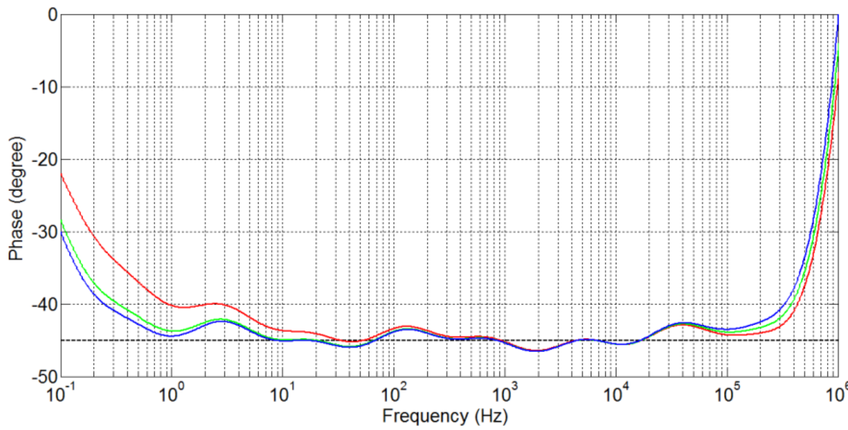

(d)

Fig. 3.12: Magnitude **(a, b)** and phase **(c, d)** responses of fractional lossy and lossless integrator

3.4 Conclusion

In this chapter, a CFOA based capacitance multiplier is presented. It requires lower component spread in order to achieve larger multiplication factor. The effect of non-idealities of CFOA on proposed multipliers is investigated and a compensation scheme is suggested. The operation of proposed circuit is verified through both SPICE simulations and experimentation. The usefulness of the multiplier is illustrated through PRB.

Alongside, four fractional capacitance multiplier topologies are also put forward. These topologies are obtained through generalization of CFOA based capacitance multipliers. The effect of non-idealities of CFOA on proposed multipliers is investigated. Functionality of these multipliers is tested through MATLAB and SPICE simulations for various multiplier factors. The application of proposed multiplier is illustrated through fractional order lossy/ lossless integrators.

CHAPTER 4

REALIZATION OF A HIGHER ORDER FOE AND ITS APPLICATION

The contents and results of the following paper have been reported in this chapter:

[1] **R. Verma,** N. Pandey, R. Pandey, "Realization of a Higher Fractional Order Element based on Novel OTA based IIMC and Its Application in Filter. Analog Integrated Circuits and Signal Processing, vol. 97, no. 1, pp. 177–191, 2018. https://doi.org/10.1007/s10470-018-1315-1. (Springer) **Indexing: SCI, SCIE, SCOPUS; IF: 0.8**

4.1 Introduction

It is well known that behavior of dynamic systems can be modeled more accurately using fractional order system (FOS) [1-3] than their integer order counterparts. The system accuracy increases with increasing the order of the FOS. The fractional order circuits are an example of FOS which can be designed using FOE with lower fractional order ($0 < \alpha < 1$) or higher order FOEs ($\alpha > 1$; where α is a compound value).

The realization method of FOE with order α ($0 < \alpha < 1$) has already been discussed in Chapter 2. This chapter is devoted to realization of FOE with order ($\alpha >1$) which has also been referred as order alteration in literature.

In open literature, two techniques are available for order alteration namely (i) generalized impedance converter (GIC) [15, 19, 25, 32, 33, 39, 40, 44, 156] and (ii) fractional stepping [54, 56, 61, 62, 69, 99, 157, 158]. The former approach is detailed in [25] in general form where the type/ order of FOE is varied by selecting appropriate passive components and it can provide FO variation in range $0 < \alpha \leq 2$. The structures reported in [15, 19, 32, 33, 39, 40, 44, 156] may be viewed as specific cases of design procedure of [25]. The later approach is based on developing functional block diagram (FBD) of FOE's transfer function for given fractional order using follow the leader feedback (FLF)/ inverse follow the leader feedback (IFLF) topology.

This chapter presents OTA based inverted impedance multiplier circuit (IIMC) and its generalization in fractional domain for deigning higher order FOE. This is followed by the design of a higher order FOF realized through IIMC based higher order FOE.

4.2 OTA Based Impedance Inverter Multiplier

This section begins with generalization of OTA based impedance inverter circuit (IIC) in fractional domain. The OTA based IIMC, which is designed using IIC and its generalization in fractional domain, is presented next. This fractional order IIMC is used for order alteration of FC and FI.

4.2.1 Generalization of OTA Based Impedance Inverter

An impedance inverter circuit (IIC) gives input impedance which is inversely proportional to the impedance connected at its other end. It is primarily used for simulating inductors for IC applications via inverting capacitive reactance and impedance matching circuit. The schematic of OTA based IIC [159] is shown in Fig. 4.1(a). The input impedance of the circuit is given as

$$Z_{in} = \frac{1}{g_{m1} g_{m2} Z_1} \tag{4.1}$$

where g_{m1} and g_{m2} correspond to transconductances of OTA1 and OTA2 respectively.

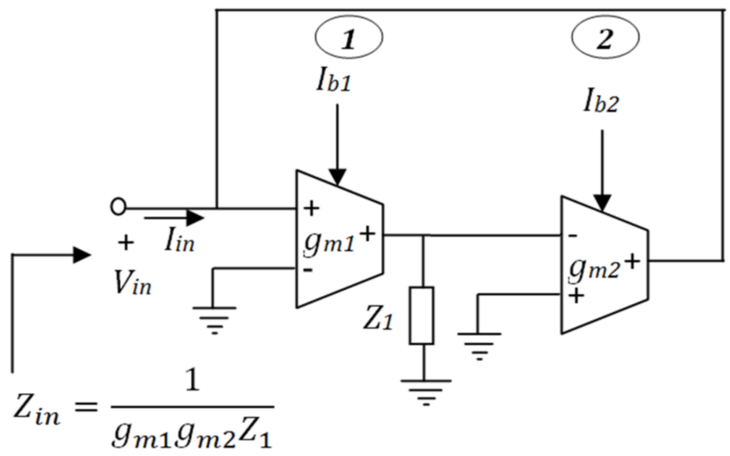

(a)

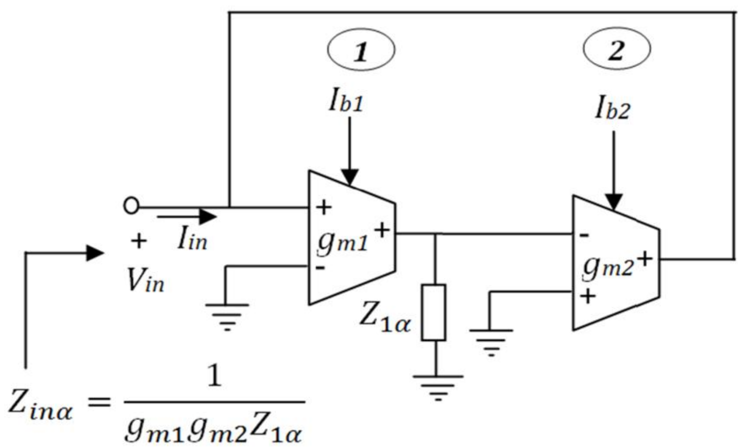

(b)

Fig. 4.1: OTA based **(a)** impedance inverter circuit [159] **(b)** generalization in fractional domain

The circuit of Fig. 4.1 (a) can be generalized to fractional domain by replacing Z_1 by $Z_{1\alpha}$ where $Z_{1\alpha}$ represents FO impedance of order α. Fig. 4.1(b) shows the resulting circuit and its input impedance is expressed as

$$Z_{in\alpha} = \frac{1}{g_{m1}g_{m2}Z_{1\alpha}} \tag{4.2}$$

An FI of order α may be obtained from (4.2) if $Z_{1\alpha}$ corresponds to an FC of order α. The impedance of the resulting FI can be expressed as

$$Z_{in\alpha} = \frac{s^{\alpha}C_{\alpha}}{g_{m1}g_{m2}} \tag{4.3}$$

4.2.2 Proposed Impedance Inverter Multiplier

The OTA based IIMC is shown in Fig.4.2. It uses (n+1) OTAs and n impedances. The input impedance of IIMC is given by

$$Z_{in-IIMC} = \frac{1}{g_{m0}(g_{m1}g_{m2}\ \ldots .\ g_{mn})(Z_1Z_2\ \ldots .\ Z_n)} \tag{4.4}$$

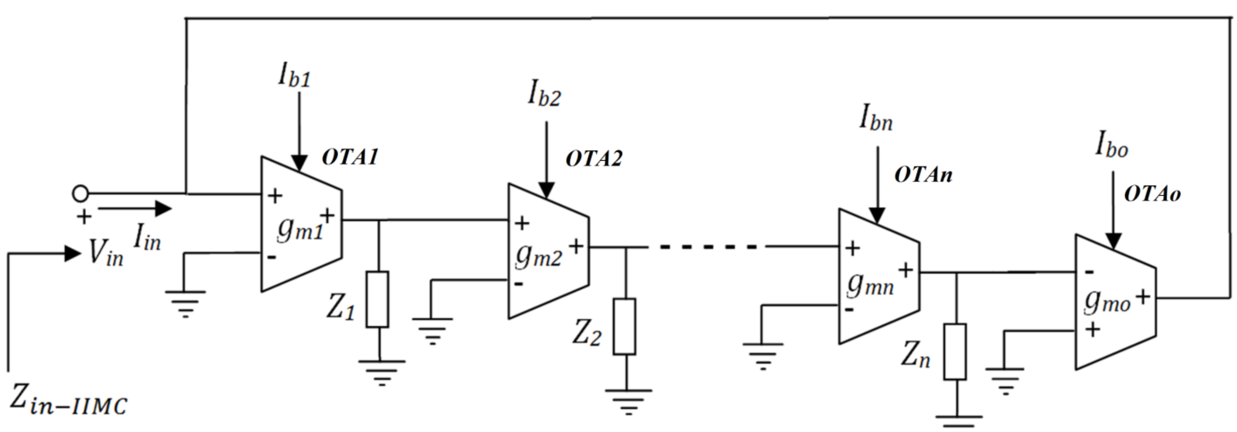

Fig. 4.2: Proposed OTA based IIMC

For $Z_i = 1/sC_i$ (i=1, 2, … ,n), the input impedance of (4.4) becomes

$$Z_{in-IIMC} = \frac{s^n C_1 C_2 \ldots . C_n}{g_{m0}(g_{m1} g_{m2} \ldots . g_{mn})} \tag{4.5}$$

The IIMC can be generalized in fractional domain by replacing Z_1 by FC of order α while other capacitances remain the same and the input impedance of (4.5) modifies to

$$Z_{in-IIMC_{(n-1+\alpha)}} = \frac{s^{n-1+\alpha} C_{1\alpha} C_2 \ldots . C_n}{g_{m0}(g_{m1} g_{m2} \ldots . g_{mn})} \tag{4.6}$$

Equation (4.6) represents input impedance of an FI of order (n-1+α) and its pictorial representation is given in Fig. 4.3. To realize fractional capacitor of same order the circuit of Fig. 4.1(b) is used where $Z_{1\alpha}$ will be replaced by an inductor having impedance as represented by (4.6).

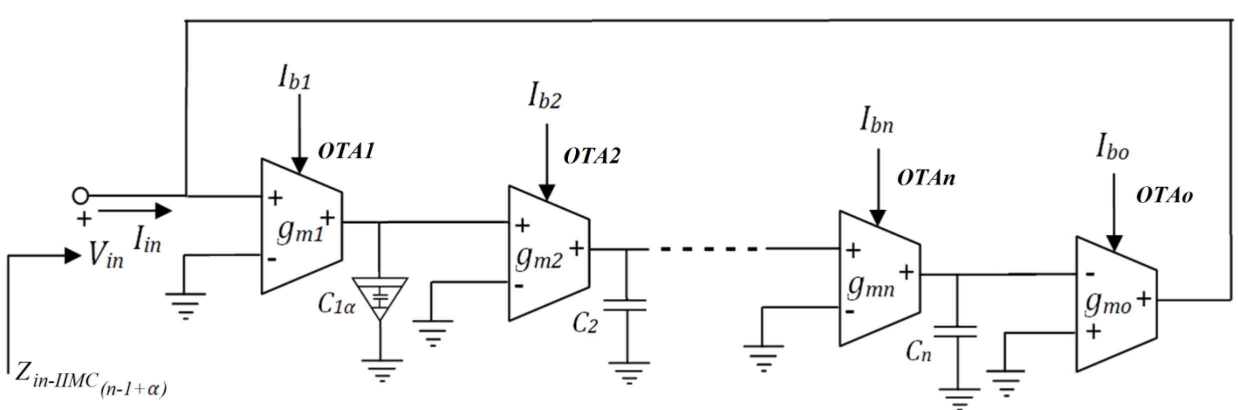

Fig. 4.3: Generalization of IIMC in fractional domain

4.2.3 Performance Evaluation

In this section FI and FC of order (1+α) are designed for validation of the proposed scheme. The FI and FC of order (1+α) are shown in Fig. 4.4 (a) and (b) respectively. The corresponding equivalent values of FI and FC are given as

$$L_{1+\alpha} = \frac{C_{1\alpha}C_2}{g_{m0}g_{m1}g_{m2}} \tag{4.7}$$

$$C_{1+\alpha} = \frac{g_{m3}g_{m4}C_{1\alpha}C_2}{g_{m0}g_{m1}g_{m2}} \tag{4.8}$$

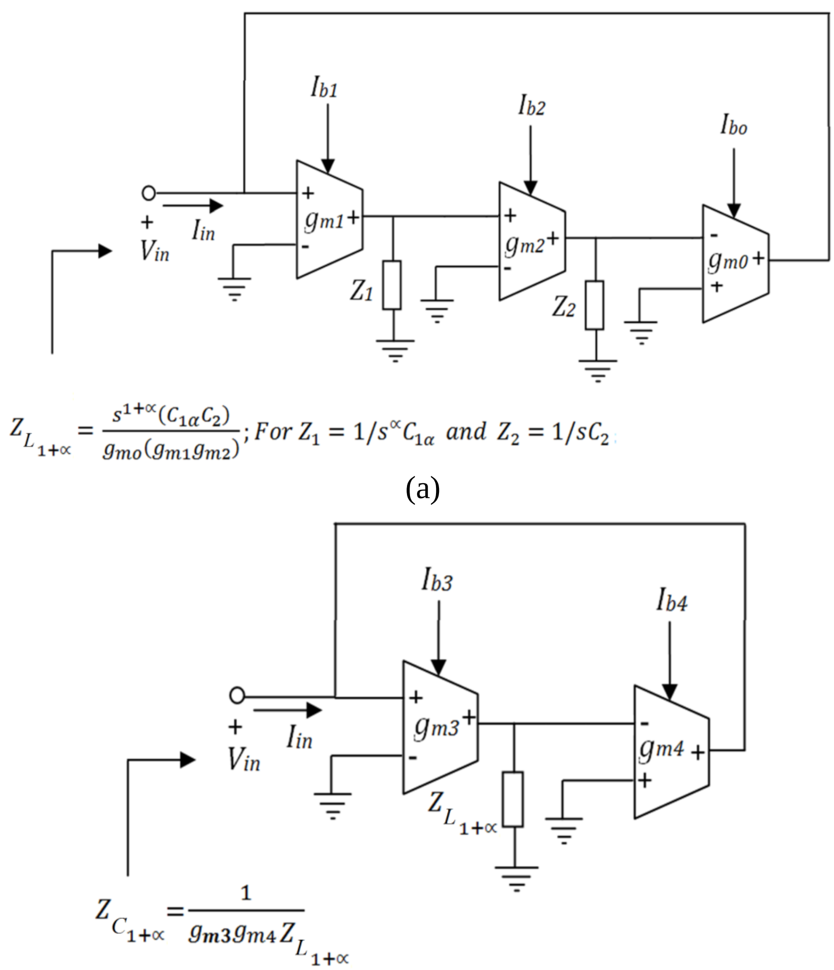

(a)

(b)

Fig. 4.4: Proposed IIMC based **(a)** FI **(b)** FC of order (1+α)

4.2.3.1 Simulation Results

The functionality of (1+α) order FI and FC is verified through simulation results in this section. The CMOS OTA of Fig. 2.7 with supply voltages ±1.8 V and 0.18 µm TSMC process parameters is used for simulation. The transconductance gain of OTA (g_m) is set as 100 µA/V.

Two instances of FI (order (1+α) = 1.2 and 1.5) are simulated by selecting $Z_{1\alpha}$ to be impedances of two different FCs of value C_α = 25 µ℧/s^α, order 0.2 and C_α=3.75 µ℧/s^α, order 0.5 respectively in Fig. 4.4(a). The integer order capacitances of 50 nF and 10 nF are used respectively for the two instances. The FC is emulated using infinite order domino RC ladder network truncated to 12 numbers of blocks [25] as shown in Fig. 3.9 which is reproduced as Fig. 4.5 for ready reference.

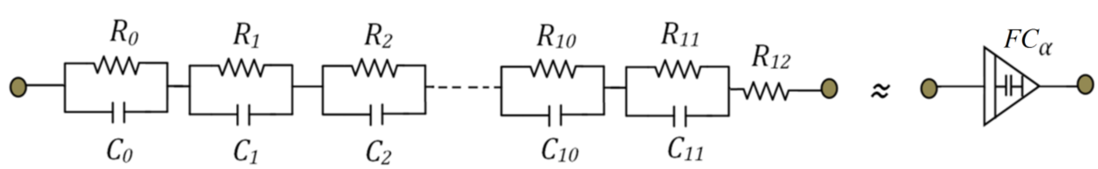

Fig. 4.5: Truncated RC domino ladder network realizing FC [25]

The values for Fig. 4.5 FC having (i) α=0.2 and C_α=25µF are R_0 = 16kΩ, R_1 = 9.1kΩ, R_2 = 6.6kΩ, R_3=4.7kΩ, R_4 = 3.3kΩ, R_5 = 2.4kΩ, R_6 = 1.8Ω, R_7 = 1.5 Ω, R_8 = 1kΩ, R_9 = 680Ω, R_{10} = 470 Ω, R_{11} = 180 Ω, R_{12}=1.1kΩ, C_0 = 51.7 µF, C_1 = 20 µF, C_2 = 4.7 µF, C_3 = 1.33 µF, C_4 = 330nF, C_5 = 100nF, C_6 = 27nF, C_7 = 8.2nF, C_8 = 2.2nF, C_9 = 560pF, C_{10} = 150pF, C_{11}=82pF (ii) α=0.5 and C_α=3.75µF are R_0 = 330kΩ, R_1 = 82kΩ, R_2 = 33kΩ, R_3=12kΩ, R_4 = 4.7kΩ, R_5 = 2kΩ, R_6 =

736Ω, $R_7 = 270$ Ω, $R_8 = 120$Ω, $R_9 = 47$Ω, $R_{10} = 8.2$ Ω, $R_{11} = 18.2$ Ω, $C_0 = 4.7$ μF, $C_1 = 3.1$ μF, $C_2 = 1$ μF, $C_3 = 470$nF, $C_4 = 168$nF, $C_5 = 68$nF, $C_6 = 27$nF, $C_7 = 10$nF, $C_8 = 4.7$nF, $C_9 = 1$nF, $C_{10} = 2.2$nF. The resulting impedance of 1.2 and 1.5 orders FIs are represented as $Z_{L1.2} = 1.25\ \Omega/s^{1.2}$, $Z_{L1.5} = 37.5\ m\Omega/s^{1.5}$ respectively.

For simulation of higher order FCs ((1+α) = 1.2 and 1.5), the $Z_{L(1+\alpha)}$ in Fig. 4.4 (b) is replaced by $Z_{L(1.2)}$ and $Z_{L(1.5)}$ respectively. The integer order capacitors are chosen to be 10 nF and 1 nF respectively. The impedance of 1.2 and 1.5 orders FCs are computed to be $Z_{C1.2} = 2.5\ n\Omega/s^{1.2}$ and $Z_{C1.5} = 0.0375\ m\Omega/s^{1.5}$.

The theoretical and simulated frequency responses for impedance of 1.2 and 1.5 orders FIs ($L_{1.2} = 1.25\ \Omega/s^{1.2}$, $L_{1.5} = 37.5\ m\Omega/s^{1.5}$) and FCs ($C_{1.2} = 2.5$ n℧/$s^{1.2}$, $C_{1.5} = 0.0375$ n℧/$s^{1.5}$ are shown in Figs. 4.6 and 4.7 respectively. The frequency range of operation for different FIs and FCs are summarized in Table 4.1 with ±5dB and $\pm 5^0$ maximum possible deviation for impedance magnitude and phase responses respectively.

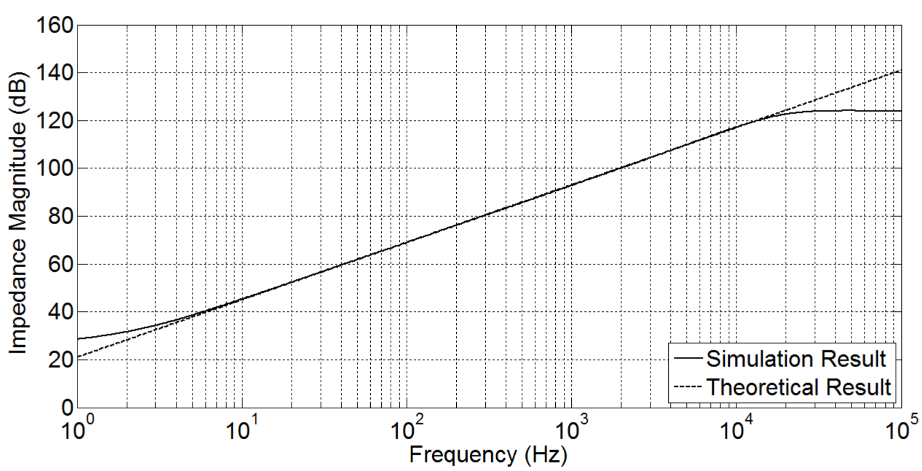

(a)

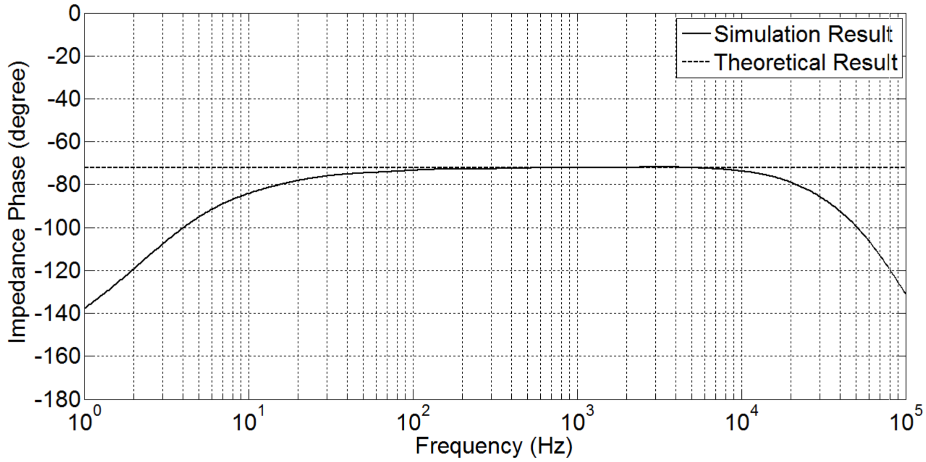

(b)

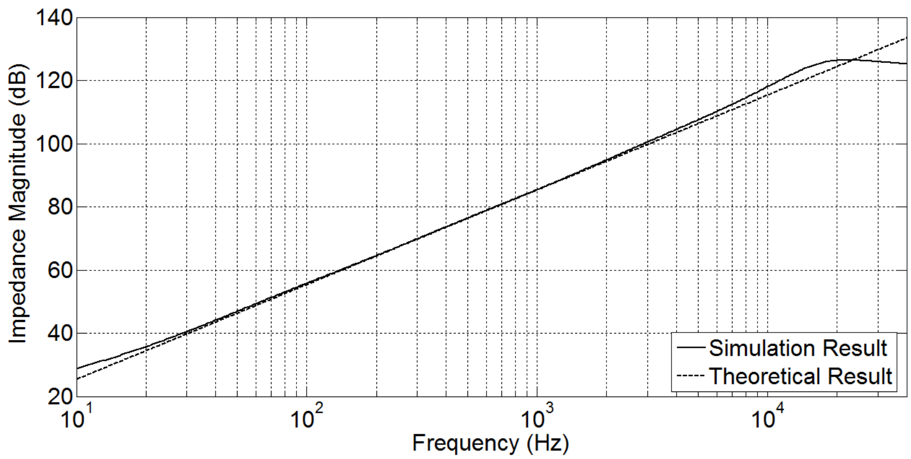

(c)

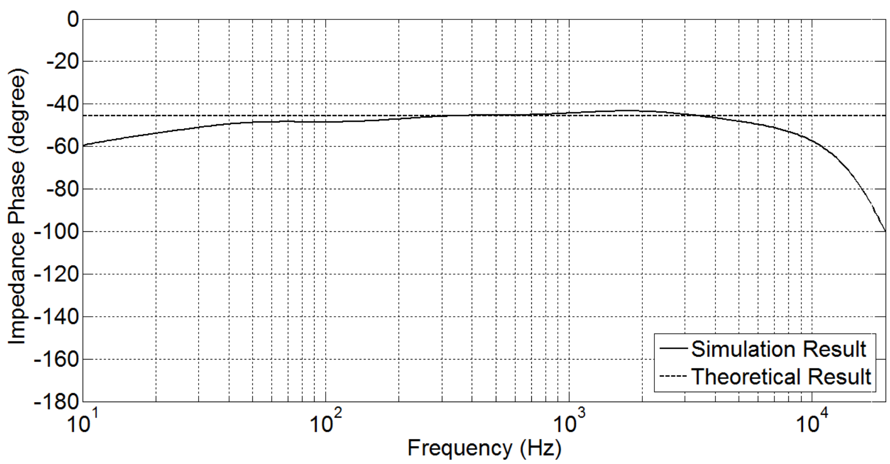

(d)

Fig. 4.6: Impedance responses of **(a),(b)** 1.2 order; and **(c),(d)** 1.5 order FIs

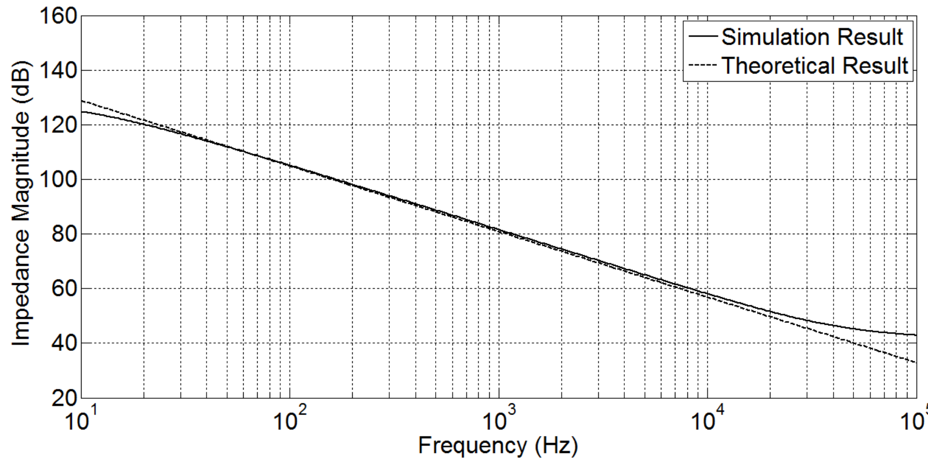
160
140
120
100
80
60
40
20
Impedance Magnitude (dB)
10^1
10^2
10^3
10^4
10^5
Frequency (Hz)
Simulation Result
Theoretical Result

(a)

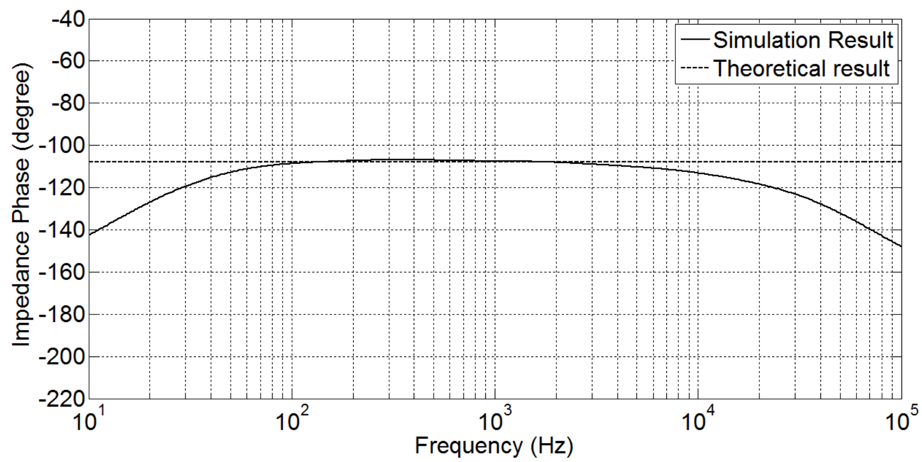
-40
-60
-80
-100
-120
-140
-160
-180
-200
-220
Impedance Phase (degree)
10^1
10^2
10^3
10^4
10^5
Frequency (Hz)
Simulation Result
Theoretical result

(b)

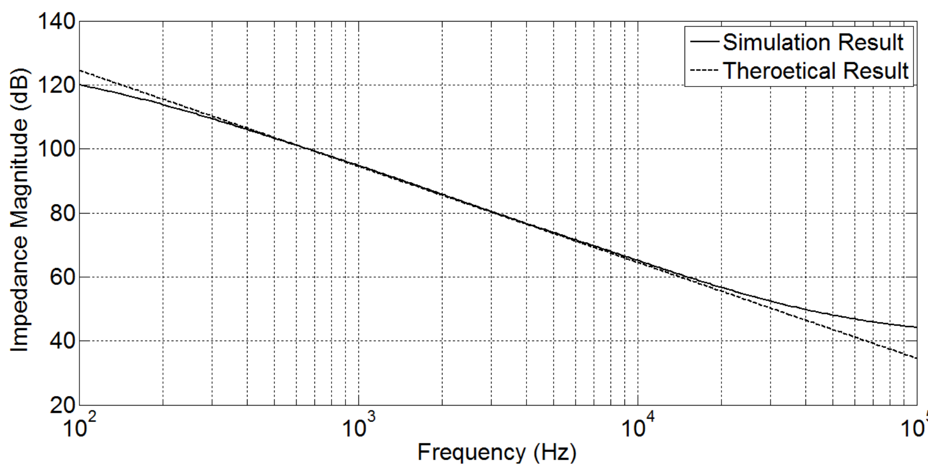
140
120
100
80
60
40
20
Impedance Magnitude (dB)
10^2
10^3
10^4
10^5
Frequency (Hz)
Simulation Result
Theroetical Result

(c)

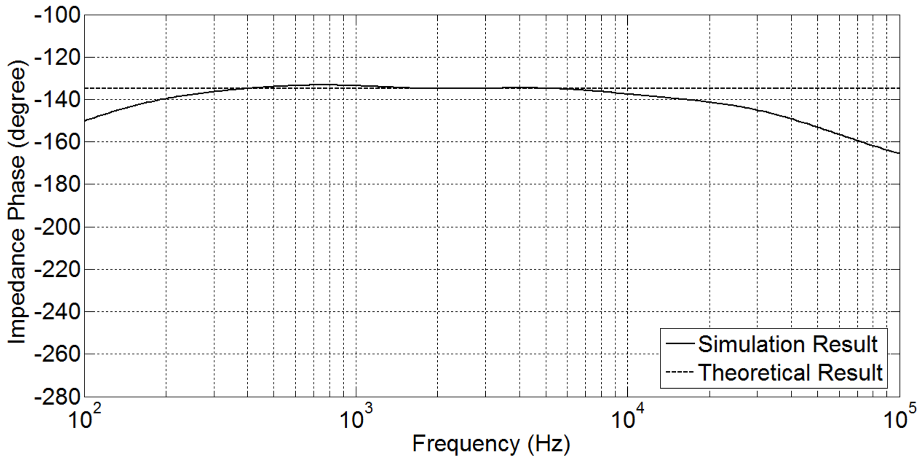

(d)

Fig. 4.7: Impedance responses **(a), (b)** 1.2 order; and **(c), (d)** 1.5 order FCs

Table 4.1: Frequency range for different FIs and FCs

Impedance Response	Frequency range of operation			
	Order of FI		Order of FC	
	1.2	1.5	1.2	1.5
Magnitude	1.48Hz-30.5kHz	7.4Hz-32.3kHz	8.7Hz-47.9kHz	92Hz-53.7kHz
Phase	33.8Hz-14.2kHz	51.2Hz-5.4kHz	48.9Hz-9.77kHz	194Hz-16kHz

4.2.3.2 Experimental Results

The experimental setup for FI of order $\alpha = 0.5$ is shown in Fig. 4.8 (a) where dual output OTAs ICs LM 13600N is used with supply voltage of ±10V. The transconductance gains of OTAs are set at $g_{m1}=g_{m2}=$ 0.393mA/V. The FC is realized using domino RC ladder circuit with component values same as taken for simulations. The response of the circuit is shown in Fig. 4.8 (b) for sinusoidal input signal (100 mV_{pp}) and its corresponding Lissajous pattern is depicted in Fig. 4.8(c).

Further experimental verification of FI of order 1+α is carried out using normal capacitor of 0.47 μF and g_{m1}=g_{m2}= 0.393mA/V, g_{m3}=0.732mA/V. The experimental setup is shown in Fig. 4.9 (a). The response of the circuit is shown in Fig. 4.9 (b) for sinusoidal input signal (100 mV_{pp}) and its corresponding Lissajous pattern is depicted in Fig. 4.9 (c). It may be noted that FI having 1+α order is 90^0 in advance than α order.

Experimental impedance phase response is shown in Fig. 4.10 along with theoretical result for 1.5 order FI. It may be noted that experimental impedance response follows theoretical curve in frequency range of 50 Hz – 4 kHz within $\pm 5^0$ phase error band.

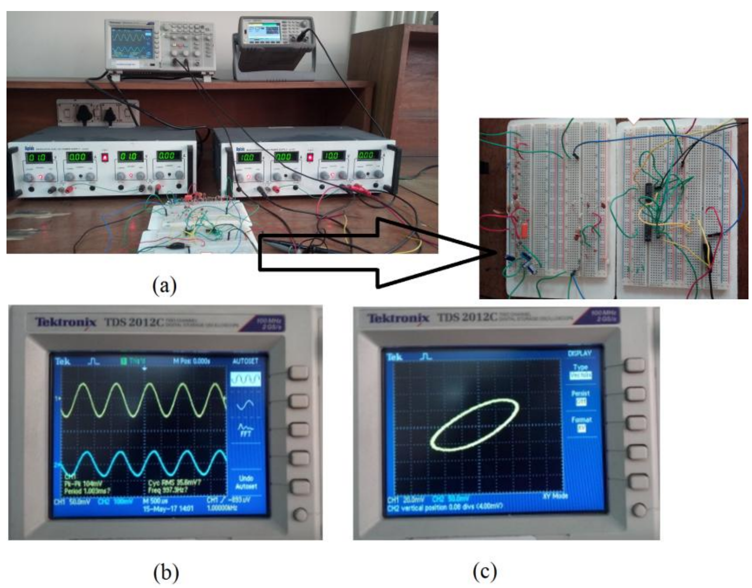

Fig. 4.8: (a) Hardware setup **(b)** experimental results **(c)** Lissajous pattern of OTA based α order FI

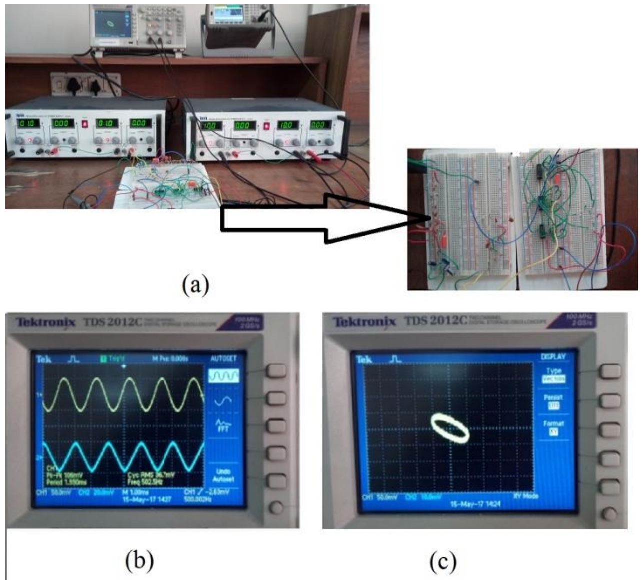

Fig. 4.9: **(a)** Hardware setup **(b)** experimental results **(c)** Lissajous pattern of OTA based FI having $1+\alpha$ order

The measurements are taken at supply voltage of ±10V. The transconductance gains of OTAs for FIs' order α and $(1+\alpha)$ are set at $g_{m1}=g_{m2}=$ 0.393mA/V; and $g_{m1}=g_{m2}=$ 0.393mA/V, g_{m3}=0.732mA/V respectively. In the designing of α and $(1+\alpha)$ order FIs, the normal capacitor of 0.47 µF is used. The responses obtained across the output capacitor of impedance inverter circuit (IIC) (Fig. 4.1 (b)) and proposed IIMC configuration realizing FI of $(1+\alpha)$ order (Fig. 4.4 (a)) for sinusoidal input signal ($100mV_{pp}$) are shown in Figs. 4.8 and 4.9 respectively. The Lissajous patterns also verify that FI having $1+\alpha$ order is 90^0 in advance than α order. Experimental impedance phase responses of FI having $1+\alpha$ ($\alpha = 0.5$) order is shown in Fig. 4.10 along with theoretical result. It may be noted that experimental impedance response of proposed FI of order 1.5 follows theoretical curve in frequency range of 50 Hz – 4 kHz within $\pm5^0$ phase error band.

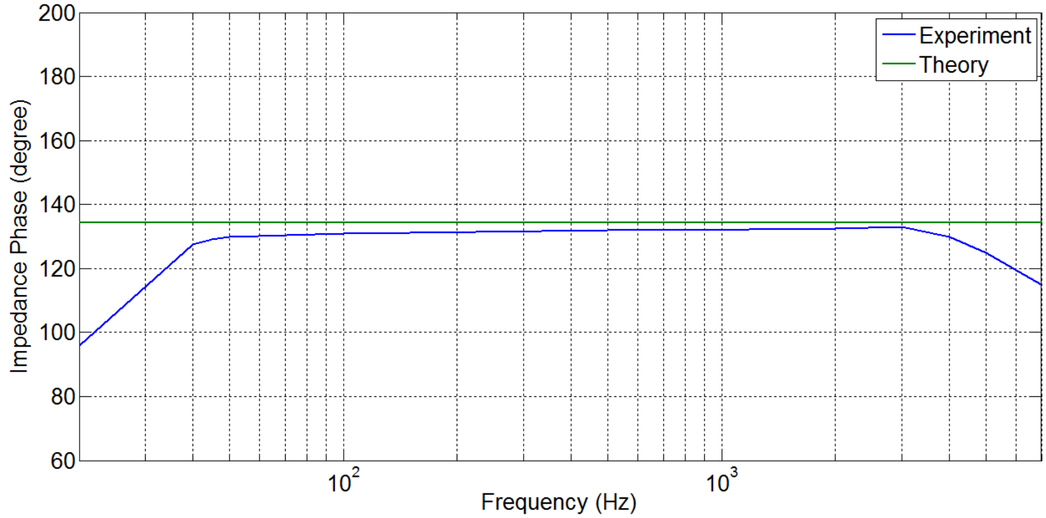

Fig. 4.10: Impedance phase response of FI of 1+α (α = 0.5) order

4.2.4 Comparison

Comparison of the presented scheme with the available ones yields in the following points:

- The FOE reported in [25] uses GIC structure and realizes fractional elements of order less than 2 only. Thus this method gives limited order alteration in higher domain. The proposed scheme realizes 1+ α order FOE. Any further integer increment may be obtained by placing OTA and integer order capacitor in the loop thus leading to a modular structure.
- In [25], the magnitude of FOE is varied by changing the value of one of the resistances employed in GIC. Therefore, electronic tuning of FOE's magnitude can be accomplished by electronic implementation of that resistance. In the proposed structure, magnitude variation is attained through bias current variation.

4.3 Proposed higher order FOF

Higher order filters are useful to achieve faster roll off rate. A higher order FOF may be designed replacing integer order fundamental elements by higher order FOEs. This section presents higher order FOF using higher order FOE proposed in section 4.2.2.

The proposed higher order current mode FOF (Fig. 4.11) is based on parallel resonator block (PRB) wherein the inductor and capacitor of conventional PRB are replaced by FI and FC of order (n + α) respectively. The OTA based realization of Fig. 4.11(a) is depicted in Fig. 4.11 (b).

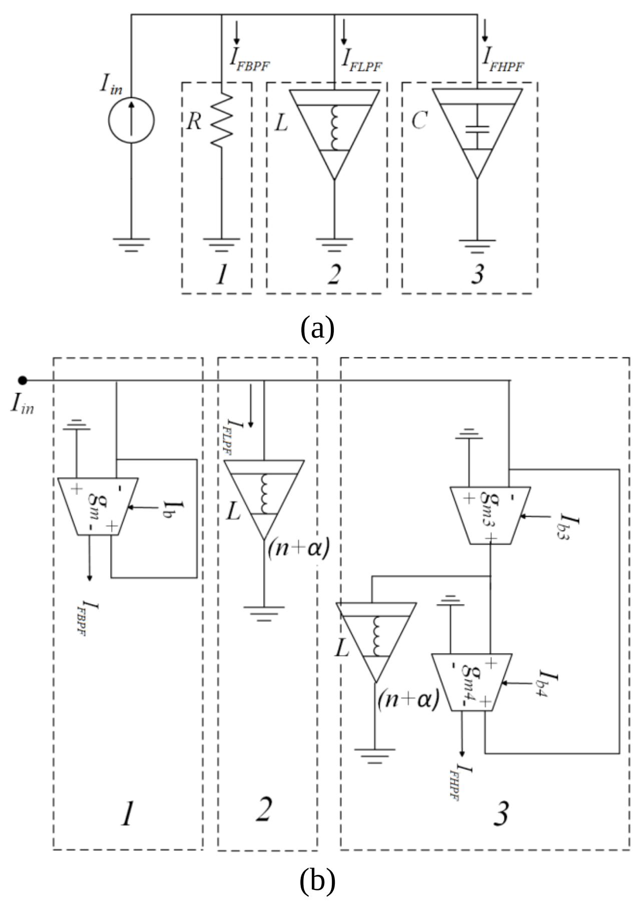

Fig. 4.11: (a) Higher order fractional parallel $RL_{(n+\alpha)}C_{(n+\alpha)}$ circuit and **(b)** its realization using OTA

The circuit analysis of Fig. 4.11 (a) yields following filter transfer functions:

i. Transfer function (TF) of FLPF

$$T(s)_{FLPF}^{2(n+\alpha)} = \frac{I_{FLPF}(s)}{I_{in}(s)} = \frac{\frac{1}{L_{\mathrm{n+\alpha}}C_{\mathrm{n+\alpha}}}}{s^{2(n+\alpha)} + \frac{s^{(n+\alpha)}}{RC_{\mathrm{n+\alpha}}} + \frac{1}{L_{\mathrm{n+\alpha}}C_{\mathrm{n+\alpha}}}} \tag{4.9}$$

ii. TF of FBPF

$$T(s)_{FBPF}^{2(n+\alpha)} = \frac{I_{FBPF}(s)}{I_{in}(s)} = \frac{\frac{s^{(n+\alpha)}}{RC_{\mathrm{n+\alpha}}}}{s^{2(n+\alpha)} + \frac{s^{(n+\alpha)}}{RC_{\mathrm{n+\alpha}}} + \frac{1}{L_{\mathrm{n+\alpha}}C_{\mathrm{n+\alpha}}}} \tag{4.10}$$

iii. TF of FO high pass filter (FHPF)

$$T(s)_{FHPF}^{2(n+\alpha)} = \frac{I_{FHPF}(s)}{I_{in}(s)} = \frac{s^{2(n+\alpha)}}{s^{2(n+\alpha)} + \frac{s^{(n+\alpha)}}{RC_{\mathrm{n+\alpha}}} + \frac{1}{L_{\mathrm{n+\alpha}}C_{\mathrm{n+\alpha}}}} \tag{4.11}$$

It may be observed from (4.9) to (4.11) that a 2(n+α) order FOF is obtained by using (n+α) order FC and FI in PRB. The corresponding responses for proposed OTA based higher order FOF are computed as:

i. TF of FLPF

$$T(s)_{FLPF}^{2(n+\alpha)} = \frac{I_{FLPF}(s)}{I_{in}(s)} = \frac{\frac{1}{L_{\mathrm{n+\alpha}}C_{\mathrm{n+\alpha}}}}{s^{2(n+\alpha)} + s^{(n+\alpha)}\frac{g_m}{C_{\mathrm{n+\alpha}}} + \frac{1}{L_{\mathrm{n+\alpha}}C_{\mathrm{n+\alpha}}}} \tag{4.12}$$

ii. TF of FBPF

$$T(s)_{FBPF}^{2(n+\alpha)} = \frac{I_{FBPF}(s)}{I_{in}(s)} = \frac{s^{(n+\alpha)}\frac{g_m}{C_{\mathrm{n+\alpha}}}}{s^{2(n+\alpha)} + s^{(n+\alpha)}\frac{g_m}{C_{\mathrm{n+\alpha}}} + \frac{1}{L_{\mathrm{n+\alpha}}C_{\mathrm{n+\alpha}}}} \tag{4.13}$$

iii. TF of FHPF

$$T(s)_{FHPF}^{2(n+\alpha)} = \frac{I_{FHPF}(s)}{I_{in}(s)} = \frac{s^{2(n+\alpha)}}{s^{2(n+\alpha)} + s^{(n+\alpha)}\frac{g_m}{C_{\mathrm{n+\alpha}}} + \frac{1}{L_{\mathrm{n+\alpha}}C_{\mathrm{n+\alpha}}}} \tag{4.14}$$

The magnitude and phase responses for proposed higher order FOF are computed as:

$$\left|T(j\omega)_{FLPF}^{2(n+\alpha)}\right| = \frac{\frac{1}{L_{\mathrm{n+\alpha}}C_{\mathrm{n+\alpha}}}}{|D(j\omega)|}$$

$$and \quad \angle T(j\omega)_{FLPF}^{2(n+\alpha)} = -\tan^{-1}\theta \tag{4.15}$$

$$\left|T(j\omega)_{FBPF}^{2(n+\alpha)}\right| = \frac{\frac{g_m}{C_{\mathrm{n+\alpha}}}\omega^{(n+\alpha)}}{|D(j\omega)|}$$

$$and \quad \angle T(j\omega)_{FBPF}^{2(n+\alpha)} = \tan^{-1}((n+\alpha)\pi/2) - \tan^{-1}\theta \tag{4.16}$$

$$\left|T(j\omega)_{FHPF}^{2(n+\alpha)}\right| = \frac{\omega^{2(n+\alpha)}}{|D(j\omega)|}$$

$$and \quad \angle T(j\omega)_{FHPF}^{2(n+\alpha)} = \tan^{-1}\big((n+\alpha)\pi\big) - \tan^{-1}\theta \tag{4.17}$$

where

$|D(j\omega)|$

$$= \left[\begin{array}{c}\omega^{4(n+\alpha)} + 2\frac{g_m}{C_{\mathrm{n+\alpha}}}\omega^{3(n+\alpha)}\cos\frac{(n+\alpha)\pi}{2} + \left\{\frac{g_m^2}{{C_{\mathrm{n+\alpha}}}^2} + \frac{2}{L_{\mathrm{n+\alpha}}C_{\mathrm{n+\alpha}}}\cos(n+\alpha)\pi\right\}\omega^{2(n+\alpha)} \\ + \frac{2}{L_{\mathrm{n+\alpha}}C_{\mathrm{n+\alpha}}}\frac{g_m}{C_{\mathrm{n+\alpha}}}\omega^{(n+\alpha)}\cos\alpha\pi/2 + \left(\frac{1}{L_{\mathrm{n+\alpha}}C_{\mathrm{n+\alpha}}}\right)^2\end{array}\right]^{1/2}$$

and

$$\angle\theta = \tan^{-1}\left[\frac{\omega^{2(n+\alpha)}\sin(n+\alpha)\pi + \frac{g_m}{C_{\mathrm{n+\alpha}}}\omega^{(n+\alpha)}\sin(n+\alpha)\pi/2}{\omega^{2(n+\alpha)}\cos(n+\alpha)\pi + \frac{g_m}{C_{\mathrm{n+\alpha}}}\omega^{(n+\alpha)}\cos(n+\alpha)\pi/2 + \frac{1}{L_{\mathrm{n+\alpha}}C_{\mathrm{n+\alpha}}}}\right] \tag{4.18}$$

In general, three critical frequencies [41] are used to characterize FOF which are defined below:

ω_m: the maximum/minimum frequency point at which $|T(j\omega)|$ is maximum/minimum

ω_h: the half power frequency

ω_{rp}: the right phase frequency corresponding to angle = ± π/2

These critical frequencies can be obtained by solving the equation $(d/d\omega)|T(j\omega)|_{\omega=\omega_m} = 0$, $|T(j\omega)|_{\omega=\omega_h}$ = $(1/\sqrt{2})|T(j\omega)|$ in pass-band and $\angle\, T(j\omega)_{\ \omega=\omega_{rp}}$ $=\pm\pi/2$ respectively.

4.3.1 Stability Analysis

This section first presents a brief about stability analysis of a generic FOF, explained in detail in [38], and is followed by assessment of stability of proposed designs. The stability of a FOF is examined using its characteristic equation which is used to identify the locations of poles, in fractional domain s-plane, and their quality factor. These calculated locations are then traced and illustrated for further studies by transformation of s-plane into fractional domain i.e F- or W-plane. The general transfer function of higher order FOF can be expressed as

$$T(s) = \frac{N(s)}{s^{2(n+\alpha)} + 2as^{(n+\alpha)} + b} \tag{4.19}$$

where numerator N(s) will take different values according to the function type. The characteristic equation of (4.19) gives the pole locations at $\{-a \pm$ $jb-a2=be\pm j\delta$ in F-domain complex plane where δ=cos$-1(-a/b)$ (assuming all coefficients are positive and $b > a^2$ or $k = b/a^2 > 1$). The stability analysis of proposed higher order FOF is carried out by using transformation of F-plane into s-plane and comparing with a classical second order system whose poles are located at $\left\{-\omega_0/2Q \pm j\omega_0\sqrt{1-(1/4Q^2)}\right\} = \omega_0 e^{\pm j\theta}$ where $\theta = \cos^{-1}(-1/$ $2Q$. This comparison results in $\omega0=b1/2(n+\alpha)$, $Q=-12$cos$\delta/(n+\alpha)$ (both must be positive) and stability condition as $(\mathrm{n}+\alpha) < 2\delta/\pi$ for higher order FOF.

The stability analysis of proposed higher order FOF is also carried out using method outlined above. The stability condition, root location in F-domain (transformation of s-domain into fractional domain i.e. $s^{n+\alpha}$) complex plane, pole frequency ω_0 and quality factor Q are given in Table 4.2. It is noteworthy that all denominator coefficients in (4.12), (4.13) and (4.14) are positive.

Table 4.2: Stability constraints for proposed higher order FOF

$k=\frac{4C_{n+\alpha}}{L_{n+\alpha}g_m^2}$	Stability condition	Root location in F-domain complex plane	ω0	Q
k ≤ 1	(n+α)<2	$r_{1,2} = \frac{-g_m/C_{n+\alpha} \pm \sqrt{(g_m/C_{n+\alpha})^2 - 4\left(\frac{1}{L_{n+\alpha}C_{n+\alpha}}\right)}}{2} = g_{1,2}e^{j\pi}$	${g_{1,2}}^{1/(n+\alpha)}$	$\frac{-1}{2\cos\pi/(n+\alpha)}$
k > 1	(n+α) < 2δ/π, δ = $\cos^{-1}-(1/\sqrt{k})$	$r_{1,2} = \sqrt{\frac{1}{L_{n+\alpha}C_{n+\alpha}}}e^{\pm j\delta}$	$\left(\frac{1}{L_{n+\alpha}C_{n+\alpha}}\right)^{1/2(n+\alpha)}$	$\frac{-1}{2\cos\delta/(n+\alpha)}$

4.3.2. Simulation Results

The operation of proposed higher order FOF using FI and FC of order $(1+\alpha) = 1.2$ and 1.5 is examined through SPICE simulation. The simulation settings for impedances of FI and FC 1.2 and 1.5 orders FIs ($L_{1.2} = 0.25\ \Omega/s^{1.2}$, $L_{1.5} = 37.5\ m\Omega/s^{1.5}$) and FCs ($C_{1.2} = 2.5\ \mho/s^{1.2}$, $C_{1.5} = 3.75\ n\ \mho/s^{1.5}$) The resistive branch of PRB is implemented using OTA and the resistance is chosen as $R=1/g_m = 20\ k\Omega$. The simulated and theoretical responses of proposed FOF are shown in Fig. 4.12 and various performances are summarized in Table 4.3 for FLPF, FHPF and FBPF. The simulation results for FLPF, FHPF and FBPF are found to be in close agreement with theoretical results.

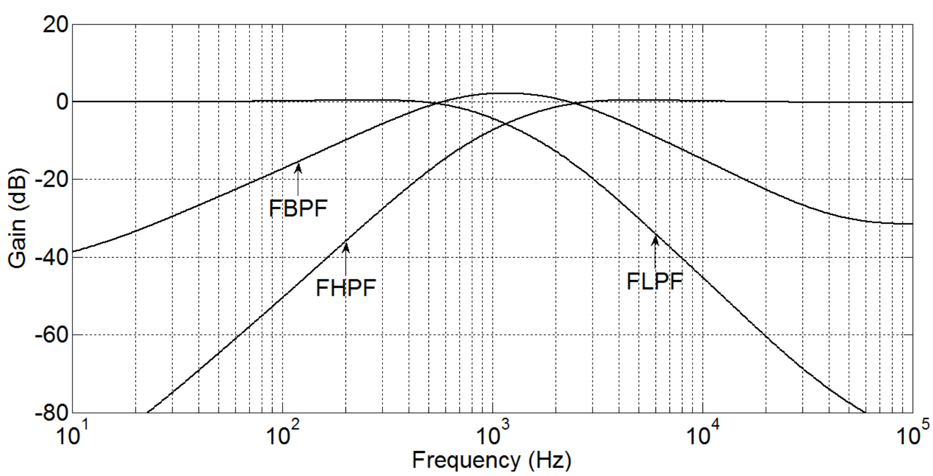

(a)

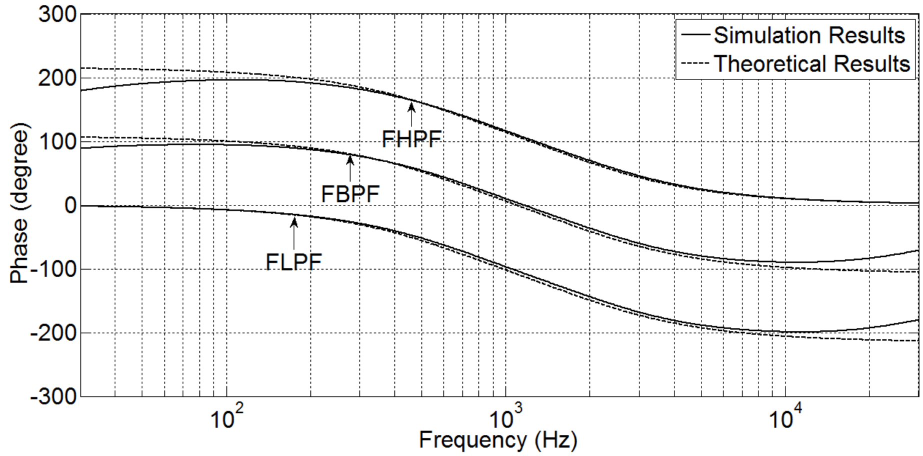

(b)

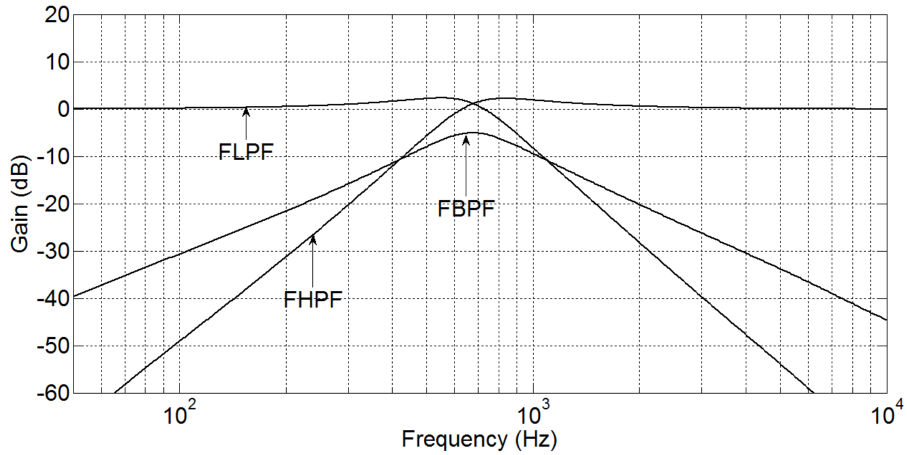

(c)

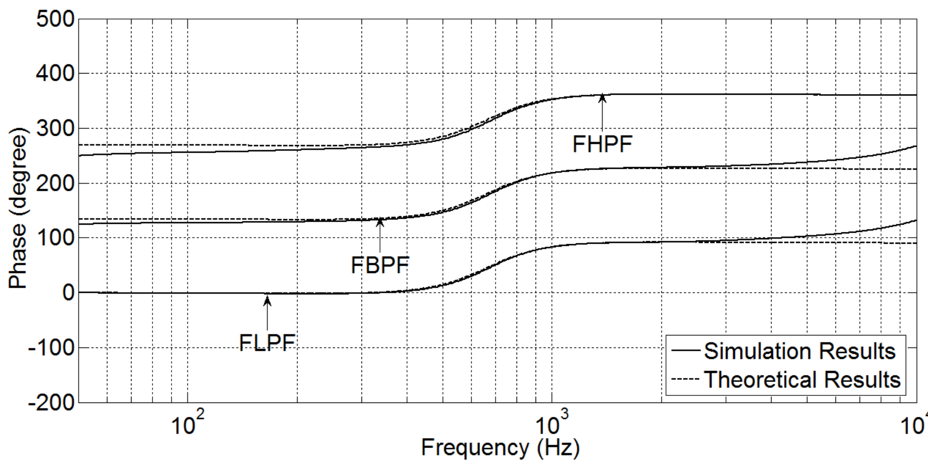

(d)

Fig. 4.12: Simulation frequency response of proposed FOF employing FOE of **(a -b)** 1.2 order and **(c-d)** 1.5 order

Table 4.3: Performance parameters for FLPF, FHPF and FBPF for order of $2(n+\alpha)$

Filter	Parameters Measured	$2(n+\alpha)=2(1.2)$		$2(n+\alpha)=2(1.5)$	
		Simulation Results	**Theoretical Results**	**Simulation Results**	**Theoretical Results**
FLPF	$\|T(j\omega\|$ in pass-band	0.992	1	0.998	1
	ω_h (Hz)	812.775	832.7	828	800
	ω_m (Hz)	254	261.72	550.28	523.3
	ω_{rp} (Hz)	900	840	1.35k	1.32k
	$\|T(j\omega)\|_{\omega=\omega_m}$	1.05	1.07	1.3	1.27
FHPF	$\|T(j\omega\|$ in pass-band	0.98	1	0.994	1
	ω_h (Hz)	1.65k	1.423k	549	543.47
	ω_m (Hz)	4.7k	4.28k	831	831.764
	ω_{rp} (Hz)	1.4k	1.411k	331	329.62
	$\|T(j\omega)\|_{\omega=\omega_m}$	1.05	1.07	1.28	1.27
FBPF	ω_{h1} (Hz)	519	484.72	494.735	478.14
	ω_{h2} (Hz)	2.597k	2.445k	917.438	909.5
	ω_m (Hz)	1.14k	1.09k	676	659.37
	ω_{rp} (Hz)	192.75, 6.166k	192.959, 6.136k	None	None
	$\|T(j\omega)\|_{\omega=\omega_m}$	1.29	1.32	0.557	0.55

Simulations are also performed to examine the stability of proposed FOF. The root-location in F-domain complex plane, pole frequency and quality factor of proposed higher order FOF are enlisted in Table 4.4.

Table 4.4: Stability Analysis

Order (n+α)	F-domain complex Plane	Root location	Pole frequency	Stability condition			Quality factor
		$r_{1,2}$	$f_{01,02}$ (Hz)	(i) $\delta = \cos^{-1}\left(-\frac{1}{\sqrt{k}}\right) > (n+\alpha)\times 90^0$ $if\ k > 1$ (ii) $\delta = 180^0 > (n+\alpha)\times 90^0\ if\ k < 1$	$(n+\alpha) < 2\delta/\pi$	Performance	Q
1.2	$F=s^{1.2}$	$-2x10^4$, $-8x10^4$	610.96, 1.94k	$180^0 > 108^0$	1.2 < 2	Stable	0.577
1.5	$F=s^{1.5}$	$-6.67x10^4 \pm j25.82x10^4$	659.375	$255.52^0 > 135^0$	1.5 <2.839	Stable	0.507

The root locus technique provides stability analysis of fractional order system [160] and its graphical representation can be illustrated through W-plane transformation. The root locus of realized FLPF and FBPF having order $2(1+\alpha)$= 2(1.2) and 2(1.5) respectively are plotted in Fig. 4.13 using forlocus function in MATLAB program. The plot of the Riemann surface has 5 and 2 Riemann sheets for order $2\ (1+\alpha)$ =2(1.2) and 2(1.5) respectively. The boundaries of unstable region (shown by dashed dotted lines in Fig. 4.14) $\{-\pi/10 \leq \arg(w)_{(1+\alpha)=1.2} \leq \pi/10\}$ and $\left\{-\frac{\pi}{4} \leq \arg(w)_{(1+\alpha)=1.5} \leq \frac{\pi}{4}\right\}$ for FOFs of order 2(1.2) and 2(1.5) respectively thus confirming the stability of the said FOFs.

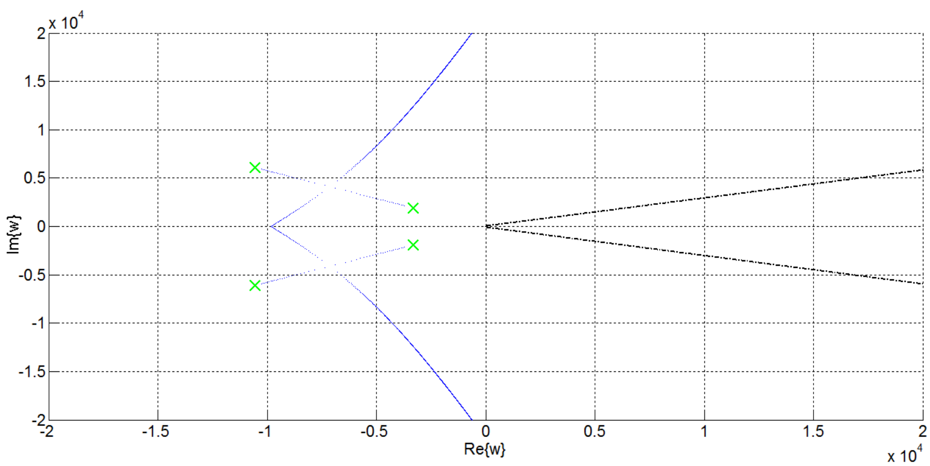

(a)

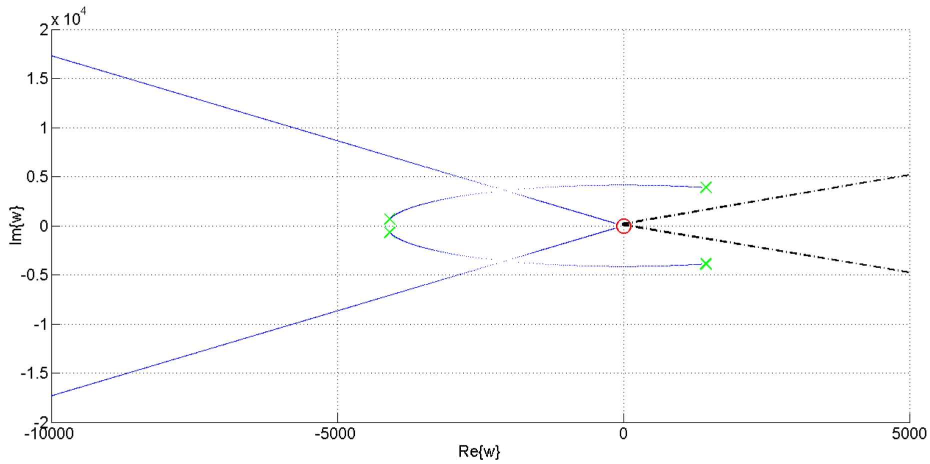

(b)

Fig. 4.13: Root-locus plots of the proposed FOFs having order 2(1+α) = 2(1.2) and 2(1.5) in **(a)** and **(b)** respectively with dashed line is the unstable region

4.4 Conclusion

An approach for designing higher order fractional element has been presented in this chapter. This approach is based on the concept of OTA IIC of integer domain which is first generalized in fractional domain by replacing the integer order capacitor by α order FC. The resulting fractional order impedance inverter is further used to propose fractional order IIMC of order (n + α). A higher order FOF is then developed as an application of the proposed IIMC. All proposed circuits are functionally verified through SPICE simulations using 0.18 µm TSMC CMOS technology parameter. The fractional capacitors (FCs) (with α = 0.2 and 0.5), are realized using truncated infinite order domino RC ladder network and are considered for all simulations in this work. The proposed IIMC is experimentally verified through hardware prototyping using LM 13600N dual OTAs IC. The simulation and experimental results are observed to be in close resemblance with theoretical prepositions.

CHAPTER 5

ELECTRONICALLY TUNABLE FOFs

The contents and results of the following papers have been reported in this chapter:

[1] **R. Verma,** N. Pandey, R. Pandey, "Electronically Tunable Fractional Order All Pass Filter", IOP: Materials Science and Engineering, vol. 225: 012229, 2017. **(SCOPUS)**. https://doi:10.1088/1757-899X/225/1/012229

[2] **R. Verma,** N. Pandey, R. Pandey, "Electronically Tunable Fractional Order Filter", Arabian Journal for Science and Engineering, vol. 42, no. 8, pp 3409–22, 2017. https://doi.org/10.1007/s13369-017-2500-8. (Springer) **Indexing: SCIE, SCOPUS; IF: 1.092**

5.1 Introduction

Active filters are widely used in applications pertaining to data acquisition, noise reduction, equalizing delay etc. Traditionally, op-amp is used for active filter design; its usage is limited due to finite gain bandwidth product. Further, the filter parameters of op-amp filters can be changed only by changing resistors and capacitors used therein. To add electronic tunability in opamp based filters, the resistors are replaced by MOSFETs working in triode region with appropriate differential connections for cancellation of associated signal nonlinearities. The OTA based filters, on the other hand, add electronic tunability through transconductance which can be adjusted via bias current.

In this chapter, generalization of OTA based filters in fractional domain is presented and two topologies one each from first [159] and second order [161] are derived. These topologies are termed as topology I and topology II in the context of this chapter. Topology I is derived from first order all pass filter whereas a second order filter providing low pass and band pass responses is considered for Topology II.

5.2 Topology I

This section presents generalization of first order filter in fractional domain and present various filter parameters. A generic OTA based structure, providing LP and AP responses, is presented next and is followed by its generalization.

5.2.1 Generalization of first order FOF

The general transfer function of first order filter is given by

$$T(s) = \frac{bs + d}{s + a} \tag{5.1}$$

and its generalization in fractional domain results in α order FOF. Its transfer function is given by

$$T(s)_{FO}^{\alpha} = \frac{bs^{\alpha} + d}{s^{\alpha} + a} \tag{5.2}$$

where a, b and d are the constant terms and appropriate selection of these results in different FOF responses which are summarized in Table 5.1

Table 5.1: Condition for α order FOFs responses

Condition	**Response**
b = 0	FLPF
d = 0	FHPF
d = -a	FAPF

The magnitude and phase responses of (5.2) are given as below:

$$|T(s)_{FO}^{\alpha}| = \sqrt{\frac{b^2\omega^{2\alpha} + d^2 + 2bd\omega^{\alpha}\cos \alpha\pi/2}{\omega^{2\alpha} + a^2 + 2a\omega^{\alpha}\cos \alpha\pi/2}} \tag{5.3}$$

$$\angle T(s)_{FO}^{\alpha} = \tan^{-1}\left[\frac{b\omega^{\alpha}\sin\alpha\pi/2}{b\omega^{\alpha}\cos\alpha\pi/2 + \mathrm{d}}\right] - \tan^{-1}\left[\frac{\omega^{\alpha}\cos\alpha\pi/2 + \mathrm{a}}{\omega^{\alpha}\sin\alpha\pi/2}\right] \tag{5.4}$$

5.2.2 Proposed Topology I

The proposed topology I is depicted in Fig. 5.1. Routine analysis of the circuit gives the output as:

$$V_{out} = \frac{s^{\alpha}V_{in1} - (g_m/C_{\alpha})V_{in2}}{s^{\alpha} + g_m/C_{\alpha}} \tag{5.5}$$

Where g_m represents transconductance gain of OTA.

Substituting $V_{in1} = V_{in2} = V_{in}$ in (5.5) results in the transfer function of FAPF and is given by

$$T(s)_{FAPF}^{\alpha} = \frac{s^{\alpha} - g_m/C_{\alpha}}{s^{\alpha} + g_m/C_{\alpha}} \tag{5.6}$$

Transfer function of FLPF, as given by (5.7), is obtained by substituting $V_{in1} = 0$ and $V_{in2} = V_{in}$ in (5.5).

$$T(s)_{FLPF}^{\alpha} = -\frac{g_m/C_{\alpha}}{s^{\alpha} + g_m/C_{\alpha}} \tag{5.7}$$

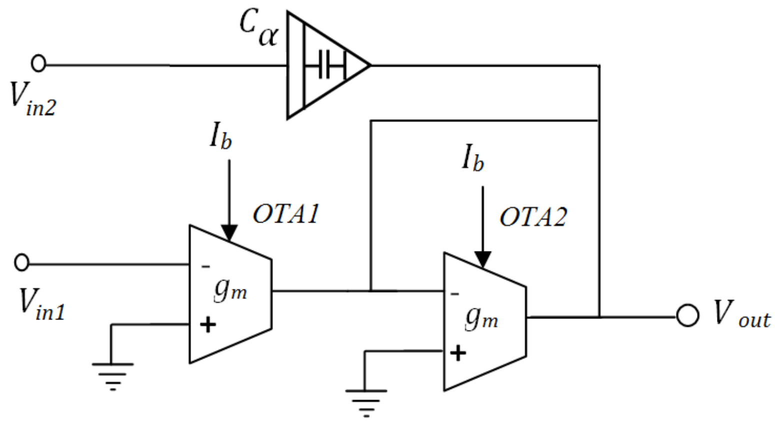

Fig. 5.1: Proposed Topology I

The magnitudes and phase of functions for (5.6) are computed respectively, as

$$|T(j\omega)_{FAPF}^{\alpha}| = \left[\frac{\omega^{2\alpha} + \frac{g_m^2}{C_\alpha^2} - 2\left(\frac{g_m}{C_\alpha}\right)\omega^\alpha \cos \alpha\pi/2}{\omega^{2\alpha} + \frac{g_m^2}{C_\alpha^2} + 2\left(\frac{g_m}{C_\alpha}\right)\omega^\alpha \cos \alpha\pi/2}\right]^{1/2} \tag{5.8}$$

$$\angle T(j\omega)_{FAPF}^{\alpha} = \tan^{-1}\left(\frac{\omega^\alpha \sin \alpha\pi/2}{\omega^\alpha \cos \alpha\pi/2 - g_m/C_\alpha}\right) - \tan^{-1}\left(\frac{\omega^\alpha \sin \alpha\pi/2}{\omega^\alpha \cos \alpha\pi/2 + g_m/C_\alpha}\right) \tag{5.9}$$

The magnitudes and phase of functions for (5.7) are computed respectively, as

$$|T(j\omega)_{FLPF}^{\alpha}| = \frac{\frac{g_m}{C_\alpha}}{\left[\omega^{2\alpha} + \frac{g_m^2}{C_\alpha^2} + 2\left(\frac{g_m}{C_\alpha}\right)\omega^\alpha \cos \alpha\pi/2\right]^{1/2}} \tag{5.10}$$

$$\angle T(j\omega)_{FLPF}^{\alpha} = \tan^{-1}\left(\frac{\omega^{\alpha}\sin\alpha\pi/2}{\omega^{\alpha}\cos\alpha\pi/2 + g_m/C_{\alpha}}\right) \tag{5.11}$$

The magnitude and phase for FAPF and FLPF at dc, $\omega_0 = \omega_{0(FAPF)} = \omega_{0(FLPF)} = (g_m/C_{\alpha})^{1/\alpha}$ and $\omega \rightarrow \infty$ are listed in Tables 5.2 and 5.3 respectively.

Table 5.2: Magnitude and phase for FAPF

ω	$\lvert T(j\omega)_{FAPF}^{\alpha}\rvert$	$\angle T(j\omega)_{FAPF}^{\alpha}$
0	1	π
$\omega_0 = (g_m/C_{\alpha})^{1/\alpha}$	$\tan\alpha\pi/4$	$\pi/2$
∞	1	0

Table 5.3: Magnitude and phase for FLPF

ω	$\lvert T(j\omega)_{FLPF}^{\alpha}\rvert$	$\angle T(j\omega)_{FLPF}^{\alpha}$
0	1	0
$\omega_0 = \left(\frac{g_m}{C_{\alpha}}\right)^{\frac{1}{\alpha}}$	$\frac{1}{2\cos\left(\frac{\alpha\pi}{4}\right)}$	$\frac{\alpha\pi}{4}$
∞	0	$\frac{\alpha\pi}{2}$

The critical frequencies of FAPF and FLPF are computed and are given as

$$\omega_{m(FAPF)} = \omega_{rp(FAPF)} = \omega_{0(FAPF)}$$
$$\omega_{h(FAPF)} == \omega_{0(FAPF)}\left[\left(2\cos\frac{\alpha\pi}{2} + \sqrt{4\cos^2\frac{\alpha\pi}{2} - 1}\right)\right]^{\frac{1}{\alpha}} \tag{5.12}$$

and

$$\omega_{m(FLPF)} = \omega_{0(FLPF)}\left(-\cos\frac{\alpha\pi}{2}\right)^{\frac{1}{\alpha}}, \omega_{rp(FLPF)} = \omega_{0(FLPF)}\left(-\frac{1}{\cos\frac{\alpha\pi}{2}}\right)^{\frac{1}{\alpha}}$$

$$\omega_{h(FLPF)} = \omega_{0(FLPF)}\left(\sqrt{1+\cos^2\frac{\alpha\pi}{2}} - \cos\frac{\alpha\pi}{2}\right)^{\frac{1}{\alpha}}$$

(5.13)

The magnitude of FAPF at $\omega = \omega_{rp}$ has a minima if $\alpha < 1$, maxima if $\alpha > 1$and flat if $\alpha = 1$ [47].

5.2.2.1 Stability Analysis

In this subsection, stability condition of proposed α order FOF is investigated for different values of α. The stability of FOF depends on its characteristic equation which is used to identify the pole-location. The stability of the FOF can be commented on by transformation of s-plane into fractional domain F- plane. It is well known that stability and physical regions for conventional s-plane are given as $+\pi/2 < \theta_S < -\pi/2$ and $+\pi > \theta > -\pi$ respectively. The mapping from s-plane into F- plane defined as $F = s^{\alpha}$, transforms the stability region by $+\alpha\pi/2 < \theta_S < -\alpha\pi/2$ and physical region by $+\alpha\pi > \theta_F > -\alpha\pi$. Thus, for $0 < \alpha < 1$ regions of unstable and physical in F-plane is smaller than s-plane whereas $\alpha > 1$, the unstable region in F-plane is larger than s-plane. The stability criterion of (5.2) maps on to conditions of positive value of coefficient ‘a’ and order α < 2 as for a positive value of ‘a’ and α = 2 the system will lead to oscillation [47].

From the characteristic equation of the proposed circuit given by (5.5) the pole location is obtained as $s^{\alpha} = -g_m/C$. It is clear that α order FOF is stable for α < 2 since the location of pole $s^{\alpha} = -g_m/C$ lies within the stable region in F-plane.

5.2.2.2 Sensitivity Analysis

The significance of sensitivity analysis of FOFs is to indicate the relative change in filters responses with respect to the circuit parameters used. In this subsection, the mathematical formulation of sensitivities of transfer functions of the proposed filters has been derived.

The sensitivity relations of FAPF with respect to α, FC value and g_m are presented in (5.14) - (5.16).

$$S_{\alpha}^{FAPF} = \frac{\frac{2g_m}{C_\alpha}\alpha s^{\alpha}\ln(s)}{\left(s^{2\alpha} - \frac{g_m^2}{C_\alpha^2}\right)} \tag{5.14}$$

$$S_{C_\alpha}^{FAPF} = \frac{\frac{2g_m}{C_\alpha}s^{\alpha}}{\left(s^{2\alpha} - \frac{g_m^2}{C_\alpha^2}\right)} \tag{5.15}$$

$$S_{g_m}^{FAPF} = -\frac{\frac{g_m^2}{C_\alpha^2}}{\left(s^{2\alpha} - \frac{g_m^2}{C_\alpha^2}\right)} \tag{5.16}$$

The sensitivity of (5.7) with respect to α, FC value and g_m are computed as

$$S_{\alpha}^{FLPF} = \frac{\alpha s^{\alpha}\ln(s)}{\left(s^{\alpha}+\frac{g_m}{C_{\alpha}}\right)} \tag{5.17}$$

$$S_{C_{\alpha}}^{FLPF} = \frac{s^{\alpha}}{\left(s^{\alpha}+\frac{g_m}{C_{\alpha}}\right)} \tag{5.18}$$

$$S_{g_m}^{FLPF} = \frac{-s^{\alpha}}{\left(s^{\alpha}+\frac{g_m}{C_{\alpha}}\right)} \tag{5.19}$$

It may be observed that transfer function sensitivities depend on α, FC value and g_m of OTA. To further illustrate the effect of various parameters MATLAB simulations are carried out and are included in simulation section.

5.2.2.3 Simulation results

The functionality of the proposed FOFs is examined through SPICE simulations using CMOS schematic of Fig. 2.7 (b) of OTA [122]. Further the FAPF is designed for different ω_0 and the corresponding simulation settings are listed in Table 5.4. The simulated and theoretical responses of proposed FAPF designed using FC of order 0.5 with a center frequency of 1 kHz are shown in Fig. 5.2. Results for FC of order 0.9 are depicted in Fig.5.3

. **Table 5.4:** Simulation settings for proposed FAPF

Order (α)	(μ℧/s$^{\alpha}$)	I_b (μA)	g_m (μA/V)	ω_0 (rad/s)
0.5	1	4.035	50	2.5 k
		9	100	10 k
		15.016	150	22.5 k
		22.34	200	40 k
0.9	1	35.175	268.58	500
		70.16	386.861	750
		140.78	501.187	1 k
		303.3	612.659	1.25 k

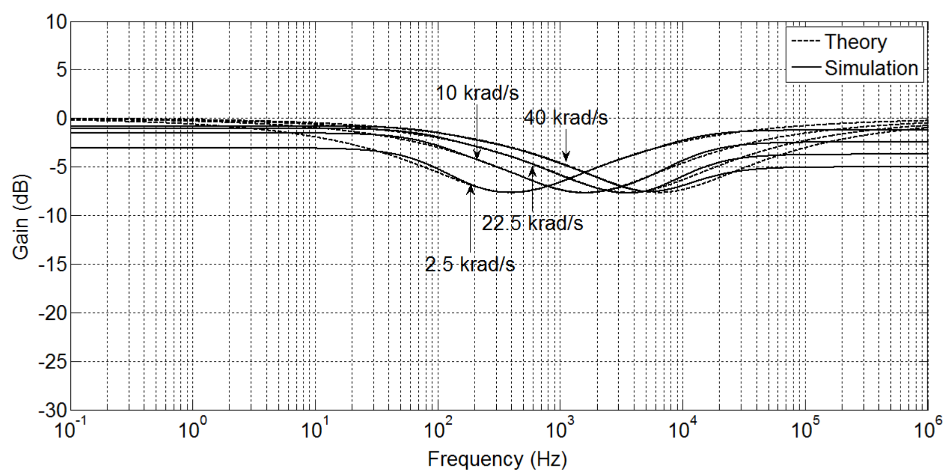

(a)

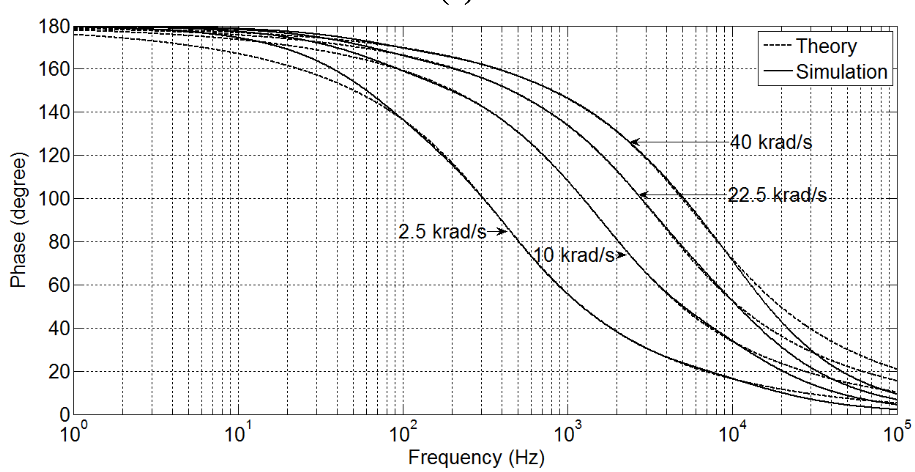

(b)

Fig. 5.2: Simulated **(a)** magnitude and **(b)** phase responses for proposed FAPF with α = 0.5

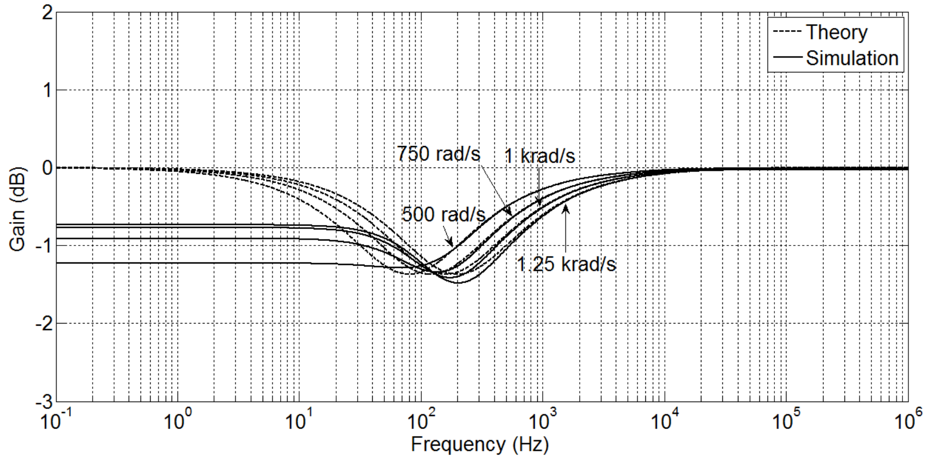

(a)

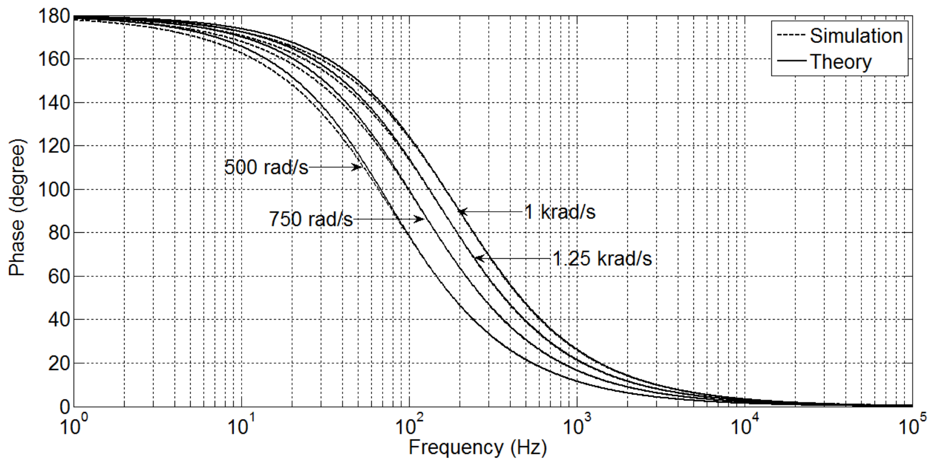

(b)

Fig. 5.3: Simulated **(a)** magnitude and **(b)** phase responses for proposed FAPF with $\alpha = 0.9$

The time domain response of proposed FAPF circuit is also examined by setting ω_{rp} as (i) 10 krad/s for order 0.5 and (ii) 500 rad/s for order 0.9. The requisite simulation settings are given in Table 5.4. Simulated responses to a 100 mV input sinusoid are shown in Fig. 5.4 and corresponding Lissajous patterns are depicted in Fig. 5.5 and 90^0 phase shift between input and output is observed.

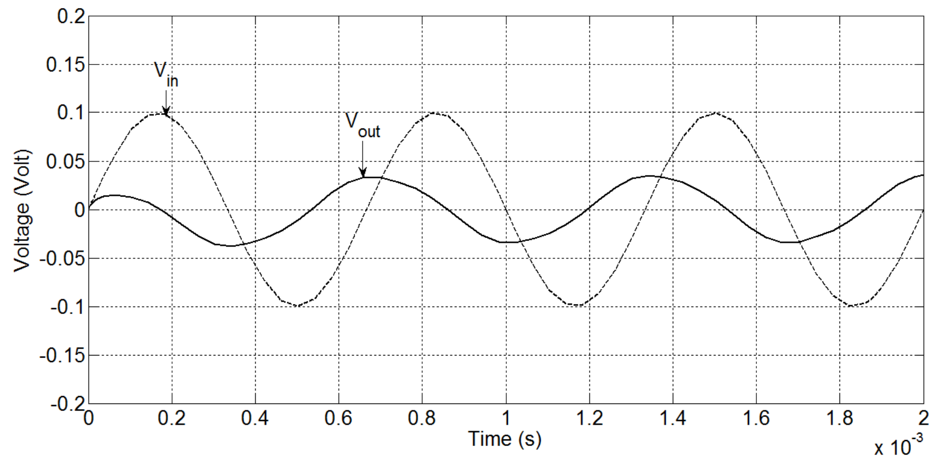

(a)

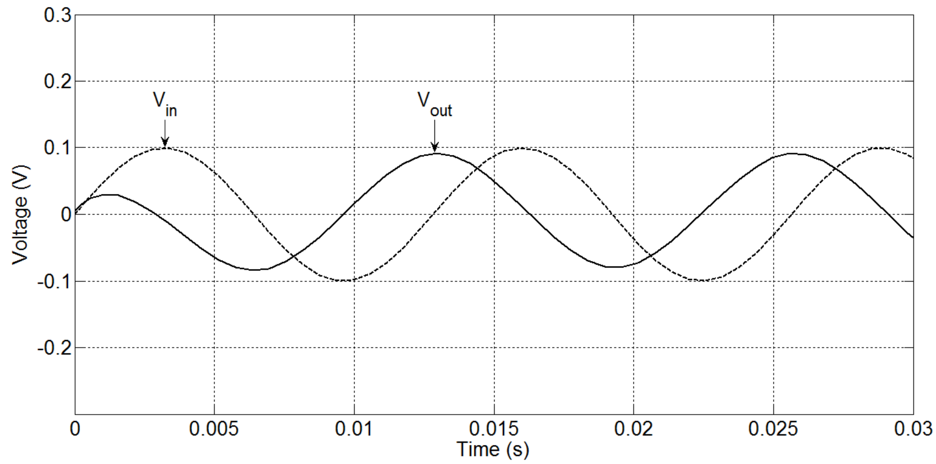

(b)

Fig. 5.4: Time domain response of proposed FAPF having **(a)** α = 0.5 and **(b)** α = 0.9

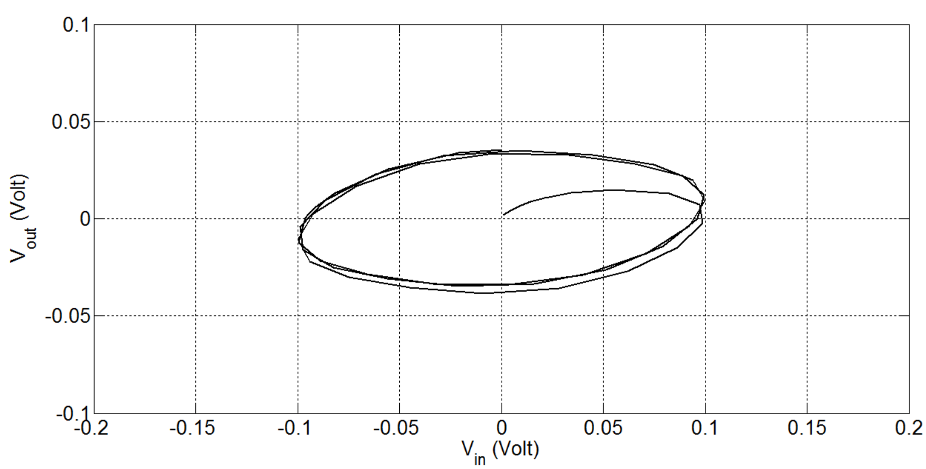

(a)

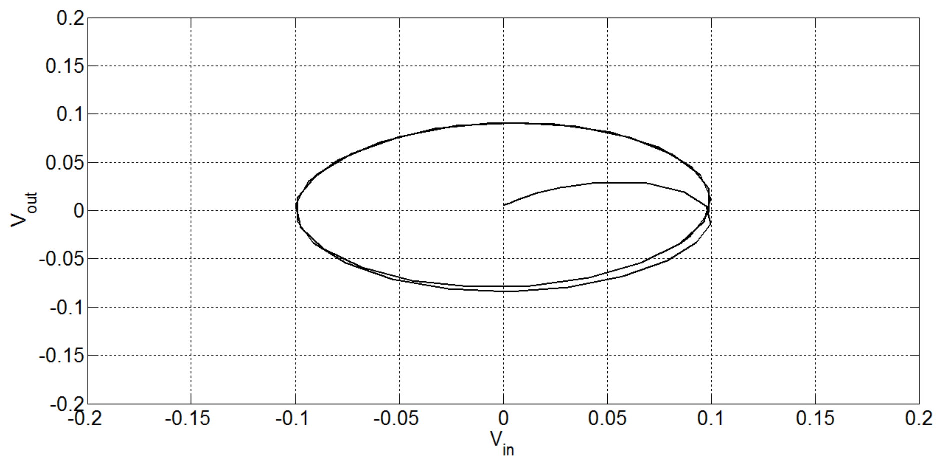

(b)

Fig. 5.5: Lissajous patterns for proposed FAPF having **(a)** α = 0.5 and **(b)** α = 0.9

The functionality of proposed FLPF is tested for α = 0.5 and 0.9 at different ω_h with the simulation settings given in Table 5.5. The simulated and theoretical responses of proposed FLPF with FC of order 0.5 and 0.9 are shown in Figs. 5.6 and 5.7 respectively. It may be noted that there is close matching between theoretical and simulated values in the range of few tens to thousand hertz frequency range.

Table 5.5: Simulation settings for proposed FLPF

Order (α)	(μ℧/s$^{\alpha}$)	I_b (μA)	g_m ($\mu A/V$)	ω_h (rad/s)
0.5	1	4.035	50	0.67 k
		9	100	2.68 k
		22.34	200	10.7 k
0.9		4.035	50	65
		9	100	140
		22.34	200	303

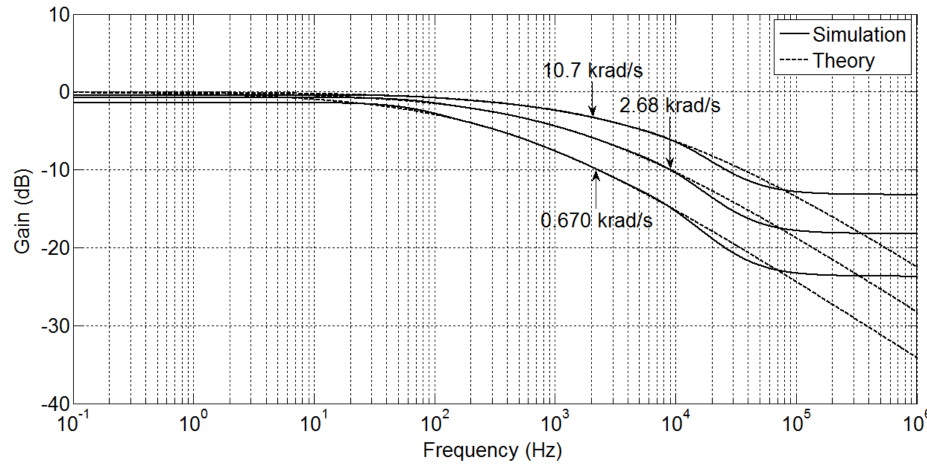

(a)

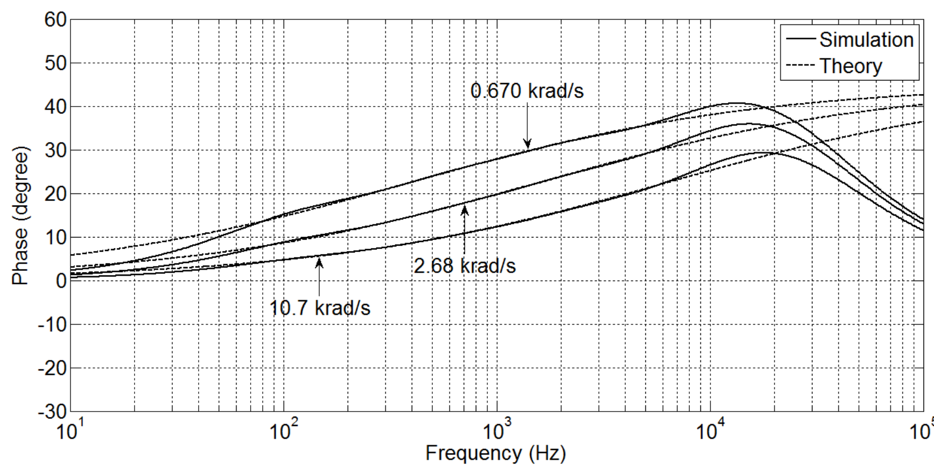

(b)

Fig. 5.6: Simulated (a) magnitude and (b) phase responses for proposed FLPF with $\alpha = 0.5$

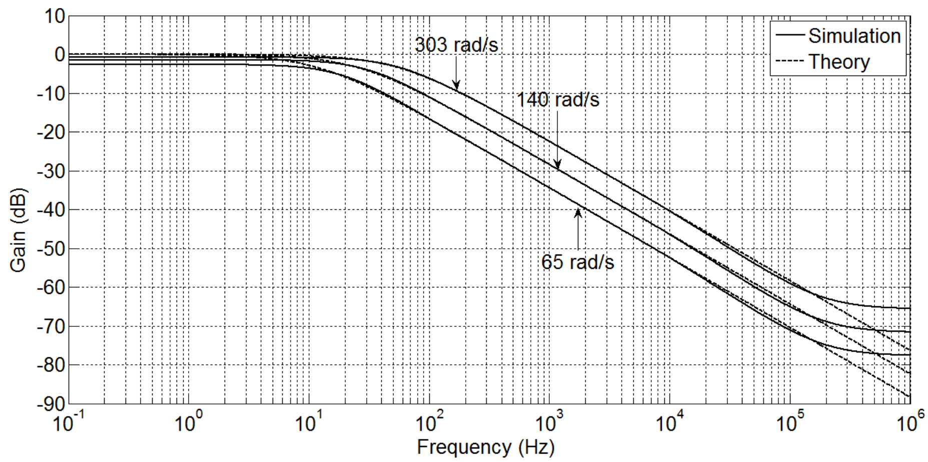

(a)

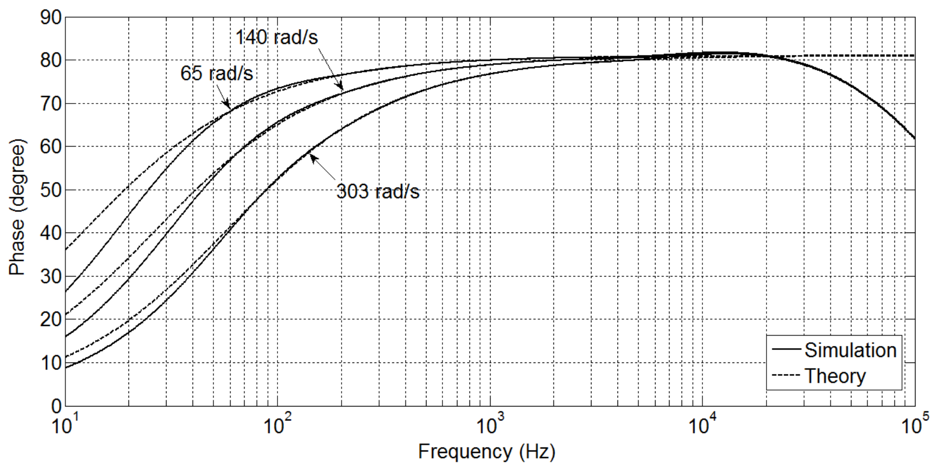

(b)

Fig. 5.7: Simulated **(a)** magnitude and **(b)** phase responses for proposed FLPF with α = 0.9

The sensitivities of proposed FAPF and FLPF are examined through MATLAB simulations at a frequency of 1 kHz. The sensitivity relations of FAPF given by (5.14) - (5.16) are plotted in Fig 5.8.Three data sets are used to examine sensitivities of FAPF with respect to α. The values of g_m are taken as 25 μA/V, 50 μA/V and 100 μA/V under data set 1, data set 2 and data set 3 respectively whereas C_α is taken as 1 μ℧/s$^\alpha$ for all cases. The resulting sensitivity plots are depicted in Fig. 5.8 (a). To plot sensitivity with respect to C_α, α is considered to be 0.5 and g_m is set as 100 μA/V. The simulated plot is shown in Fig. 5.8(b). Sensitivity variation curve of FAPF against g_m while α is chosen as 0.5 and C_α as 1 μ℧/s$^\alpha$ is presented in Fig.5.8(c). The corresponding curves for FLPF represented by (5.17) - (5.19) for similar simulation settings are plotted in Fig 5.9. From Figs. 5.8 and 5.9 it is observed that sensitivity variations of FAPF against α and g_m are found to be within unity whereas for FLPF it is within unity for all the three plots.

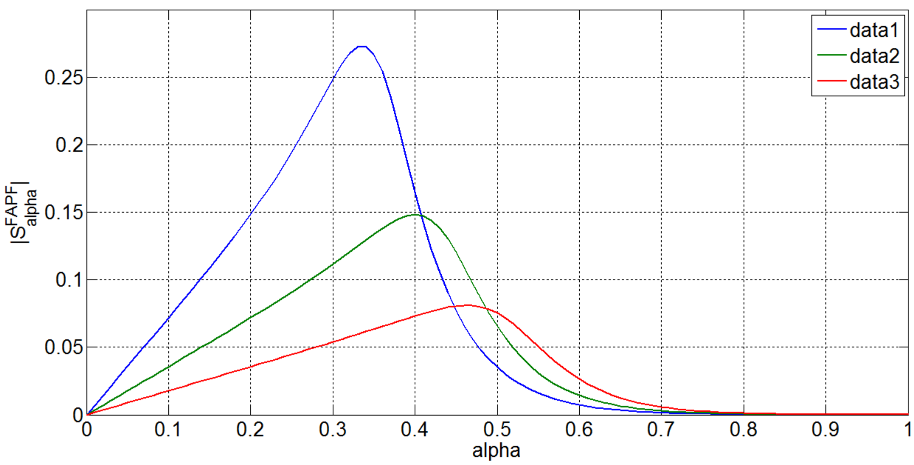

(a)

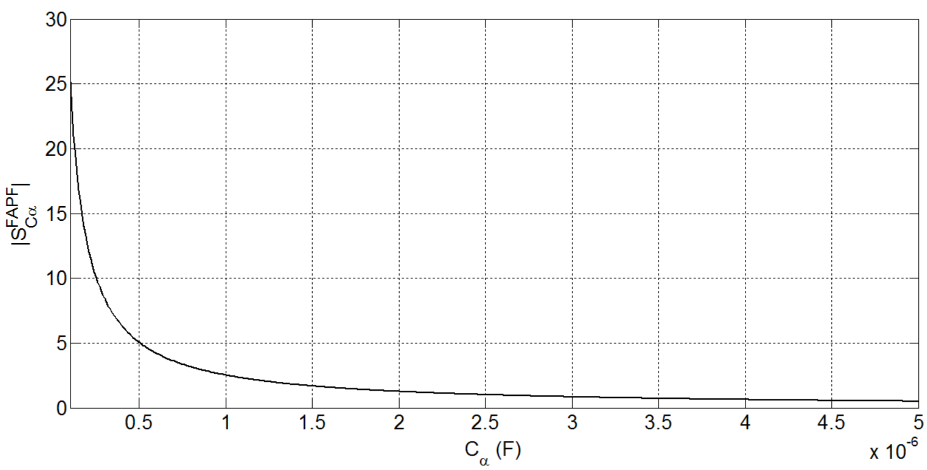

(b)

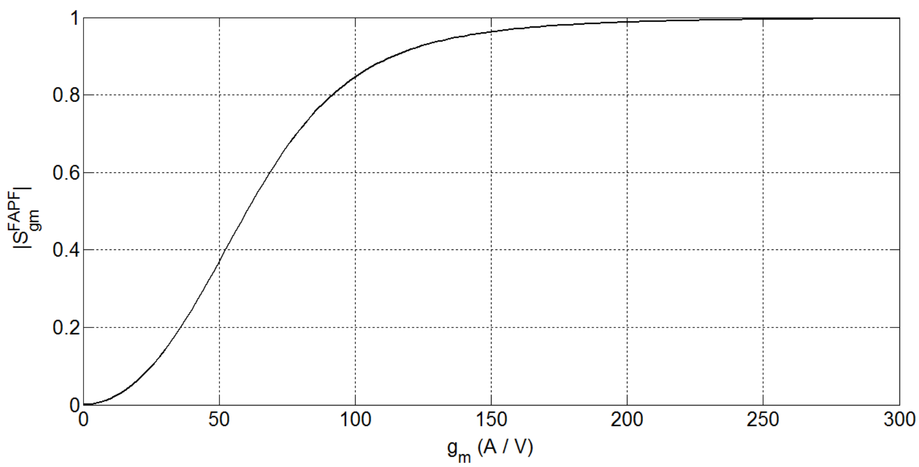

(c)

Fig. 5.8: The sensitivity magnitudes of proposed FAPF with respect to **(a)** α, **(b)** C_α and **(c)** g_m

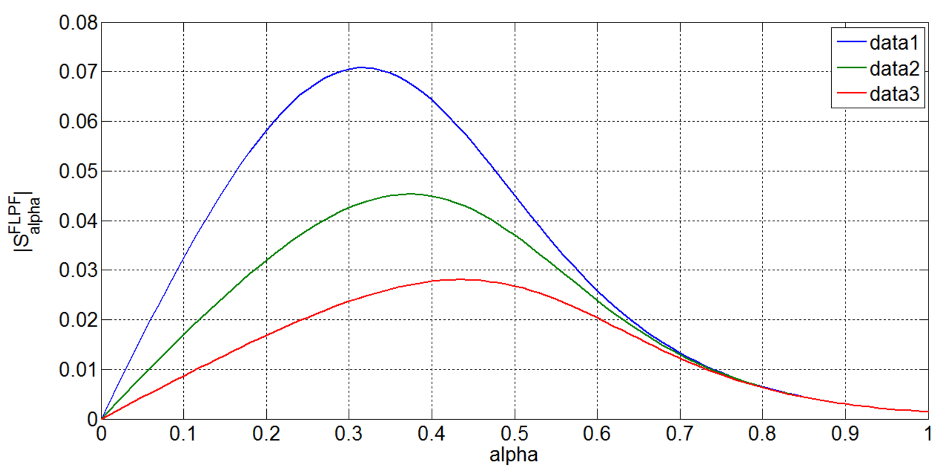

(a)

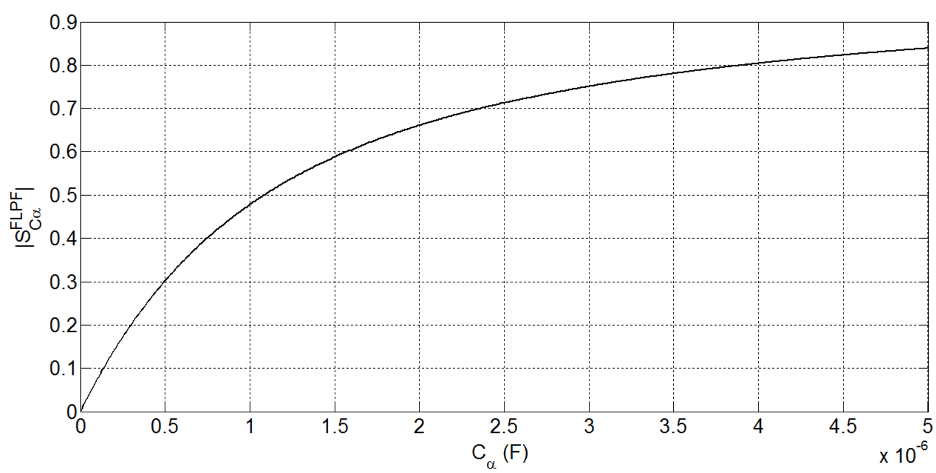

(b)

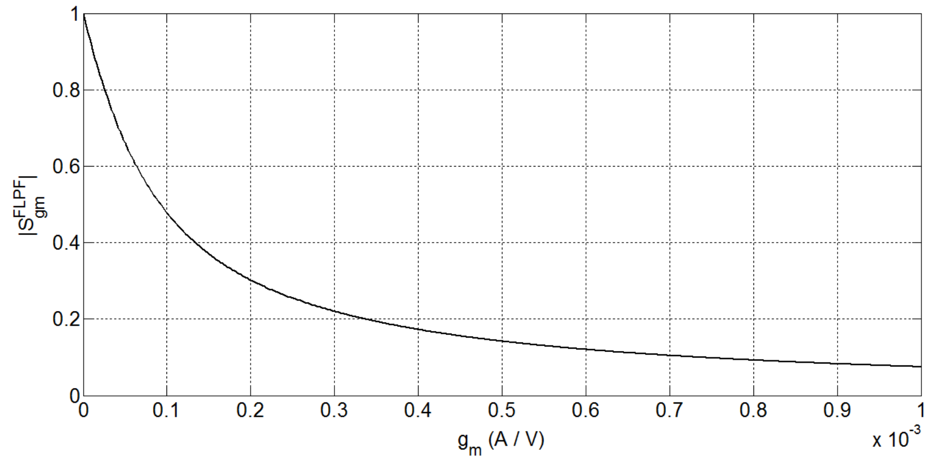

(c)

Fig. 5.9: The sensitivity magnitudes of proposed FLPF with respect to **(a)** α, **(b)** C_α and **(c)** g_m

5.3 Topology II

In this section generalization of second order filter in fractional domain is briefed first followed by description of new single input multi output OTA based FOF providing LP and BP responses.

5.3.1 Generalization of second order FOF

The general transfer function of second order filter is given by

$$T(s) = \frac{b_2 s^2 + b_1 s + b_0}{s^2 + a_1 s + a_0} \tag{5.20}$$

where coefficients b_0, b_1, b_2, a_0, a_1 are the constant terms.

The generalization of (5.20) in fractional domain using two FCs of different orders α and β results in (α + β) order FOF. Its transfer function is given by

$$T(s)_{FO}^{(\alpha+\beta)} = \frac{b_2 s^{(\alpha+\beta)} + b_1 s^{\alpha} + b_0}{s^{(\alpha+\beta)} + a_1 s^{\alpha} + a_0}$$

(5.21)

It may be noted that various FO responses may be obtained by appropriate selection of b_i's (i = 0, 1, 2). The FLPF is obtained for ($b_2 = 0$, $b_1 = 0$), FHPF can be designed by setting ($b_1 = 0$, $b_0 = 0$), FBPF is deduced by selecting ($b_2 = 0$, $b_0 = 0$) and FBSF response can be derived for $b_1 = 0$. The general transfer function represents FAPF for coefficient setting of $b_2=1$, $b_1 =(- a_1)$ and $b_0= a_0$.

Considering $\alpha = \beta$, (5.21) modifies to

$$T(s)_{FO}^{2\alpha} = \frac{b_2 s^{2\alpha} + b_1 s^{\alpha} + b_0}{s^{2\alpha} + a_1 s^{\alpha} + a_0}$$

(5.22)

Representing denominator of (5.22) as D(s), the magnitude of the characteristic equation of (5.22) [41] can be obtained as

$$|D(s)| = [\omega^{4\alpha} + 2a_1\omega^{3\alpha}\cos\alpha\pi/2 + ({a_1}^2 + 2a_0\cos\alpha\pi)\omega^{2\alpha} + 2a_1a_0\omega^{\alpha}\cos\alpha\pi/2 + {a_0}^2]^{1/2}$$

(5.23)

5.3.2 Proposed OTA based FLPF and FBPF

In this subsection, OTA-based filter topology [161] is adapted for FO domain. The capacitors are replaced by FCs of same order α and the resulting topology is depicted in Fig. 5.10. It provides electronically tunable FLPF and FBPF responses simultaneously. The routine analysis results in the following filter transfer functions:

$$T(s)^{2\alpha}_{FLPF} = \frac{g_{m1}g_{m3}/C_{1\alpha}C_{2\alpha}}{D(s)} \tag{5.24}$$

$$T(s)^{2\alpha}_{FBPF} = \frac{s^{\alpha}g_{m2}/C_{1\alpha}}{D(s)} \tag{5.25}$$

where $$D(s) = s^{2\alpha} + s^{\alpha}\, g_{m2}/C_{1\alpha} + g_{m1}g_{m3}/C_{1\alpha}C_{2\alpha} \tag{5.26}$$

and g_{m1}, g_{m2} and g_{m3} correspond to g_m of OTA1, OTA2 and OTA3 respectively.

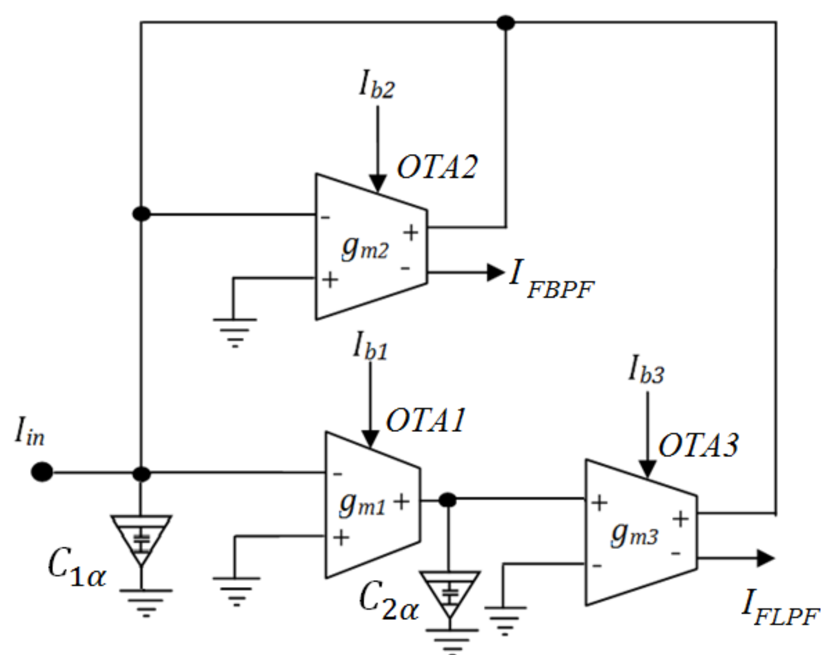

Fig. 5.10: OTA-based current mode circuit configuration

In order to determine the critical frequencies of the proposed FLPF and FBPF the magnitudes of $T(s)^{2\alpha}_{FLPF}$ and $T(s)^{2\alpha}_{FBPF}$ are computed respectively, as

$$|T(j\omega)^{2\alpha}_{FLPF}| = \frac{\frac{g_{m1}g_{m3}}{C_{1\alpha}C_{2\alpha}}}{\left[\begin{array}{c}\omega^{4\alpha} + 2\frac{g_{m2}}{C_{1\alpha}}\omega^{3\alpha}\cos\frac{\alpha\pi}{2} + \left(\frac{g_{m2}^2}{C_{1\alpha}^2} + 2\frac{g_{m1}g_{m3}}{C_{1\alpha}C_{2\alpha}}\cos\alpha\pi\right)\omega^{2\alpha} + 2\frac{g_{m1}g_{m3}}{C_{1\alpha}C_{2\alpha}}\frac{g_{m2}}{C_{1\alpha}}\omega^{\alpha}\cos\frac{\alpha\pi}{2} \\ + \left(\frac{g_{m1}g_{m3}}{C_{1\alpha}C_{2\alpha}}\right)^2\end{array}\right]^{1/2}} \tag{5.27}$$

$$|T(j\omega)^{2\alpha}_{FBPF}| = \frac{\frac{g_{m2}}{C_{1\alpha}}\omega^{\alpha}}{\left[\begin{array}{c}\omega^{4\alpha} + 2\frac{g_{m2}}{C_{1\alpha}}\omega^{3\alpha}\cos\frac{\alpha\pi}{2} + \left(\frac{g_{m2}^2}{C_{1\alpha}^2} + 2\frac{g_{m1}g_{m3}}{C_{1\alpha}C_{2\alpha}}\cos\alpha\pi\right)\omega^{2\alpha} + 2\frac{g_{m1}g_{m3}}{C_{1\alpha}C_{2\alpha}}\frac{g_{m2}}{C_{1\alpha}}\omega^{\alpha}\cos\frac{\alpha\pi}{2} \\ + \left(\frac{g_{m1}g_{m3}}{C_{1\alpha}C_{2\alpha}}\right)^2\end{array}\right]^{1/2}} \tag{5.28}$$

The frequencies $\omega_{m(FLPF)}$ and $\omega_{m(FBPF)}$ are determined by differentiating magnitudes of $T(j\omega)^{2\alpha}_{FLPF}$ and $T(j\omega)^{2\alpha}_{FBPF}$ by (5.27) and (5.28) with respect to ω^{α} and equating it to zero. Applying this to (5.27) and (5.28) results, respectively, in

$$\begin{aligned}\omega^{3\alpha}_{m(FLPF)} + 3\frac{g_{m2}}{2C_{1\alpha}}\omega^{2\alpha}_{m(FLPF)}\cos\alpha\pi/2 + \left[2\left(\frac{g_{m2}}{2C_{1\alpha}}\right)^2 + \frac{g_{m1}g_{m3}}{C_{1\alpha}C_{2\alpha}}\cos\alpha\pi\right]\omega^{\alpha}_{m(FLPF)} \\ + \frac{g_{m2}}{2C_{1\alpha}}\frac{g_{m1}g_{m3}}{C_{1\alpha}C_{2\alpha}}\cos\alpha\pi/2 = 0\end{aligned} \tag{5.29}$$

$$\left(\omega^{2\alpha}_{m(FBPF)} - \frac{g_{m1}g_{m3}}{C_{1\alpha}C_{2\alpha}}\right)\left(\omega^{2\alpha}_{m(FBPF)} + 2\omega^{\alpha}_{m(FBPF)}\frac{g_{m2}}{2C_{1\alpha}}\cos\frac{\alpha\pi}{2} + \frac{g_{m1}g_{m3}}{C_{1\alpha}C_{2\alpha}}\right) = 0 \tag{5.30}$$

The numerical values of $\omega_{m(FLPF)}$ and $\omega_{m(FBPF)}$ can be determined by solving (5.29) and (5.30) respectively. In case of FBPF, one of the $\omega_{m(FBPF)}$ value is given by $\omega_{m(FBPF)} = \left(\frac{g_{m1}g_{m3}}{C_{1\alpha}C_{2\alpha}}\right)^{1/2\propto}$ and its corresponding peak magnitude is computed as

$$\left|T(j\omega_{m(FBPF)})\right| = \frac{\frac{g_{m2}}{2C_{1\alpha}}}{\left|\frac{g_{m2}}{2C_{1\alpha}} + \sqrt{\frac{g_{m1}g_{m3}}{C_{1\alpha}C_{2\alpha}}\cos \alpha\pi/2}\right|} \tag{5.31}$$

The half power frequency for FLPF ($\omega_{h(FLPF)}$) may be determined by equating magnitude of (5.27) to $1/\sqrt{2}$. The corresponding expression is computed as

$$\begin{aligned}\omega_{h(FLPF)}^{4\alpha} + 4\frac{g_{m2}}{2C_{1\alpha}}\omega_{h(FLPF)}^{3\alpha}\cos \alpha\pi/2 \\ + \left[4\left(\frac{g_{m2}}{2C_{1\alpha}}\right)^2 + 2\frac{g_{m1}g_{m3}}{C_{1\alpha}C_{2\alpha}}\cos \alpha\pi\right]\omega_{h(FLPF)}^{2\alpha} \\ + 4\frac{g_{m2}}{2C_{1\alpha}}\frac{g_{m1}g_{m3}}{C_{1\alpha}C_{2\alpha}}\omega_{h(FLPF)}^{\alpha}\cos \alpha\pi/2 - \left(\frac{g_{m1}g_{m3}}{C_{1\alpha}C_{2\alpha}}\right)^2 = 0\end{aligned} \tag{5.32}$$

Similarly, the expression for computing half power frequency for FBPF ($\omega_{h(FBPF)}$) is given by

$$\omega_{h(FBPF)}^{4\alpha} + 4\frac{g_{m2}}{2C_{1\alpha}}\omega_{h(FBPF)}^{3\alpha}\cos\frac{\alpha\pi}{2} - \left[4\left(\frac{g_{m2}}{2C_{1\alpha}}\right)^2 - 2\frac{g_{m1}g_{m3}}{C_{1\alpha}C_{2\alpha}}\cos\alpha\pi + 8\frac{g_{m1}g_{m3}}{C_{1\alpha}C_{2\alpha}}cos^2\frac{\alpha\pi}{2} + 16\frac{g_{m2}}{2C_{1\alpha}}\sqrt{\frac{g_{m1}g_{m3}}{C_{1\alpha}C_{2\alpha}}}\cos\frac{\alpha\pi}{2}\right]\omega_{h(FBPF)}^{2\alpha} + 4\frac{g_{m2}}{2C_{1\alpha}}.\frac{g_{m1}g_{m3}}{C_{1\alpha}C_{2\alpha}}\omega_{h(FBPF)}^{\alpha}\cos\alpha\pi/2 + \left(\frac{g_{m1}g_{m3}}{C_{1\alpha}C_{2\alpha}}\right)^2 = 0 \tag{5.33}$$

The numerical values of $\omega_{h(FLPF)}$and $\omega_{h(FBPF)}$can be determined by solving (5.32) and (5.33) respectively.

The right phase frequency (corresponding to phase angle = ± π/2) for FLPF and FBPF are expressed by (5.34) and (5.35) respectively.

$$\omega_{rp(FLPF)} = \left(\frac{-\frac{g_{m2}}{2C_{1\alpha}}\cos\frac{\alpha\pi}{2} - \sqrt{\left(\frac{g_{m2}}{2C_{1\alpha}}\right)^2\cos^2\frac{\alpha\pi}{2} - \frac{g_{m1}g_{m3}}{C_{1\alpha}C_{2\alpha}}\cos\alpha\pi}}{\cos\alpha\pi}\right)^{1/\alpha} \tag{5.34}$$

$$\omega_{rp(FBPF)} = \left(\frac{-\frac{g_{m2}}{2C_{1\alpha}} \pm \sqrt{\left(\frac{g_{m2}}{2C_{1\alpha}}\right)^2 - \frac{g_{m1}g_{m3}}{C_{1\alpha}C_{2\alpha}}\cos^2\frac{\alpha\pi}{2}}}{\cos\frac{\alpha\pi}{2}}\right)^{1/\alpha} \tag{5.35}$$

The critical frequencies of FLPF and FBPF responses depend upon transconductance *(g_m)* of OTAs which can be tuned electronically through bias current variation. Therefore, various critical frequencies of OTA-based FOF can be electronically tuned.

5.3.2.1 Stability Analysis

The stability of presented FOF depends on coefficients of $s^{i\alpha}$ (i = 1, 0) in (5.26). As all coefficients of (5.26) are positive, the conditions for different parameters [38] are mentioned in Table 5.6. It may be noted from Table 5.6 that FOF is stable for δ > απ/2 for α ranging between 0 and 1.

Table 5.6: Stability constraints with ω_0 and Q of $D(s)$

Parameter $\boldsymbol{k = 4(g_{m1}g_{m3}/g_{m2}^2)}$	**Stability condition**	**Root location**	**Pole frequency ω_0**	**Q**
$\boldsymbol{k \le 1}$	α<2	$r_{1,2} = \dfrac{-g_{m2}/C_{1\alpha} \pm \sqrt{(g_{m2}/C_{1\alpha})^2 - 4(\frac{g_{m1}g_{m3}}{C_{1\alpha}C_{2\alpha}})}}{2} = g_{1,2}e^{j\pi}$	${g_{1,2}}^{1/\alpha}$	$\dfrac{-1}{2\cos\pi/\alpha}$
$\boldsymbol{k > 1}$	α < 2δ/π, δ=$\cos^{-1}-(1/\sqrt{k})$>π/2	$r_{1,2} = \sqrt{\dfrac{g_{m1}g_{m3}}{C_{1\alpha}C_{2\alpha}}}\ e^{\pm j\delta}$	$(\frac{g_{m1}g_{m3}}{C_{1\alpha}C_{2\alpha}})^{1/2\alpha}$	$\dfrac{-1}{2\cos\delta/\alpha}$

5.3.2.2 Sensitivity analysis

In this subsection, sensitivities of both the FOF transfer functions have been computed to enumerate the effect of α, FC value and g_{mi}*'s (i= 1, 2, 3)* and are expressed, respectively, as

$$S_{\alpha}^{FLPF} = -\frac{\alpha s^{\alpha} \ln(s)\,(2s^{\alpha} + g_{m2}/C_{1\alpha})}{s^{2\alpha} + s^{\alpha} g_{m2}/C_{1\alpha} + g_{m1}g_{m3}/C_{1\alpha}C_{2\alpha}} \tag{5.36}$$

$$S_{C_{1\alpha}}^{FLPF} = -\frac{s^{2\alpha}}{s^{2\alpha} + s^{\alpha} g_{m2}/\,C_{1\alpha} + g_{m1}g_{m3}/C_{1\alpha}C_{2\alpha}} = S_{C_{1\alpha}}^{FBPF} \tag{5.37}$$

$$S_{C_{2\alpha}}^{FLPF} = -\frac{s^{2\alpha} + s^{\alpha} g_{m2}/C_{1\alpha}}{s^{2\alpha} + s^{\alpha} g_{m2}/C_{1\alpha} + g_{m1}g_{m3}/C_{1\alpha}C_{2\alpha}} = -S_{g_{m1}}^{FLPF} = -S_{g_{m3}}^{FLPF} \tag{5.38}$$

$$S_{g_{m2}}^{FLPF} = -\frac{s^{\alpha} g_{m2}/C_{1\alpha}}{s^{2\alpha} + s^{\alpha} g_{m2}/C_{1\alpha} + g_{m1}g_{m3}/C_{1\alpha}C_{2\alpha}} \tag{5.39}$$

$$S_{\alpha}^{FBPF} = \frac{\alpha s^{\alpha} \ln(s)[-s^{2\alpha} + g_{m1}g_{m3}/C_{1\alpha}C_{2\alpha}]}{s^{2\alpha} + s^{\alpha} g_{m2}/C_{1\alpha} + g_{m1}g_{m3}/C_{1\alpha}C_{2\alpha}} \tag{5.40}$$

$$S_{C_{2\alpha}}^{FBPF} = \frac{g_{m1}g_{m3}/C_{1\alpha}C_{2\alpha}}{s^{2\alpha} + s^{\alpha} g_{m2}/C_{1\alpha} + g_{m1}g_{m3}/C_{1\alpha}C_{2\alpha}} = S_{g_{m1}}^{FBPF} = S_{g_{m3}}^{FBPF} \tag{5.41}$$

$$S_{g_{m2}}^{FBPF} = \frac{s^{2\alpha} + g_{m1}g_{m3}/C_{1\alpha}C_{2\alpha}}{s^{2\alpha} + s^{\alpha} g_{m2}/C_{1\alpha} + g_{m1}g_{m3}/C_{1\alpha}C_{2\alpha}} \tag{5.42}$$

Equations (5.36)–(5.42) show that the transfer functions' sensitivity depends on α, FC value and g_m of OTA. Therefore, graphs need be plotted to observe the exact effect of various parameters.

5.3.2.3 Simulation results

Workability of proposed OTA based FOF is verified through SPICE simulations for $\alpha = 0.5$ and 0.9 with a center frequency of 1 kHz. The FC emulator of Fig. 2.1 is used for simulation. The frequency responses of FLPF and FBPF with FC of order 0.5 and 0.9 are shown in Figs. 5.11 and 5.12 respectively using the simulation settings of Table 5.7. It may be noted from Table 5.7 that since $k > 1$ and $\alpha < 2\delta/\pi$ therefore the stability criteria given in Table 5.6 is satisfied.

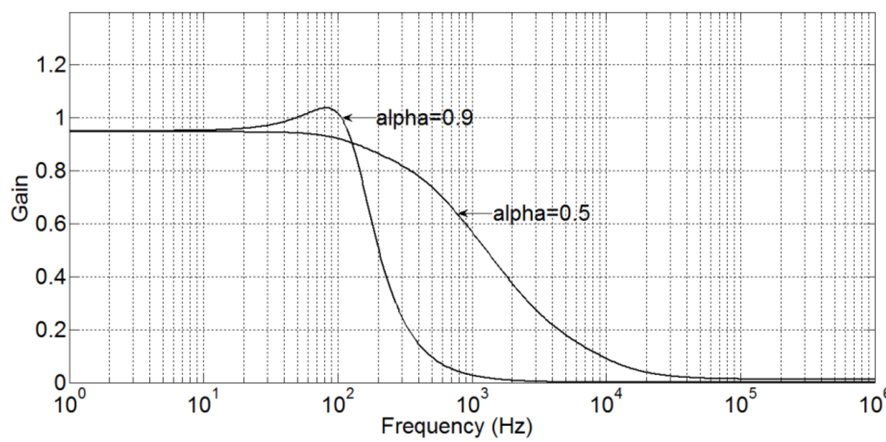

(a)

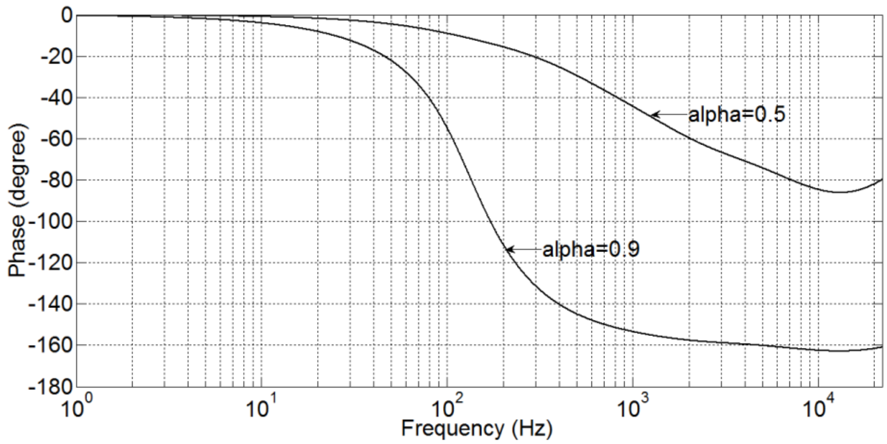

(b)

Fig. 5.11: Simulated frequency response **(a)** magnitude and **(b)** phase for proposed FLPF

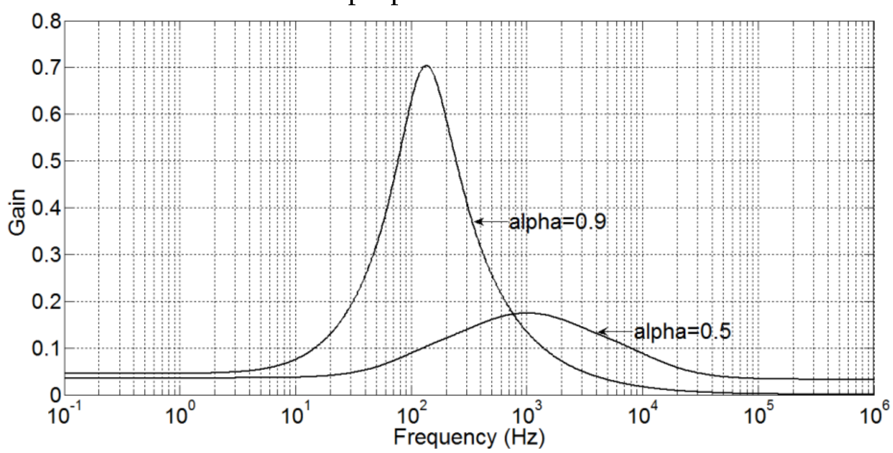

(a)

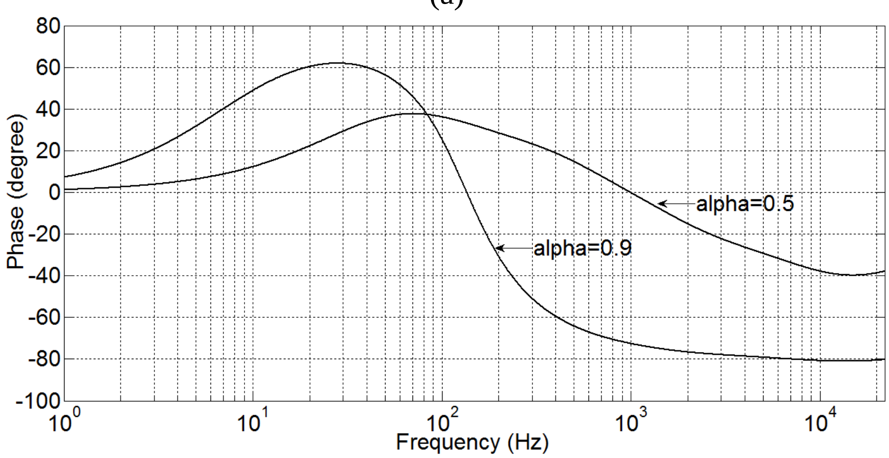

(b)

Fig.5.12: Simulated frequency response **(a)** magnitude and **(b)** phase for proposed FBPF

Table 5.7: Simulation setting for proposed FOF

Order (α)	$C_\alpha = C1\alpha = C2\alpha$ (μ℧/s$^\alpha$)	$I_{b1} = I_{b3}$ (μA)	I_{b2} (μA)	$g_{m1} = g_{m3}$ $(\mu A/V)$	g_{m2} $(\mu A/V)$	a_0	a_1	k	2δ/π
0.5	1	17.4	2.47	79.311	23.942	6290.235	23.942	43.894	1.096
0.9	0.382	98	57.73	165	134.7	186569.572	352.618	6	1.268

It is observed from Figs. 5.11(b) and 5.12(b) that right phase frequency exists only for FLPF of order 0.9 which is in sync with (5.24) and (5.25) respectively. Performance parameters for proposed FLPF and FBPF are listed in Tables 5.9 and 5.10 respectively. There is a close match between theoretical and simulated values. It is also found that the critical frequencies increase with decrease in order α.

Table 5.8: Performance parameters for FLPF for α = 0.5 and 0.9

Parameters Measured	**C_α =1μ℧/s$^\alpha$, α= 0.5**		**C_α =0.382μ℧/s$^\alpha$, α= 0.9**	
	Simulation Results	**Theoretical Results**	**Simulation Results**	**Theoretical Results**
$\lvert T(j\omega)^{2\alpha}_{FLPF}\rvert$ in pass-band	0.95	1	0.95	1
$\omega_{h(FLPF)}$ (Hz)	681	628	156.33	163.9 46
$\omega_{m(FLPF)}$ (Hz)	none	none	79.228	80.58

Table 5.9: Performance parameters for FBPF for α = 0.5 and 0.9

Parameters Measured	**C_α =1µ℧/s$^\alpha$, α= 0.5**		**C_α =0.382µ℧/s$^\alpha$, α= 0.9**	
	Simulation Results	**Theoretical Results**	**Simulation Results**	**Theoretical Results**
$\omega_{h1(FBPF)}$ (Hz)	211	224	76.77	75.37
$\omega_{h2(FBPF)}$ (Hz)	4.7k	4.47k	245	242
$\omega_{m(FBPF)}$ (Hz)	1.08k	1.001k	136	135
$\lvert T(j\omega_{(FBPF)})\rvert$ at $\omega_{m(FBPF)}$	-15.169dB	-15dB	0.705	0.723

The FLPF (α = 0.5 and 0.9) is tested for electronic tunability of half power frequency by varying I_{b2} while keeping the other settings same as listed in Table 5.7. The results are plotted in Fig. 5.13. The right phase frequency variation with respect to I_{b2} for proposed FLPF with α = 0.9 is plotted in Fig. 5.14. It may be observed that half power frequencies show downward trend with increasing bias current whereas the right phase frequency increases slightly with increasing bias current.

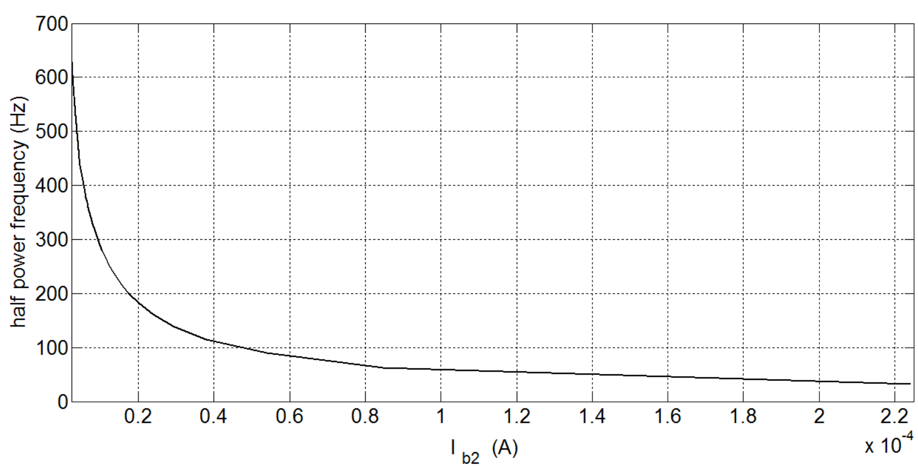

(a)

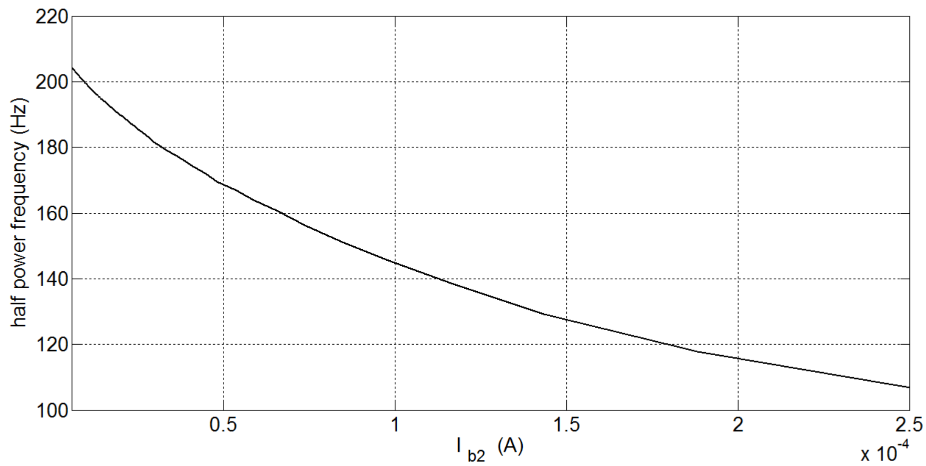

(b)

Fig. 5.13: Electronic tunability of half power frequency of proposed FLPF having α= **(a)** 0.5, **(b)** 0.9

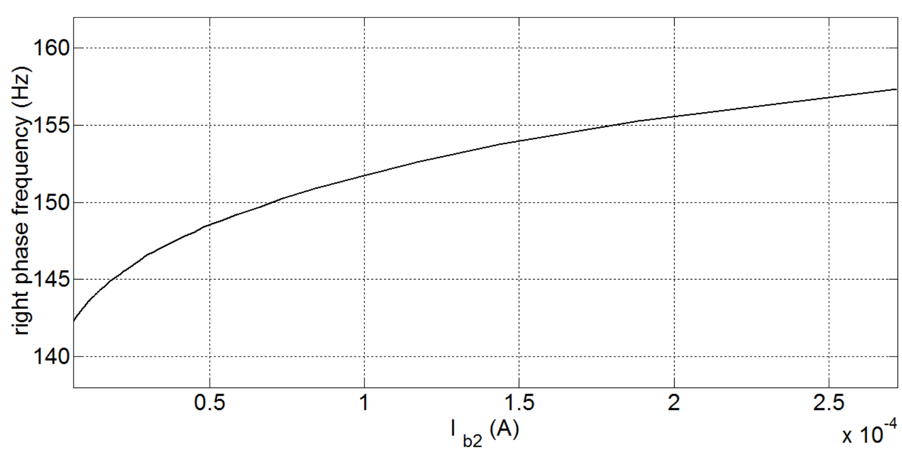

Fig. 5.14: Electronic tunability of right-phase frequency of proposed FLPF having $\alpha = 0.9$

Equations (5.36)–(5.42) are plotted in Fig.5.15 to investigate the effect of α, FC value and g_m of OTA on the transfer functions' sensitivity, wherein data are acquired at 1 kHz. The value of g_{m2} is taken as 25 µA/V (data 1), 50µA/V (data 2) and 80µA/V (data 3) for all plots except those given in Fig. 5.15e, i. The values of g_{m1} and g_{m3} are kept equal at 25µA/V (data 1), 50µA/V (data 2) and 80µA/V (data3) while observing sensitivity variation with respect to g_{m2} (Fig.5.15e, i). Sensitivities with respect to α, $C_{1\alpha}$ and $C_{2\alpha}$ are plotted while keeping g_{m1} and g_{m3} equal to 25μA/V and g_{m2} at 25μA/V. The values of α, $C_{1\alpha}$ and $C_{2\alpha}$ are kept at 0.5, 1 and 1 μ℧/s$^{\alpha}$ respectively, in all the plots for the cases where these parameter are not varied for observation. The transfer functions' sensitivity with respect to FC value and g_m of OTA remain well within unity while both FLPF and FBPF are sensitive to α variation.

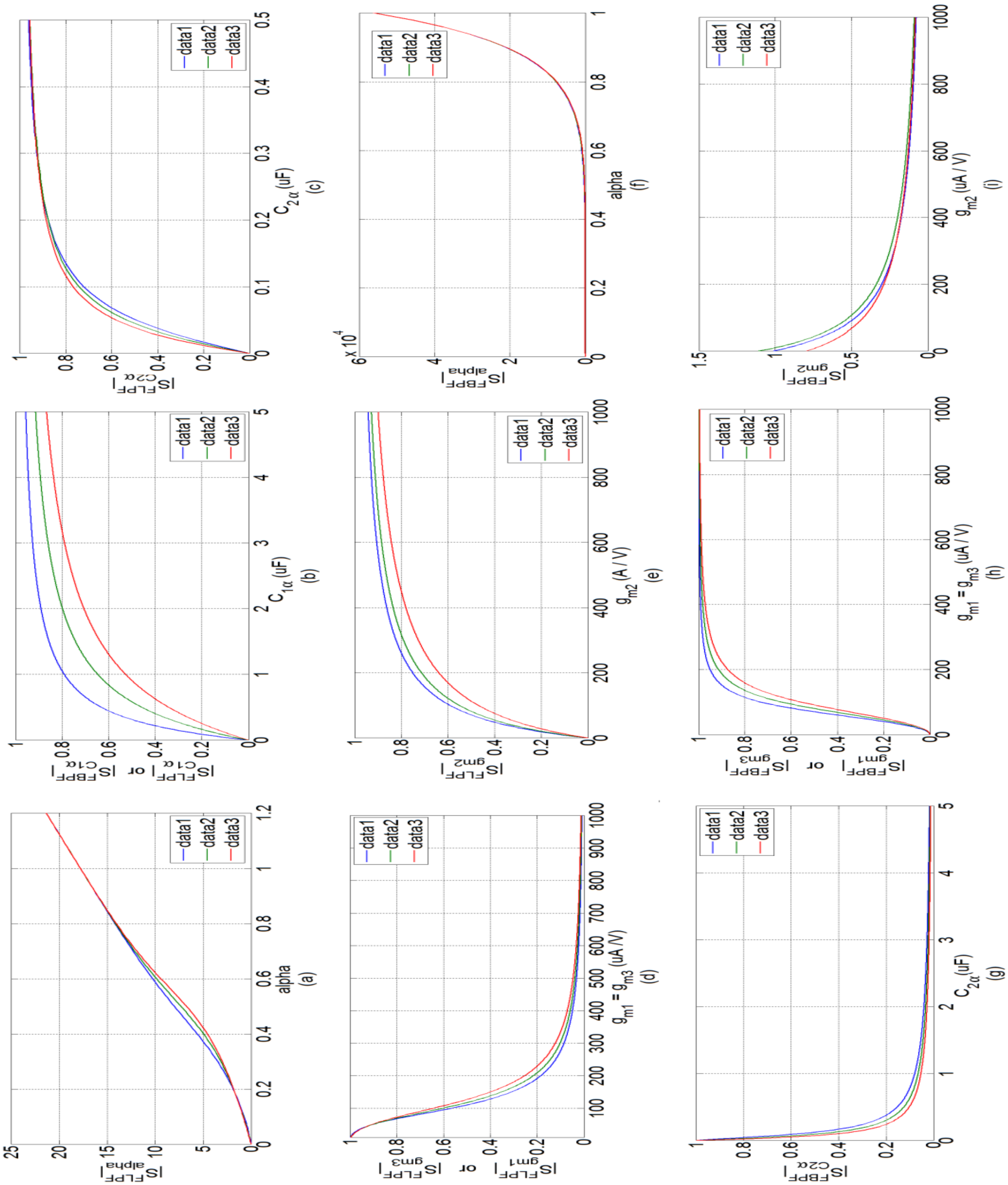

Fig. 5.15: Sensitivity: **(a)** $|S_{\alpha}^{FLPF}|$ versus α; **(b)** $\left|S_{C_{1\alpha}}^{FLPF}\right|$ versus $C_{1\alpha}$ and $\left|S_{C_{1\alpha}}^{FBPF}\right|$ versus $C_{1\alpha}$; **(c)** $\left|S_{C_{2\alpha}}^{FLPF}\right|$ versus $C_{2\alpha}$; **(d)** $\left|S_{g_{m1}=g_{m3}}^{FLPF}\right|$ versus $g_{m1}=g_{m3}$; **(e)** $\left|S_{g_{m2}}^{FLPF}\right|$versus g_{m2}; **(f)** $|S_{\alpha}^{FBPF}|$ versus α; **(g)** $\left|S_{C_{2\alpha}}^{FBPF}\right|$ versus $C_{2\alpha}$; **(h)** $\left|S_{g_{m1}=g_{m3}}^{FBPF}\right|$ versus $g_{m1} = g_{m3}$; **(i)** $\left|S_{g_{m2}}^{FBPF}\right|$ versus g_{m2}

5.4 Conclusion

In this chapter, two electronically tunable FOFs using OTAs are presented. These filters are obtained through generalization of first and second order filters. The realization of proposed FAPF and FLPF circuits are achieved from first order filter. Proposed FLPF and FBPF circuits are adaption of second order configuration in fractional domain. Mathematical formulations are outlined for various critical frequencies and transfer function sensitivities. Electronic tunability of filter parameters is achieved through bias current variation of OTA. The functionality of the proposed FOFs is verified through SPICE simulations by considering FC of orders 0.5 and 0.9. The FCs used in each configuration is designed around a centre frequency of 1 kHz. From various responses it is observed that the simulation and theoretical results are quite close for a wide range of frequencies. Electronic tunability of half power frequency and right-phase frequency is demonstrated by changing the bias currents of OTAs. The sensitivity of transfer functions with respect to various circuit parameters is also examined through simulations, and it is found that the values remain well within unity for most of the circuit parameters.

CHAPTER 6

REALIZATION OF CFOA BASED HIGHER ORDER FOFs

The contents and results of the following paper have been reported in this chapter:

[1] **R. Verma,** N. Pandey, R. Pandey, "CFOA based Low Pass and High Pass Fractional Step Filter Realizations", AEU- International Journal of Electronics and Communications, vol. 99, pp. 161-76, 2019. https://doi.org/10.1016/j.aeue.2018.11.032. (Elsevier) **Indexing: SCI, SCIE, SCOPUS; IF: 2.115**

6.1 Introduction

The essential use of a higher order filter is to provide a greater roll off/ attenuation rate in transition band. The attenuation rate in conventional n^{th} order integer filter is 20n dB/decade which puts a constraint on fine tuning of attenuation rate. By adopting the design methodology of a higher order filter in fractional domain the attenuation rate in transition band can be fine tuned as $(n+\alpha)$ order FOF provides an attenuation rate of $20(n+\alpha)$ dB/decade.

In literature two different methods are available to design a higher order FOFs- the first employs FOE in the integer order filter while the second relies on the substitution of Laplacian operator s^{α} by equivalent integer order approximation form. Chapters 4 and 5 described FOFs obtained using first method. This chapter is devoted to design of higher order i.e. $(n+\alpha)$ order FOFs using second method.

The designs based on second method follow a two step procedure: First a $(1+\alpha)$ order filter is designed based on the integer order rational approximations of fractional order operator using FBD approach. Next by cascading this $(1+\alpha)$ order FOF with an (n-1) integer order filter an $(n+\alpha)$ order FOF can be obtained. To illustrate this, and two filter configurations namely CFOA based $(5+\alpha)$ order Butterworth FLPF and FHPF are presented.

6.2 Design scheme

In this section, the design scheme (1+α) order FOF with Butterworth magnitude response is presented first followed by higher order FOFs realization scheme.

6.2.1 FLPF of (1+α) order

The general form of FLPF TF [34, 163] may be expressed as

$$H(s)_{FLPF}^{\alpha_1+\alpha_2} = \frac{k_1}{s^{\alpha_1+\alpha_2} + k_3 s^{\alpha_2} + k_2} \tag{6.1}$$

which represents a variety of transfer functions of fractional order filter. Considering α_1 and α_2 as (i) $1+\alpha = \alpha_1 + \alpha_2 = 2\beta$ (ii) $\alpha_1 = 1,\ \alpha_2 = \alpha$ $(0 < \alpha < 1)$ and (iii) $\alpha_2 = 1,\ \alpha_1 = \alpha\ (0 < \alpha < 1)$; the generalized TF of (6.1) leads to $(1+\alpha)$ order TFs of (6.2) – (6.4) which are classified as Type 1, Type 2 and Type 3 respectively.

Type 1:

$$H(s)_{FLPF}^{1+\alpha} = \frac{k_1}{s^{2\beta} + k_3 s^{\beta} + k_2} \tag{6.2}$$

Type 2:

$$H(s)_{FLPF}^{1+\alpha} = \frac{k_1}{s^{1+\alpha} + k_3 s^{\alpha} + k_2} \tag{6.3}$$

Type 3:

$$H(s)_{FLPF}^{1+\alpha} = \frac{k_1}{s^{1+\alpha} + k_3 s + k_2} \tag{6.4}$$

A detailed analysis of three types of TFs with Butterworth magnitude responses is presented in [34, 162] wherein MATLAB optimization tool is used to determined coefficients ($k_1,\ k_2,\ k_3$). It is shown that the magnitude responses of TFs differ in terms of least squares error (LSE), stability and 3dB frequency. Magnitude response of Type 2 TF is closest to Butterworth response over widest 3 dB frequency ranges and is suitable over others for higher order FLPF realization [34].

Considering Type 2 TF of (1+α) order FLPF to approximate Butterworth response with scaling frequency of $\omega_0 = 1/\tau$, (6.3) may be written as [61]

$$H(s)_{FLPF}^{1+\alpha} = \frac{k_1}{(s\tau)^{1+\alpha} + k_3 (s\tau)^{\alpha} + k_2} \tag{6.5}$$

The coefficients k_i*'s* may be obtained by optimization method [34], numerical search method [70], Gravitational Search Algorithm (GSA) approach [55], Laguerre based approach [120], numerical least squares optimization method [162], Real coded Genetic Algorithm (RGA) [163] and Particle Swarm Optimization (PSO) [164]. This work considers the coefficients given in [70] which are reproduced in (6.6) for ready reference.

$$k_1 = 1$$
$$k_2 = 0.2937\alpha + 0.71216$$
$$k_3 = 1.068\alpha^2 + 0.161\alpha + 0.3324 \tag{6.6}$$

The CFE approximation is one of the methods used to express $(s\tau)^\alpha$ [26]. The order of approximation affects frequency response. A comparison study shows that 4th order approximation has a wider frequency range than 2nd order; however, the number of elements used for realization of $(s\tau)^\alpha$ is more [54]. Here, 2nd order approximation of $(s\tau)^\alpha$ as given in (6.7) is considered.

$$(s\tau)^\alpha = \frac{(\alpha^2 + 3\alpha + 2)(s\tau)^2 + (8 - 2\alpha^2)(s\tau) + (\alpha^2 - 3\alpha + 2)}{(\alpha^2 - 3\alpha + 2)(s\tau)^2 + (8 - 2\alpha^2)(s\tau) + (\alpha^2 + 3\alpha + 2)} \tag{6.7}$$

Combining (6.7) and (6.5) gives

$$H(s)_{FLPF}^{1+\alpha} = \frac{a_2 s^2 + a_1 s + a_0}{s^3 + b_2 s^2 + b_1 s + b_0} \tag{6.8}$$

where

$$a_2 = \frac{1}{\tau}\frac{(\alpha^2 - 3\alpha + 2)}{(\alpha^2 + 3\alpha + 2)}k_1$$

$$a_1 = \frac{1}{\tau^2}\frac{(8 - 2\alpha^2)}{(\alpha^2 + 3\alpha + 2)}k_1$$

$$a_0 = \frac{1}{\tau^3}k_1$$

$$b_2 = \frac{1}{\tau}\frac{(k_2+k_3-2)\alpha^2 - 3(k_2-k_3)\alpha + (8+2k_2+2k_3)}{(\alpha^2+3\alpha+2)}$$

$$b_1 = \frac{1}{\tau^2}\frac{(1-2k_2-2k_3)\alpha^2 - 3\alpha + (2+8k_2+8k_3)}{(\alpha^2+3\alpha+2)}$$

$$b_0 = \frac{1}{\tau^3}\frac{(k_2+k_3)\alpha^2 + 3(k_2-k_3)\alpha + 2(k_2+k_3)}{(\alpha^2+3\alpha+2)}$$

(6.9)

The TF of (6.8) can be realized using FBD approach. The derived FLF topology is shown in Fig. 6.1 which uses one lossy integrator and two lossless integrators.

The TF of Fig. 6.1 is computed as

$$H(s)_{FLPF}^{1+\alpha} = \frac{\frac{A_1}{\tau_1}s^2 + \frac{A_2}{\tau_1\tau_2}s + \frac{A_3}{\tau_1\tau_2\tau_3}}{s^3 + \frac{1}{\tau_1}s^2 + \frac{1}{\tau_1\tau_2}s + \frac{1}{\tau_1\tau_2\tau_3}}$$

(6.10)

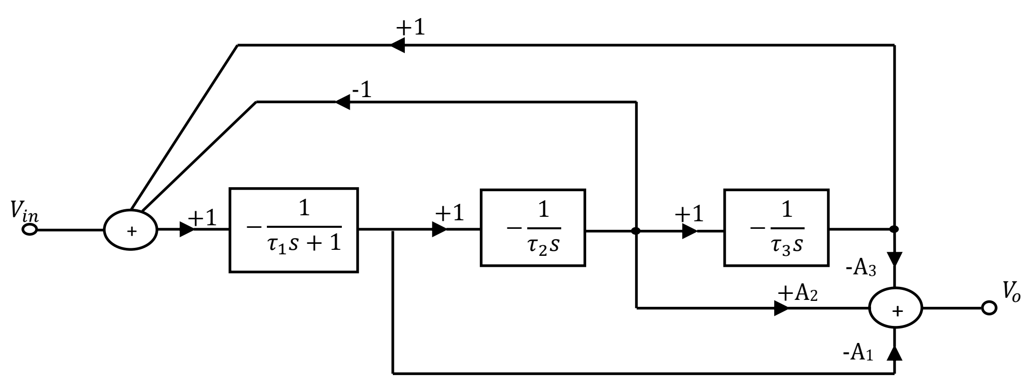

Fig. 6.1: FBD of integer (3rd) order FLF for (1+α) order FLPF

Equating the TFs of (6.8) and (6.10), the coefficients used in (6.10) are determined as

$$\tau_1 = 1/b_2, \quad \tau_2 = b_2/b_1, \quad \tau_3 = b_1/b_0$$

$$A_1 = a_2/b_2, \quad A_2 = a_1/b_1, \quad A_3 = a_0/b_0 \tag{6.11}$$

6.2.2 Fractional order high-pass filter (FHPF) of (1+α) order

The TF of FHPF may be obtained by applying frequency transformation i.e. $(s\tau) \rightarrow 1/(s\tau)$ to (6.5). The resultant TF is given by (6.12).

$$H(s)_{FHPF}^{1+\alpha} = \frac{k_1(s\tau)^{1+\alpha}}{k_2(s\tau)^{1+\alpha} + k_3(s\tau) + 1} \tag{6.12}$$

Using the CFE approximation of $(s\tau)^{\alpha}$ as given in (6.7) the (6.12) modifies to

$$H(s)_{FHPF}^{1+\alpha} = \frac{a_2 s^3 + a_1 s^2 + a_0 s}{s^3 + b_2 s^2 + b_1 s + b_0} \tag{6.13}$$

The FBD approach based FLF realization of (6.13) is shown in Fig. 6.2 and the corresponding TF is expressed as

$$H(s)_{FHPF}^{1+\alpha} = \frac{A_1 s^3 + \frac{A_1 + A_2}{\tau_1} s^2 + \frac{A_3}{\tau_1 \tau_2} s}{s^3 + \frac{1}{\tau_1} s^2 + \frac{1}{\tau_1 \tau_2} s + \frac{1}{\tau_1 \tau_2 \tau_3}} \tag{6.14}$$

It may be observed from Fig. 6.2 that the FHPF topology is also realized using one lossy and two lossless integrators

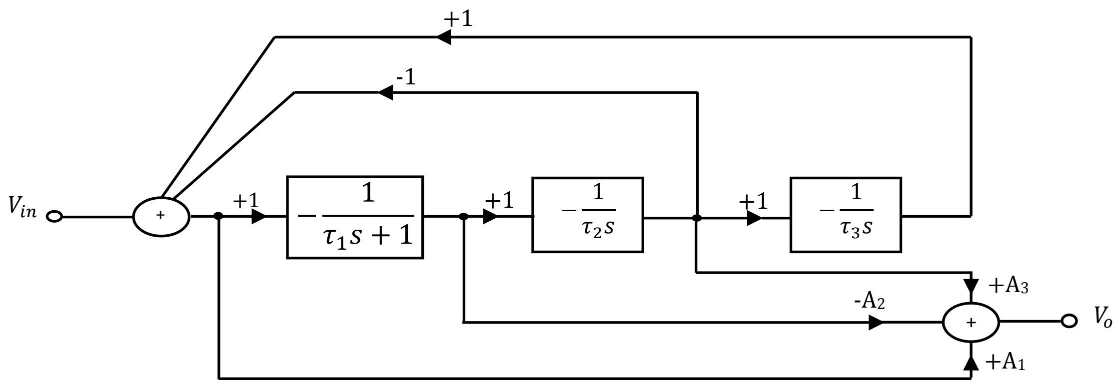

Fig. 6.2: FBD of integer (3rd) order FLF for (1+α) order FHPF

Solving (6.12), (6.13) and (6.14), the relations between various coefficients are found as

$$a_2 = A_1 = \frac{k_1(\alpha^2+3\alpha+2)}{k_2(\alpha^2+3\alpha+2)+k_3(\alpha^2-3\alpha+2)}$$

$$a_1 = \frac{A_1+A_2}{\tau_1} = \frac{1}{\tau}\frac{k_1(8-2\alpha^2)}{k_2(\alpha^2+3\alpha+2)+k_3(\alpha^2-3\alpha+2)}$$

$$a_0 = \frac{A_3}{\tau_1\tau_2} = \frac{1}{\tau^2}\frac{k_1(\alpha^2-3\alpha+2)}{k_2(\alpha^2+3\alpha+2)+k_3(\alpha^2-3\alpha+2)}$$

$$b_2 = \frac{1}{\tau_1} = \frac{1}{\tau}\frac{(k_2+k_3)(8-2\alpha^2)+(\alpha^2-3\alpha+2)}{k_2(\alpha^2+3\alpha+2)+k_3(\alpha^2-3\alpha+2)}$$

$$b_1 = \frac{1}{\tau_1\tau_2} = \frac{1}{\tau^2}\frac{k_2(\alpha^2-3\alpha+2)+k_3(\alpha^2+3\alpha+2)+(8-2\alpha^2)}{k_2(\alpha^2+3\alpha+2)+k_3(\alpha^2-3\alpha+2)}$$

$$b_0 = \frac{1}{\tau_1\tau_2\tau_3} = \frac{1}{\tau^3}\frac{(\alpha^2+3\alpha+2)}{k_2(\alpha^2+3\alpha+2)+k_3(\alpha^2-3\alpha+2)}$$

(6.15)

6.2.3 Sensitivity Analysis

The sensitivity analysis of proposed FOFs is presented in this section.

6.2.3.1 Sensitivity analysis of FLPF

The sensitivity expressions for the TF of (1+α) order FLPF in (6.8) with respect to coefficients a_2, a_1, a_0, b_2, b_1, b_0 are computed as:

$$S_{a_2}^{H(s)_{FLPF}^{1+\alpha}} = \frac{a_2 s^2}{N_1(s)}\ , \quad S_{a_1}^{H(s)_{FLPF}^{1+\alpha}} = \frac{a_1 s}{N_1(s)}\, , \quad S_{a_0}^{H(s)_{FLPF}^{1+\alpha}} = \frac{a_0}{N_1(s)}$$

$$S_{b_2}^{H(s)_{FLPF}^{1+\alpha}} = -\frac{b_2 s^2}{D_1(s)}\ , \quad S_{b_1}^{H(s)_{FLPF}^{1+\alpha}} = -\frac{b_1 s}{D_1(s)}\ , \quad S_{b_0}^{H(s)_{FLPF}^{1+\alpha}} = -\frac{b_0}{D_1(s)}$$

(6.16)

where $N_1(s)$ and $D_1(s)$ correspond to numerator and denominator of (6.8) respectively.

Using (6.8) and (6.10) the coefficients a_2, a_1, a_0, b_2, b_1, b_0 may be expressed in terms of gains and time constants (A_i and τ_i $(i = 1, 2, 3)$) as

$$a_2 = \frac{A_1}{\tau_1}, \quad a_1 = \frac{A_2}{\tau_1 \tau_2}, \quad a_0 = \frac{A_3}{\tau_1 \tau_2 \tau_3}, \quad b_2 = \frac{1}{\tau_1}, \quad b_1 = \frac{1}{\tau_1 \tau_2}, \quad b_0 = \frac{1}{\tau_1 \tau_2 \tau_3}$$

(6.17)

and the sensitivities of a_j's and b_j's (j = 0,1,2) are computed respectively as

$$S^{a_2}_{A_2,A_3,\tau_{2,}\tau_3} = S^{a_1}_{A_1,A_3,\tau_3} = S^{a_0}_{A_1,A_2} = 0$$

$$S^{a_2}_{A_1} = S^{a_1}_{A_2} = S^{a_0}_{A_3} = 1$$

$$S^{a_2}_{\tau_1} = S^{a_1}_{\tau_1,\tau_2} = S^{a_0}_{\tau_{1,}\tau_2\tau_3} = -1 \tag{6.18}$$

$$S^{b_2}_{A_1,A_2,A_3,\tau_{2,}\tau_3} = S^{b_1}_{A_1,A_2,A_3,\tau_3} = S^{b_0}_{A_1,A_{2,}A_3} = 0$$

$$S^{b_2}_{\tau_1} = S^{b_1}_{\tau_1,\tau_2} = S^{b_0}_{\tau_1,\tau_2,\tau_3} = -1 \tag{6.19}$$

Thus, the sensitivities of coefficients a_j *and* b_j *(j= 0, 1, 2)* with respect to gains and time constants are within unity and may be considered low.

6.2.3.2 Sensitivity analysis of FHPF

The sensitivities of $H(s)^{1+\alpha}_{FHPF}$ with respect to its coefficients are computed as:

$$S^{H(s)^{1+\alpha}_{FHPF}}_{a_2} = \frac{a_2 s^3}{N_2(s)}\ ,\ S^{H(s)^{1+\alpha}_{FHPF}}_{a_1} = \frac{a_1 s^2}{N_2(s)}\ ,\quad S^{H(s)^{1+\alpha}_{FHPF}}_{a_0} = \frac{a_0 s}{N_2(s)}$$

$$S^{H(s)^{1+\alpha}_{FHPF}}_{b_2} = -\frac{b_2 s^2}{D_2(s)}\ ,\quad S^{H(s)^{1+\alpha}_{FHPF}}_{b_1} = -\frac{b_1 s}{D_2(s)}\ ,\quad S^{H(s)^{1+\alpha}_{FHPF}}_{b_0} = -\frac{b_0}{D_2(s)} \tag{6.20}$$

where $N_2(s)$ and $D_2(s)$ represent numerator and denominator of (6.13).

Using (6.13) and (6.14) the coefficients a_j *and* b_j *(j= 0, 1, 2)* may be expressed in terms of gains and time constants (A_i and τ_i $(i = 1, 2, 3)$) as

$$a_2 = A_1, \quad a_1 = \frac{A_1 + A_2}{\tau_1}, \quad a_0 = \frac{A_3}{\tau_1 \tau_2}, \quad b_2 = \frac{1}{\tau_1}, \quad b_1 = \frac{1}{\tau_1 \tau_2}, \quad b_0 = \frac{1}{\tau_1 \tau_2 \tau_3} \tag{6.21}$$

Various sensitivities of a_j's (j = 0, 1, 2) are computed as

$$S^{a_2}_{A_2, A_3, \tau_1, \tau_2, \tau_3} = S^{a_1}_{A_3, \tau_2, \tau_3} = S^{a_0}_{A_1, A_2, \tau_3} = 0$$

$$S^{a_2}_{A_1} = S^{a_0}_{A_3} = 1\,, \quad S^{a_1}_{A_1} = \frac{A_1}{A_1 + A_2}\,, \quad S^{a_1}_{A_2} = \frac{A_2}{A_1 + A_2}$$

$$S^{a_1}_{\tau_1} = S^{a_0}_{\tau_1, \tau_2} = -1 \tag{6.22}$$

and the sensitivities of b_j *(j= 0, 1, 2)* remain same as those in case of FLPF (6.19).

Thus, the sensitivities of coefficients a_j *and* b_j *(j= 0, 1, 2)* with respect to gains and time constants always remain within unity and may be considered to be low.

6.3 Higher Order fractional order filters

From the stability point of view, the design of higher order FOF (order = n+α > 2) requires Butterworth approach for maximally flat response. Higher order (n+α > 2) FOF with maximally flat response may be obtained by cascading (1+α) order FLPF (FHPF) of Section 6.2.1 (6.2.2) with Butterworth LP (HP) filter of integer order i.e. (n-1). Therefore, the Butterworth response of (n+α) order FOF can be defined [61] as follows

$$H(s)_{FLPF}^{n+\alpha} = \frac{H(s)_{FLPF}^{1+\alpha}}{B(s)_{LPF}^{n-1}} \tag{6.23}$$

$$H(s)_{FHPF}^{n+\alpha} = \frac{H(s)_{FHPF}^{1+\alpha}}{B(s)_{HPF}^{n-1}} \tag{6.24}$$

where $B(s)_{LPF}^{n-1}$, $B(s)_{HPF}^{n-1}$ are (n-1) order Butterworth polynomials for LP and HP filters, respectively.

6.4 Proposed Designs

In this section CFOA based realizations of design schemes discussed in section 6.2 are presented. The (1+α) order FLPF and FHPF implementations are presented first followed by CFOA based realizations of 4th order Butterworth LP and HP filters designed using leapfrog structure. Subsequently, realization of CFOA based (5+α) order FOF may be obtained by cascading of (1+α) order FOF with 4th order filters.

6.4.1 Fractional order filters using CFOA

The proposed CFOA based realization of FBD of Fig. 6.1, representing (1+α) order FLPF, is depicted in Fig. 6.3. The CFOA1 performs the addition and lossy integration operations. The input and feedback with positive transfers are connected to X terminal through resistors and feedback with negative transfer is connected to Z terminal through resistor. The inverting integrators are realized by CFOA2 and CFOA3 by placing a resistor and capacitor to their corresponding X and Z terminals. Finally, CFOA4 combines the feedforward transfers where the positive (negative) gains are obtained via resistors placed between specific node and Z(X) terminal.

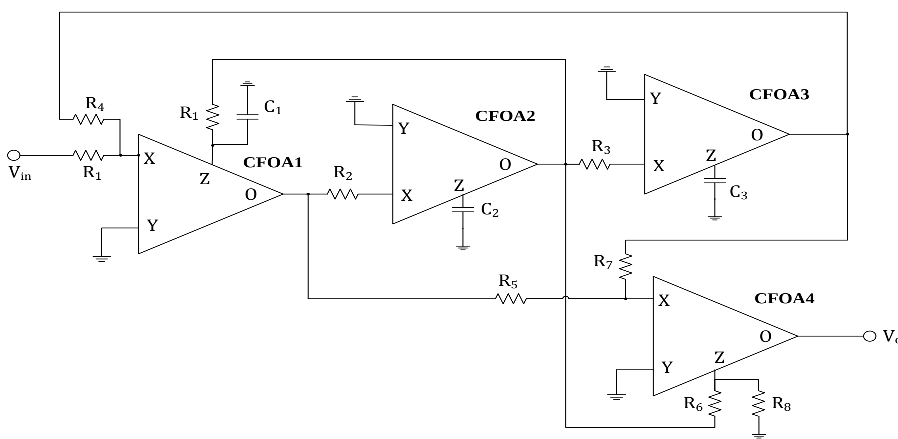

Fig. 6.3: Proposed CFOA based realization of (1+α) order FLPF

The routine analysis of the circuit of Fig. 6.3 provides (assuming $R_1 = R_4$)

$$\frac{V_o}{V_{in}} = \frac{\frac{1}{R_1C_1}\cdot\frac{R_6R_8}{R_5(R_6+R_8)}s^2 + \frac{1}{R_1C_1R_2C_2}\cdot\frac{R_8}{R_6+R_8}s + \frac{1}{R_1C_1R_2C_2R_3C_3}\cdot\frac{R_6R_8}{R_7(R_6+R_8)}}{s^3 + \frac{1}{R_1C_1}s^2 + \frac{1}{R_1C_1R_2C_2}s + \frac{1}{R_1C_1R_2C_2R_3C_3}} \tag{6.25}$$

The comparison of (6.25) with general topology expressed in (6.10) gives

$$\tau_i = R_iC_i, \quad \mathrm{i} = 1,2,3$$

$$A_1 = \frac{R_6R_8}{R_5(R_6+R_8)}, \qquad A_2 = \frac{R_8}{R_6+R_8}, \quad A_3 = \frac{R_6R_8}{R_7(R_6+R_8)} \tag{6.26}$$

A close observation of FBDs of Figs. 6.1 and 6.2 reveals that these two differ in feedforward connections only. The former uses connection after lossy integrator while the later relies on connection from a node prior to lossy integration operation. This requirement translates into simply placing an additional CFOA and few resistors in Fig. 6.3 which leads to increase in overall active blocks count. The same operation may also be obtained by simply placing a parallel resistor - capacitor combination between lossy integrator output and X terminal of CFOA4. The CFOA implementation, of FBD of (1+α) order FHPF (Fig. 6.2), so obtained is placed as Fig. 6.4.

The circuit analysis of Fig. 6.4 yields following TF

$$H(s) = \frac{\frac{R_6R_8}{R_1(R_6+R_8)}s^3 + \frac{1}{R_1C_1}\cdot\frac{R_6R_8}{R_5(R_6+R_8)}s + \frac{1}{R_1C_1R_2C_2}\cdot\frac{R_8}{R_6+R_8}s}{s^3 + \frac{1}{R_1C_1}s^2 + \frac{1}{R_1C_1R_2C_2}s + \frac{1}{R_1C_1R_2C_2R_3C_3}} \tag{6.27}$$

Comparing (6.10) and (6.27) gives the following relation between coefficients

$$\tau_i = R_iC_i, \quad \mathrm{i} = 1,2,3$$

$$A_1 = \frac{R_6R_8}{R_1(R_6+R_8)}, \quad A_1 + A_2 = \frac{R_6R_8}{R_5(R_6+R_8)}, \quad A_3 = \frac{R_8}{R_6+R_8} \tag{6.28}$$

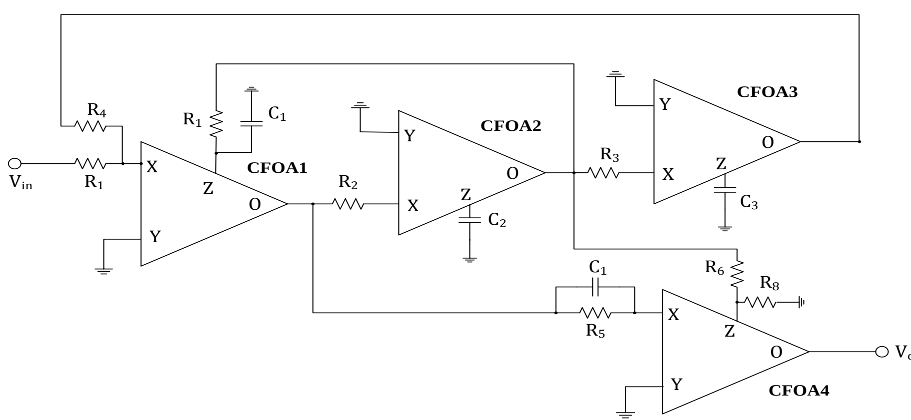

Fig. 6.4: Proposed CFOA based realization of (1+α) order FHPF

6.4.2 Realization of 4th order LP and HP Butterworth filters using CFOA

To realize CFOA based 4th order LP Butterworth filter, normalized ladder of Fig. 6.5 (a) is considered. Adopting the method outlined in [165], the leapfrog structure of Fig. 6.5 (b) is obtained which uses two lossy and two lossless integrators. Proposed CFOA based realization of Fig. 6.5 (b) is shown in Fig. 6.5 (c) which employs 4 CFOAs, 9 resistors and 4 capacitors. Applying frequency transformation (i.e. $s \rightarrow 1/s$) to normalized 4th order LP Butterworth filter a normalized 4th order HP Butterworth filter may be obtained. The corresponding CFOA based realization is given in Fig. 6.5 (d). It is worth mentioning that CFOA based 3rd and 4th order LP/HP filters are available in literature [166]. These filters are designed using multiple loop feedback (MLF) such as FLF and IFLF configurations. The FLF approach employs more ABBs than those used in leapfrog method [167]. Moreover, the leapfrog configuration enjoys minimum sensitivity compared to others MLFs [168].

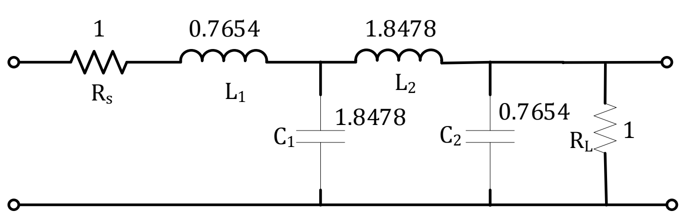

(a)

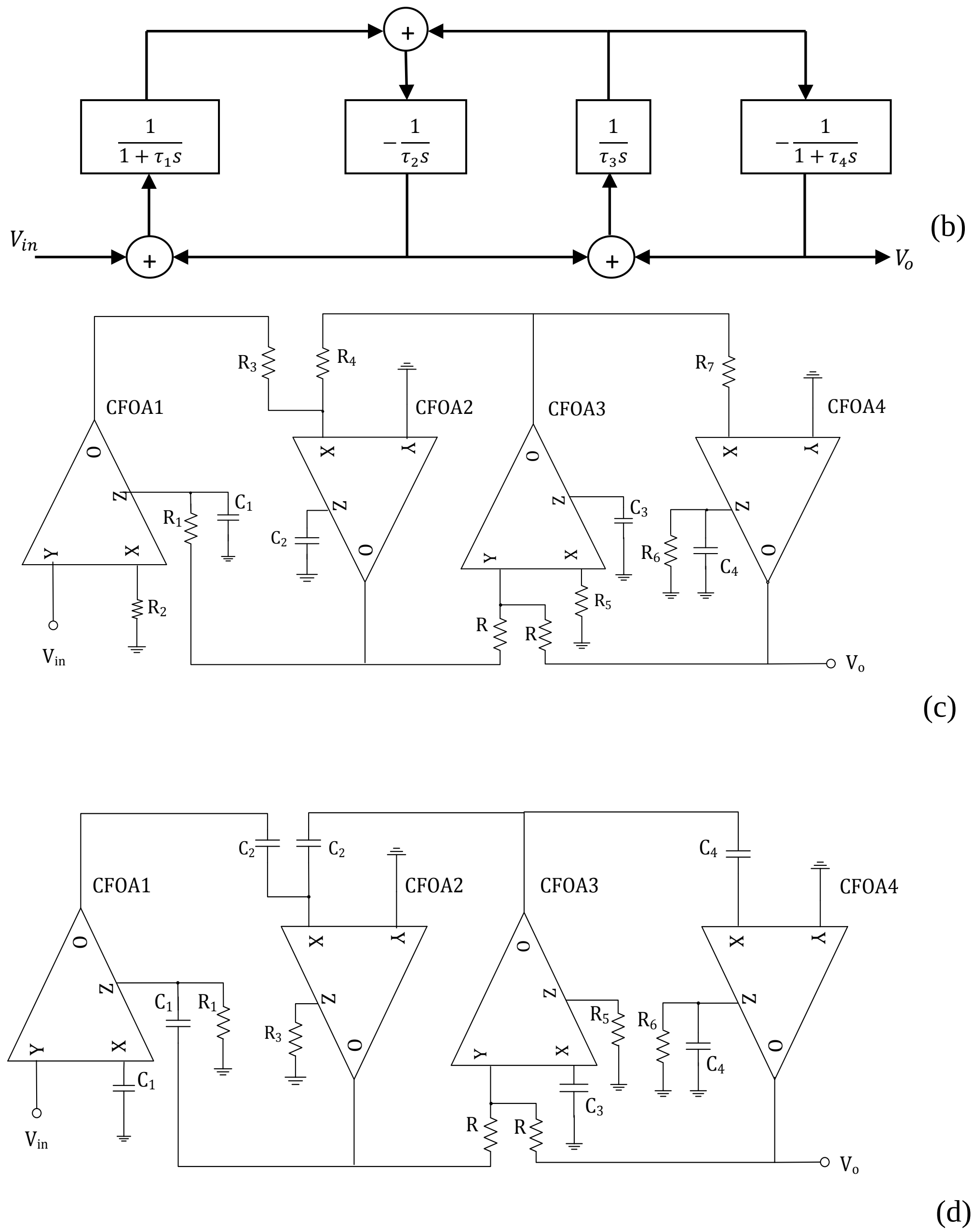

Fig. 6.5: The 4th order Butterworth LP filter **(a)** Normalized configuration **(b)** leapfrog configuration **(c)** Proposed CFOA based realization (R_1= R_2, R_3= R_4, R_6= R_7, τ_1=R_1C_1, τ_2=R_3C_2, τ_3=2.(R_5C_3), τ_4=R_6C_4) and its **(d)** Frequency transformed HP

6.4.3 Stability analysis

In this section stability analysis of $(n + \alpha)$ order FOFs is carried out using the root-locus technique for FO linear system. The transformation of *s*-plane defined for integer order linear system into fractional domain s^{α} plane changes the region of stability from $\pm \pi/2$ to $\pm \alpha\pi/2$ and non-physical region from $\pm \pi$ to $\pm \alpha\pi$ [11, 12]. The stability of proposed FOFs can be examined by considering the characteristic equation of (6.5) defining TF of $(1 + \alpha)$ order FLPF/ FHPF along with left half poles of Butterworth polynomial of normalized 4th order LP/ HP.

6.5 Functional Verification

In this section, the functionality of proposed FOFs is examined through both simulation and experimentation.

6.5.1 Simulation Results

The workability of proposed higher order FOFs is examined through SPICE simulation using macro model of CFOA IC (AD844AN). The supply voltage used is ± 10V. The performance of proposed circuits is examined at 1 kHz half power frequency. The components value for proposed $((1+\alpha);\ (\alpha = 0.25, 0.5 \text{ and } 0.75))$ order FLPF and FHPF are computed and listed in Table 6.1.

Table 6.1: Circuit components values of proposed FLPFs and FHPFs of (1+α) order filters

Circuit	Filter Order	$R_1 = R_4$ (kΩ)	R_2 (kΩ)	C_1 (nF)	C_2 (nF)	R_3 (kΩ)	C_3 (nF)	R_5 (kΩ)	R_6 (kΩ)	R_7 (kΩ)	R_8 (kΩ)
FLPF (Fig. 6.3)	1.25	56	56	0.788	2.63	100	6.26	100.033	18.015	12.824	46
	1.5	56	56	0.97	2.47	100	5.243	255.692	29.89	17.823	46
	1.75	56	56	1.12	2.49	100	4.615	914.83	47.462	23.38	46
FHPF (Fig. 6.4)	1.25	4.502	18.22	8.987	9.439	45	12.754	6.324	35.116	None	5.22
	1.5	4.829	18.22	10	10.04	45	10.08	7.955	69.209	None	5.22
	1.75	5.091	18.22	10.78	9.97	45	8.994	10.335	199.208	None	5.22

Simulated frequency responses for FLPF and FHPF with component setting of Table 6.1 are shown in Figs. 6.6 and 6.7 respectively. The FLPF responses from (6.5) and (6.8) are also plotted in Fig. 6.6 and are designated as ideal and approximated respectively. Same notation is adopted for FHPF responses depicted in Fig. 6.7. The stop-band attenuation slopes of simulated, approximated and ideal FLPF having order 1.25, 1.5 and 1.75 are (-24.03 dB/decade, -24.867 dB/decade, -25 dB/decade), (-29.66 dB/decade, -30.745 dB/decade, -30 dB/decade) and (-34.11 dB/decade, -34.85 dB/decade, -35 dB/decade) respectively. Stop-band attenuation rates of simulated, approximated and ideal FHPF having order 1.25, 1.5 and 1.75 are (24.06 dB/decade, 24.2 dB/decade, 25 dB/decade), (29.09 dB/decade, 30.5 dB/decade, 30 dB/decade) and (34.05 dB/decade, 35.03 dB/decade, 35 dB/decade) respectively. It may be noted that simulated, approximated and ideal stop band attenuations for FLPF and FHPF are in close agreement within 3 decades of frequency band. The deviation beyond this frequency band may be attributed to limitation of validity range of 2nd order approximation form for $(s\tau)^{\alpha}$ is restricted to about 3 to 4 decades of operating frequency [21].

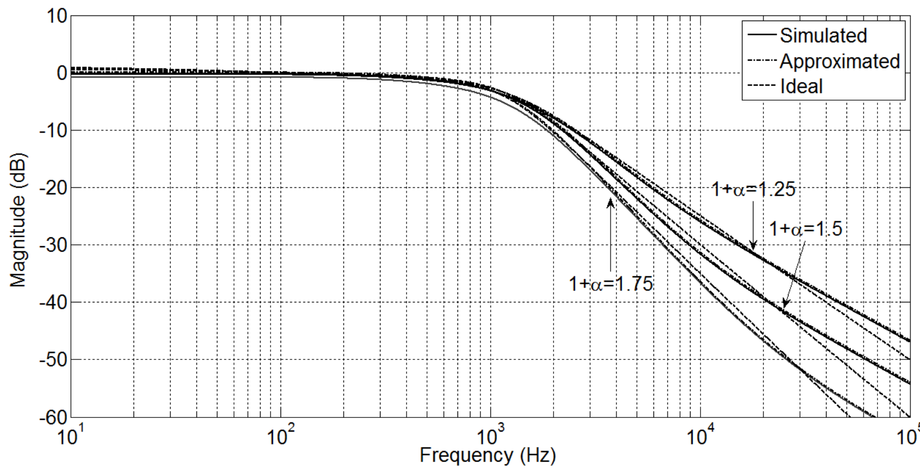

(a)

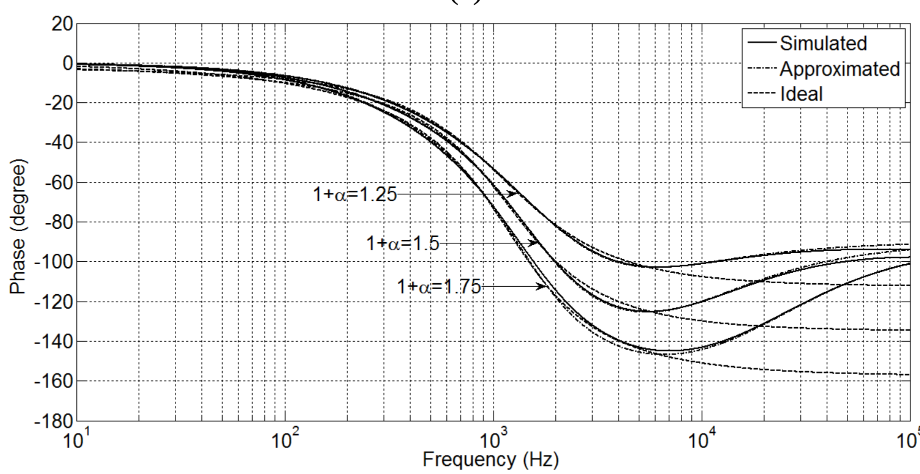

(b)

Fig. 6.6: Frequency response of proposed 1.25, 1.5 and 1.75 order FLPF **(a)** Magnitude **(b)** Phase responses

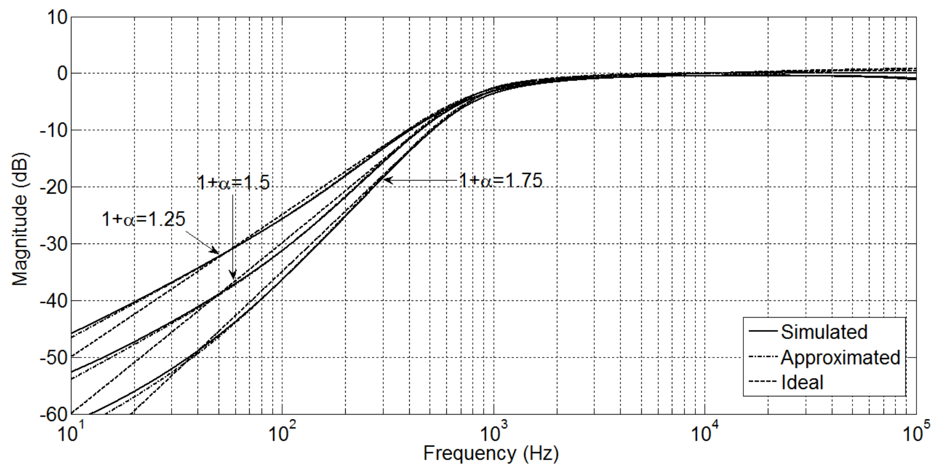

(a)

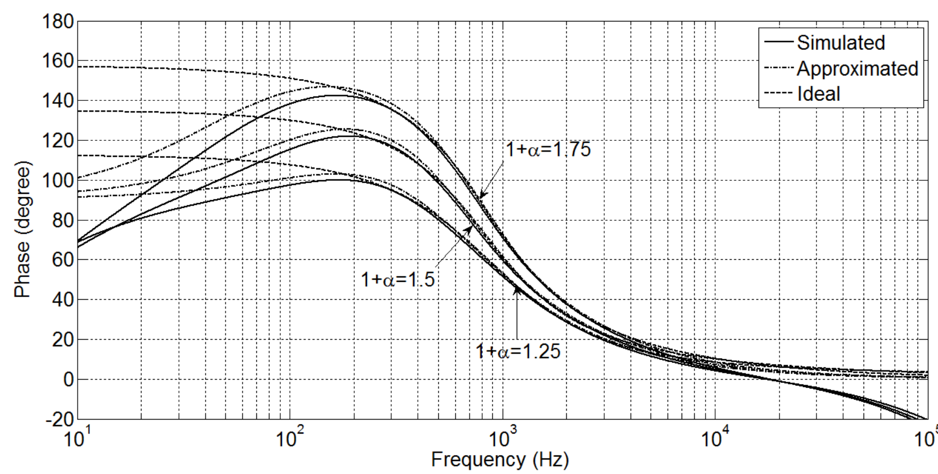

(b)

Fig. 6.7: Frequency response of proposed 1.25, 1.5 and 1.75 order FHPF **(a)** Magnitude **(b)** Phase responses

The component values for proposed 4th order LP and HP Butterworth filters of Fig. 6.5 are computed for half power frequency of 1 kHz as given in Table 6.2. Simulated frequency responses for proposed 4th order LP, HP Butterworth filters and corresponding theoretical counterparts are shown in Figs. 6.8 and 6.9. The simulated stop-band attenuation slopes of 4th order LP and HP are observed to be

-78.3 dB/decade and 78.67 dB/decade respectively against the theoretical values are -80 dB/decade and 80 dB/decade.

Table 6.2: Circuit components values of proposed 4th order LP and HP

Filter Type	R_1 (kΩ)	R_2 (kΩ)	R_3 (kΩ)	R_4 (kΩ)	R_5 (kΩ)	R_6 (kΩ)	R_7 (kΩ)	$C_1 = C_2 = C_3 = C_4$ (nF)
LP	1.2184	1.2184	2.9417	2.9417	1.4709	1.2184	1.2184	100
HP	20.7975	None	8.6148	None	17.229	20.7985	None	10

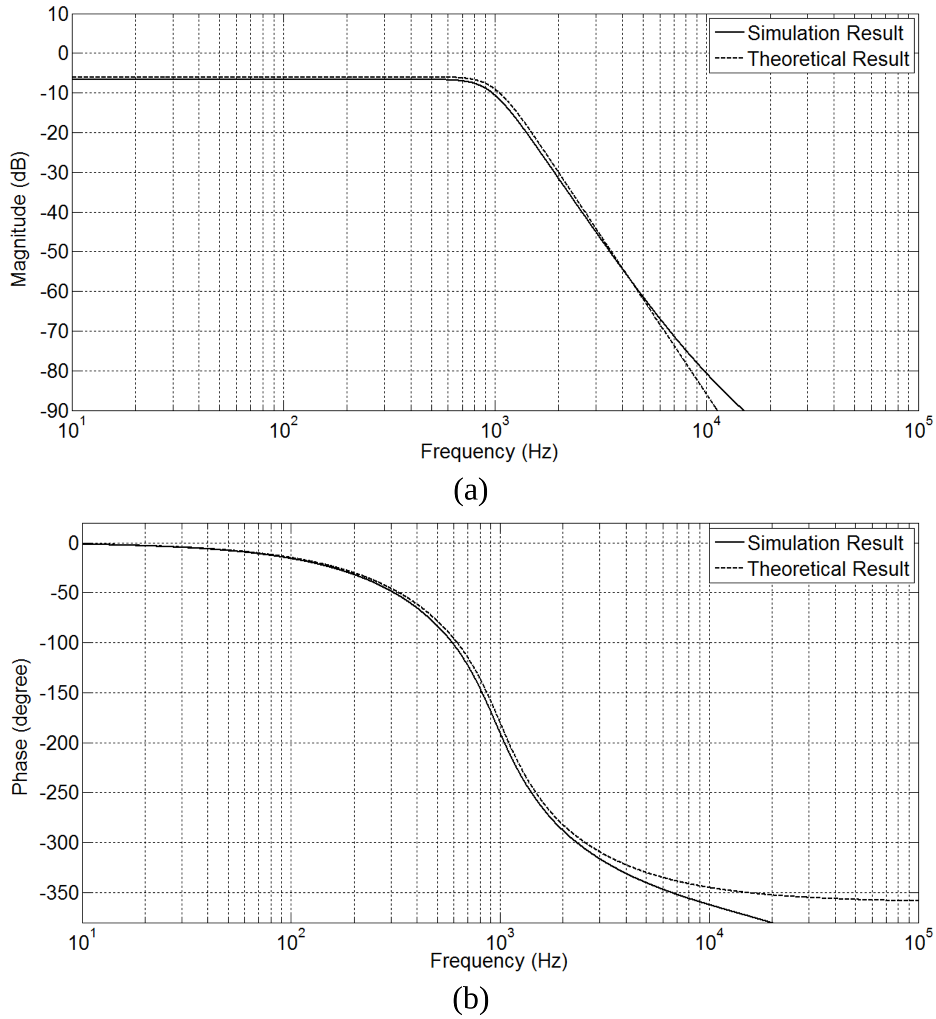

Fig. 6.8: Frequency response of proposed 4th order LP Butterworth filter **(a)** Magnitude **(b)** Phase responses

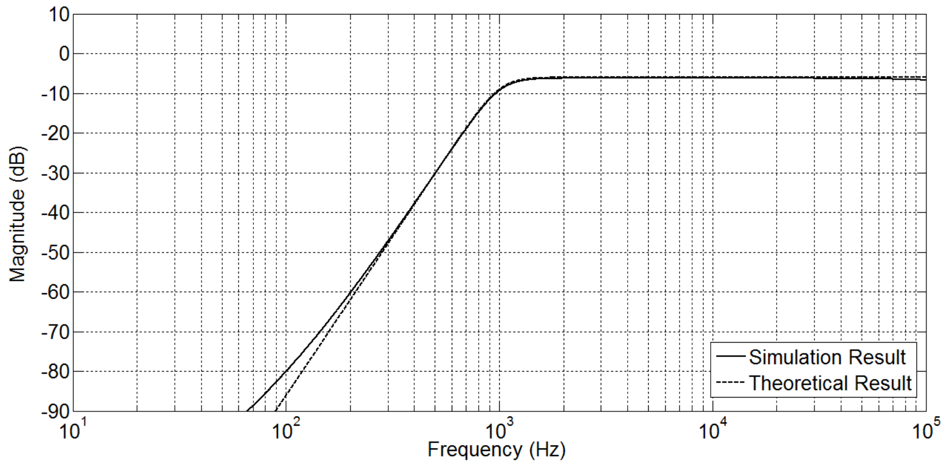

(a)

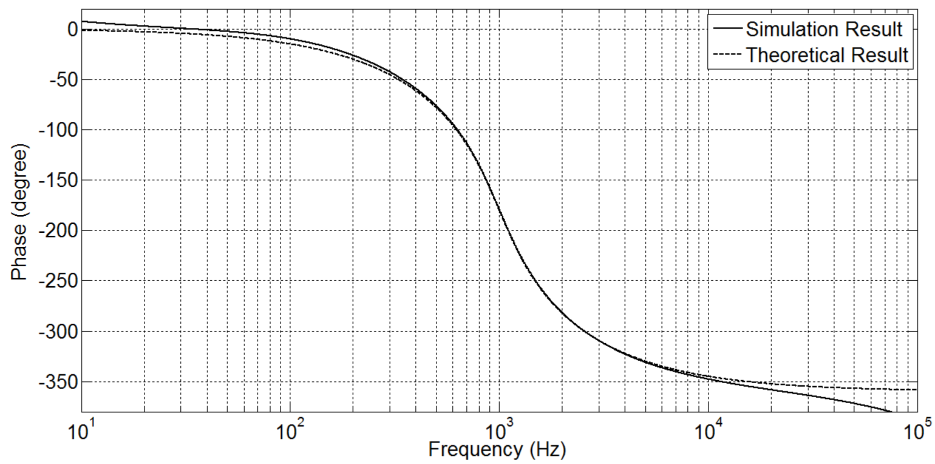

(b)

Fig. 6.9: Frequency response of proposed 4th order HP Butterworth filter **(a)** Magnitude **(b)** Phase responses

The proposed FOFs of order (1+α) and 4th order Butterworth filters are cascaded to achieve the functionality of (5+α) order FOF. The resulting FLPF and FHPF are simulated for test case orders of 5.25, 5.5 and 5.75; and corresponding simulated and theoretical results are depicted in Figs. 6.10 and 6.11. Simulated stop-band attenuation slopes for 5.25, 5.5 and 5.75 order FLPFs are found to be -103.84 dB/decade, -108.71 dB/decade, -113.78 dB/decade respectively against theoretical values of -105 dB/decade, -110 dB/decade and -115 dB/decade. Simulated stop-band attenuation slopes for 5.25, 5.5 and 5.75 order FHPFs are obtained as 103.21 dB/decade, 107.73 dB/decade and 113.1 dB/decade respectively while the corresponding theoretical values are as 105 dB/decade, 110 dB/decade and 115 dB/decade.

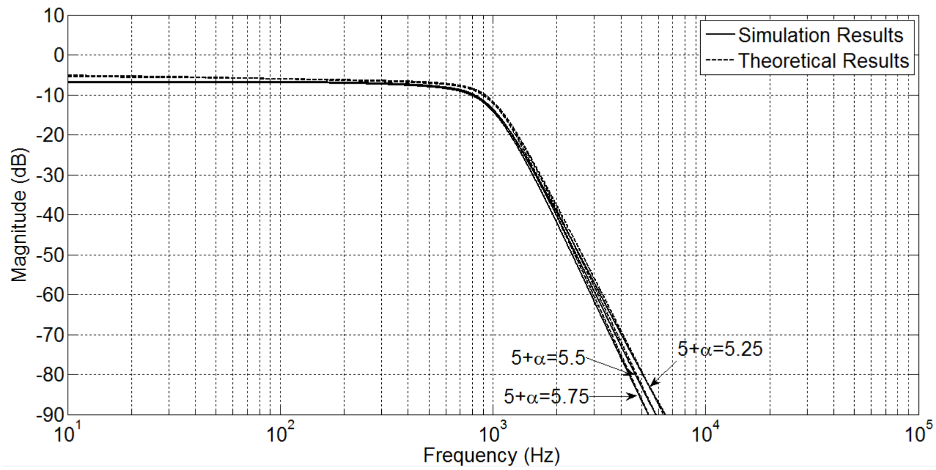

(a)

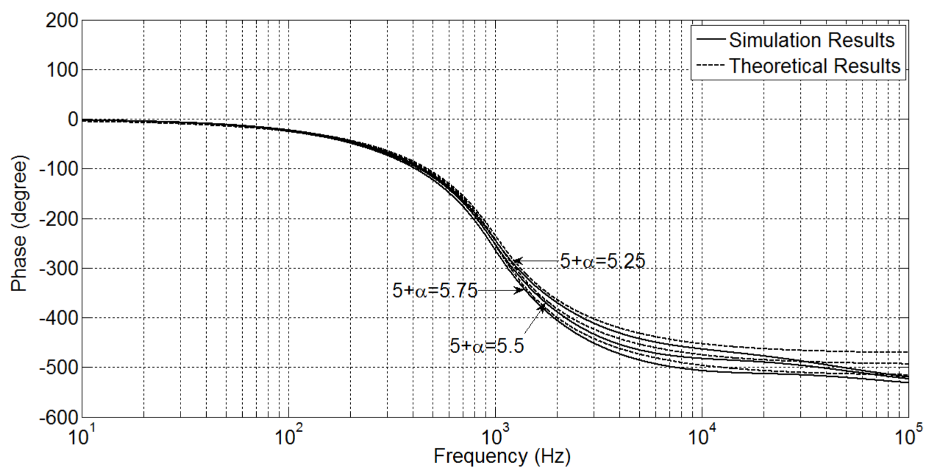

(b)

Fig. 6.10: Frequency response of proposed 5.25, 5.5 and 5.75 order FLPF **(a)** Magnitude **(b)** Phase responses

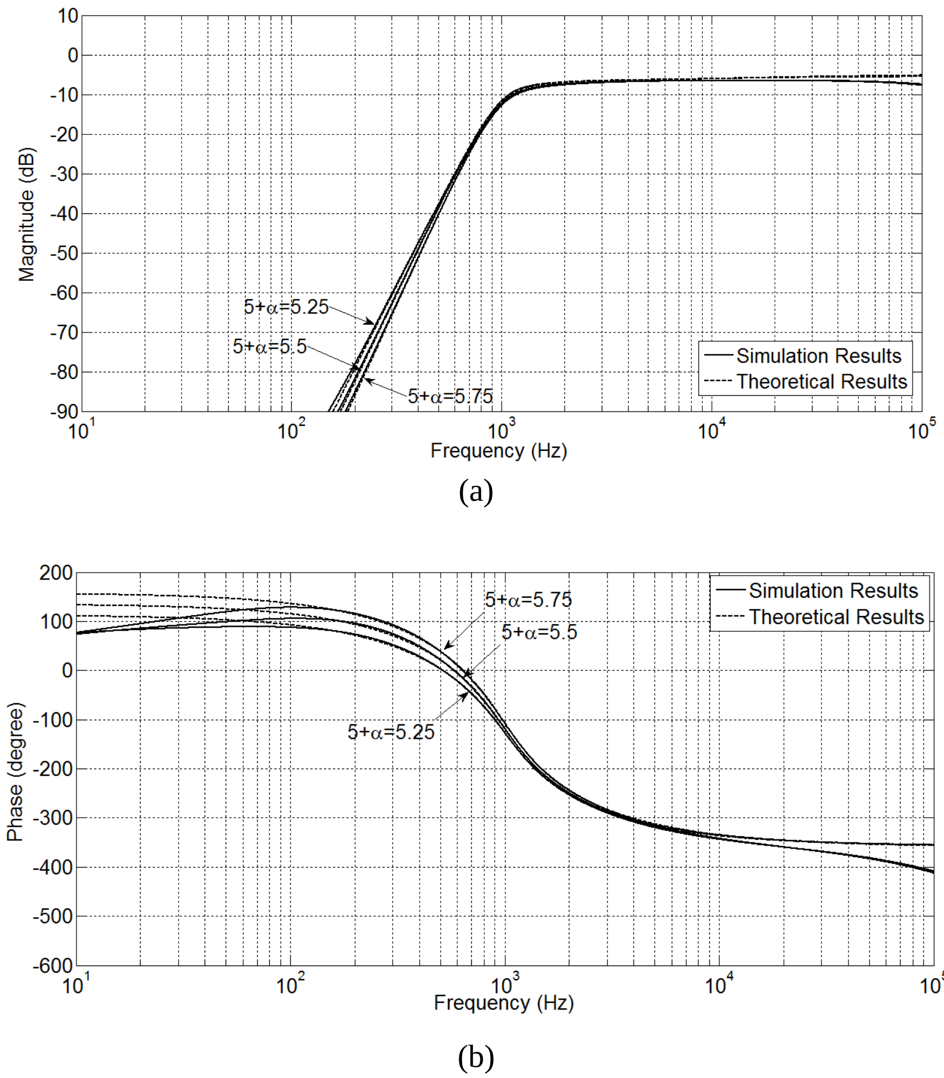

Fig. 6.11: Frequency response of proposed 5.25, 5.5 and 5.75 order FHPF **(a)** Magnitude **(b)** Phase responses

To examine the stability of proposed FLFPs, root-locus plots for (1 + α) and (5 + α) order FLPFs (assuming pass-band half power frequency ω_0 = 1 rad/s; α = 0.25, 0.5, 0.75) are obtained through forlocus function of MATLAB [169] and are shown in Figs. 6.12 and 6.13 respectively. For characteristic equation of (1 + α) (= 1.25, 1.5, 1.75) order FLPFs, the lowest common divisor λ is obtained as (= 4, 2, 4) which results in number of roots R (= 5, 3, 7). Similarly, λ = 4, 2, 4 in (5+α)

= 5.25, 5.5, 5.75 order FLPF respectively gives 21, 11, 23 number of roots respectively. The boundaries of unstable and stable regions are separated by phase angle $\pm\pi/2\lambda$ as sketched in solid lines. For order 1.25/ 1.75/ 5.25/ 5.75 ($\lambda = 4$) and 1.5/ 5.5 order ($\lambda = 2$), the unstable regions θ_s are $-\pi/8 < \theta_s < \pi/8$ and $-\pi/4 < \theta_s < \pi/4$ respectively. It may be noted from Figs. 6.12 and 6.13 that all roots lie in stable region. Similar plots are also obtained for proposed FHPFs and are omitted for the sake of brevity.

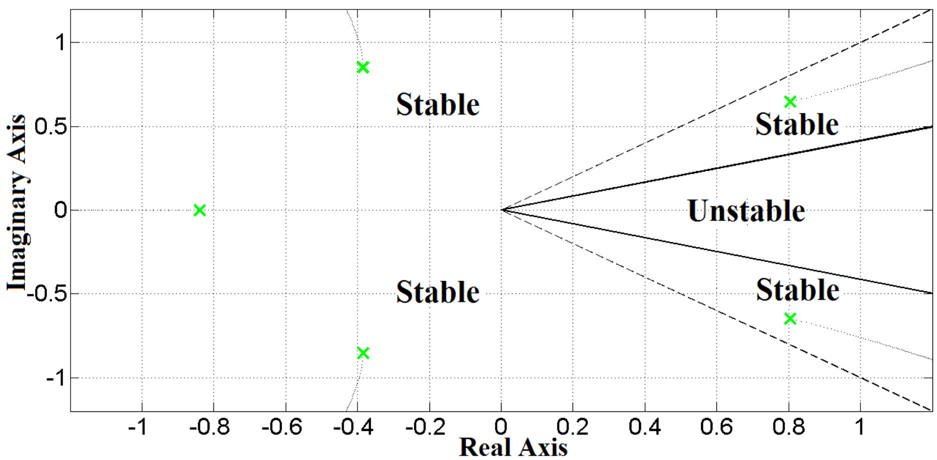

(a)

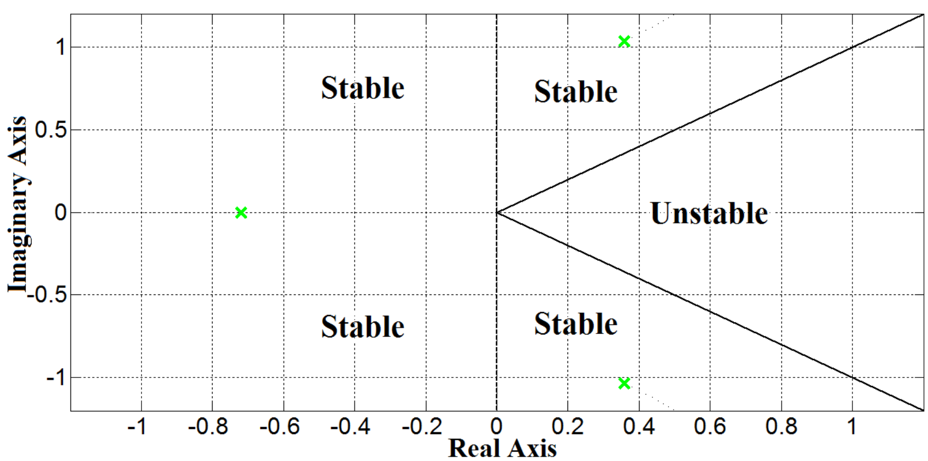

(b)

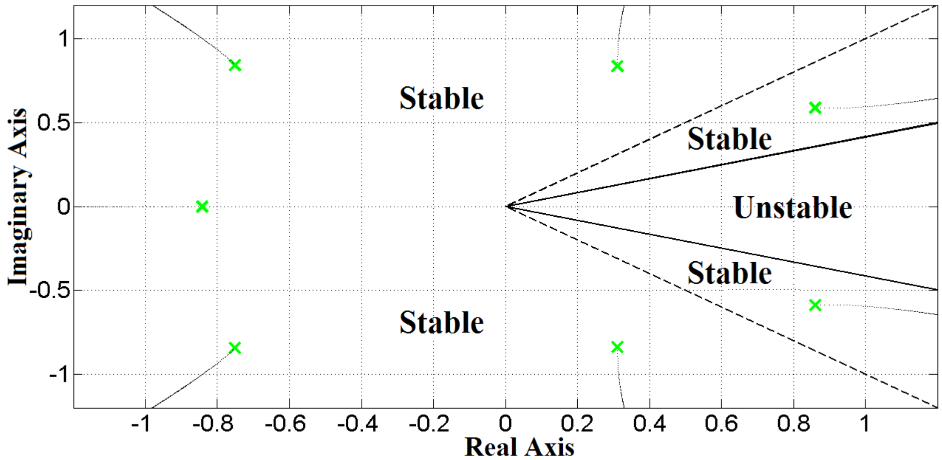

(c)

Fig. 6.12: Root-locus plot of **(a)** 1.25 **(b)** 1.5 and **(c)** 1.75 order FLPFs

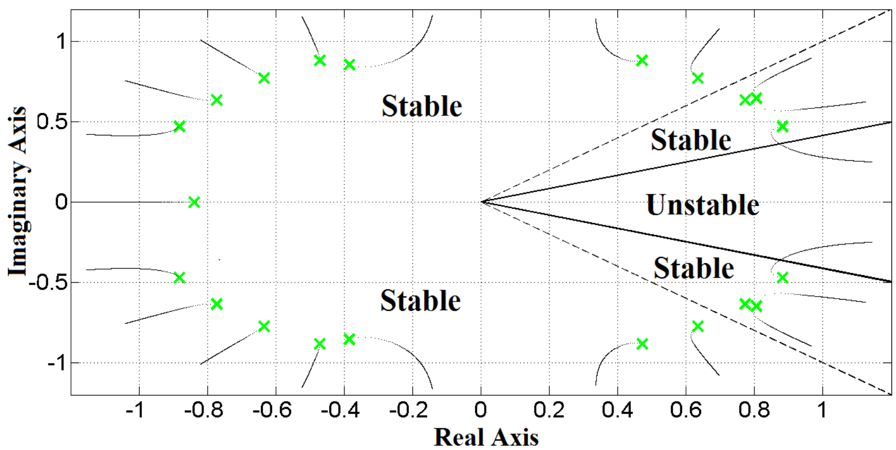

(a)

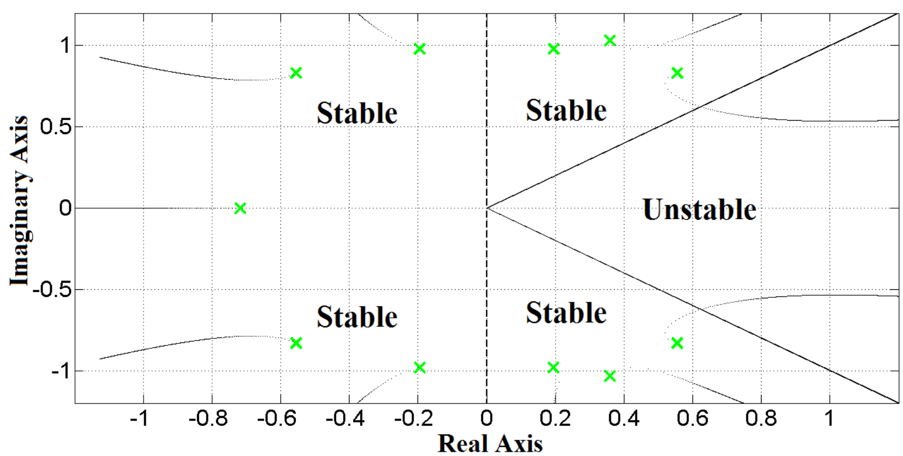

(b)

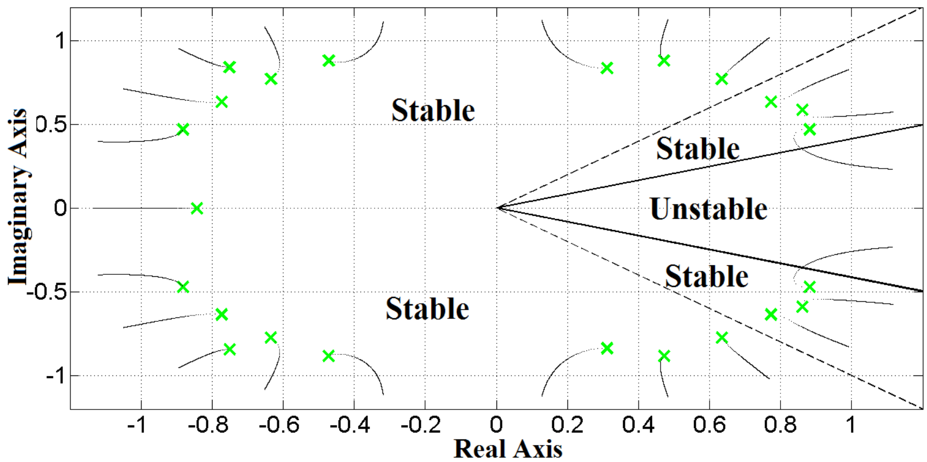

(c)

Fig. 6.13: Root-locus plot of **(a)** 5.25 **(b)** 5.5 and **(c)** 5.75 order FLPFs

The effect of passive component variations on proposed (1+α) and (5+α) order filters behavior is examined through Monte Carlo analysis by taking 150 samples and uniform Gaussian distribution. Figs. 6.14 and 6.15 show simulated magnitude and phase responses due to 5% of resistance and capacitance tolerances for proposed FLPF and FHPFs of 1.25, 1.5, 1.75, 5.25, 5.5, 5.75 order respectively. The maximum spread in passband (stopband) magnitude and phase for (1+α = 1.25, 1.5, 1.75) order FLPFs is observed to be within 1.8 dB (2.188 dB) and 10.03° (10.678°) respectively. Corresponding spread for (5+α = 5.25, 5.5, 5.75) order FLPFs are found to be 2.07 dB (3.71 dB) and 11.593° (11.78°).

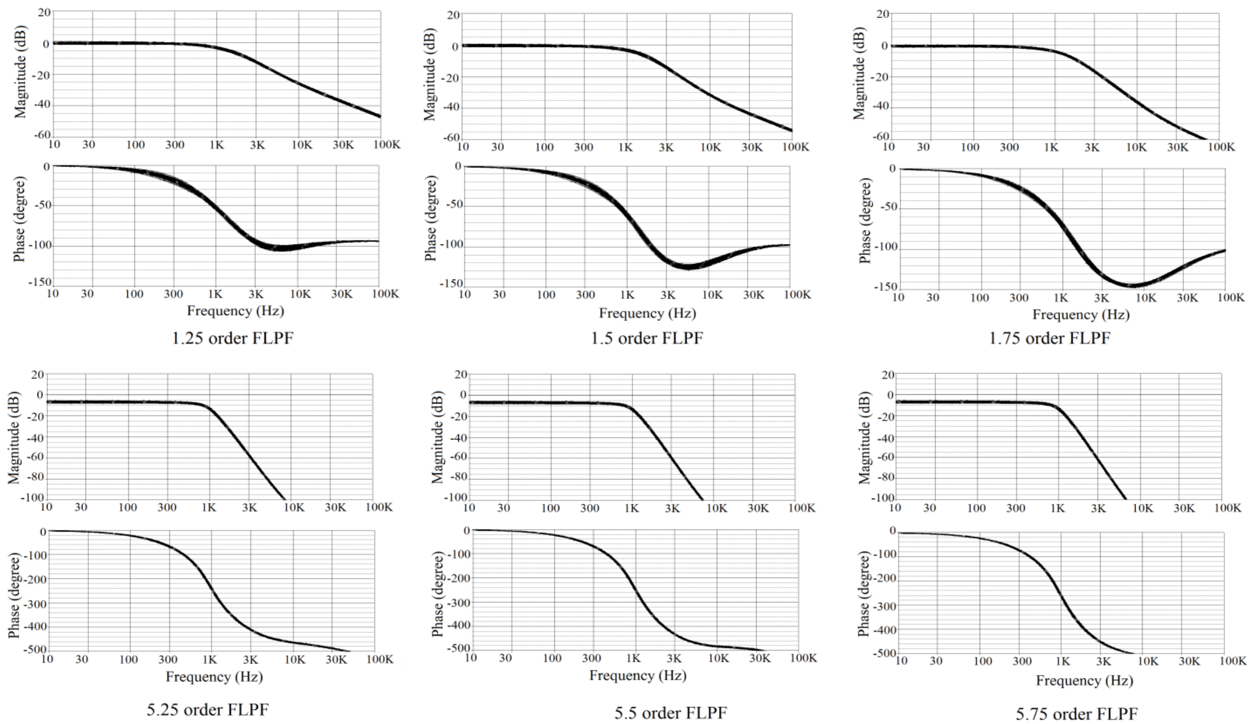

Fig. 6.14: Magnitude and phase responses under Monte Carlo analysis for proposed FLPFs

Similar observations for 1+α (= 1.25, 1.5, 1.75) order FHPFs are made and it is found the maximum magnitude and phase variations in passband (stopband) remain within 1.968 dB (2.97 dB) and 11° (10.887°) respectively. Corresponding spread for 5+α (= 5.25, 5.5, 5.75) order FHPFs are 2.8 dB (3.718 dB) and 12.71° (11.341°). It may be noted that the spread in the magnitude and phase responses of proposed (5+α) order FOFs varies slightly from (1+α) order FOFs which may be attributed to smaller component sensitivity of proposed 4th order leapfrog structure.

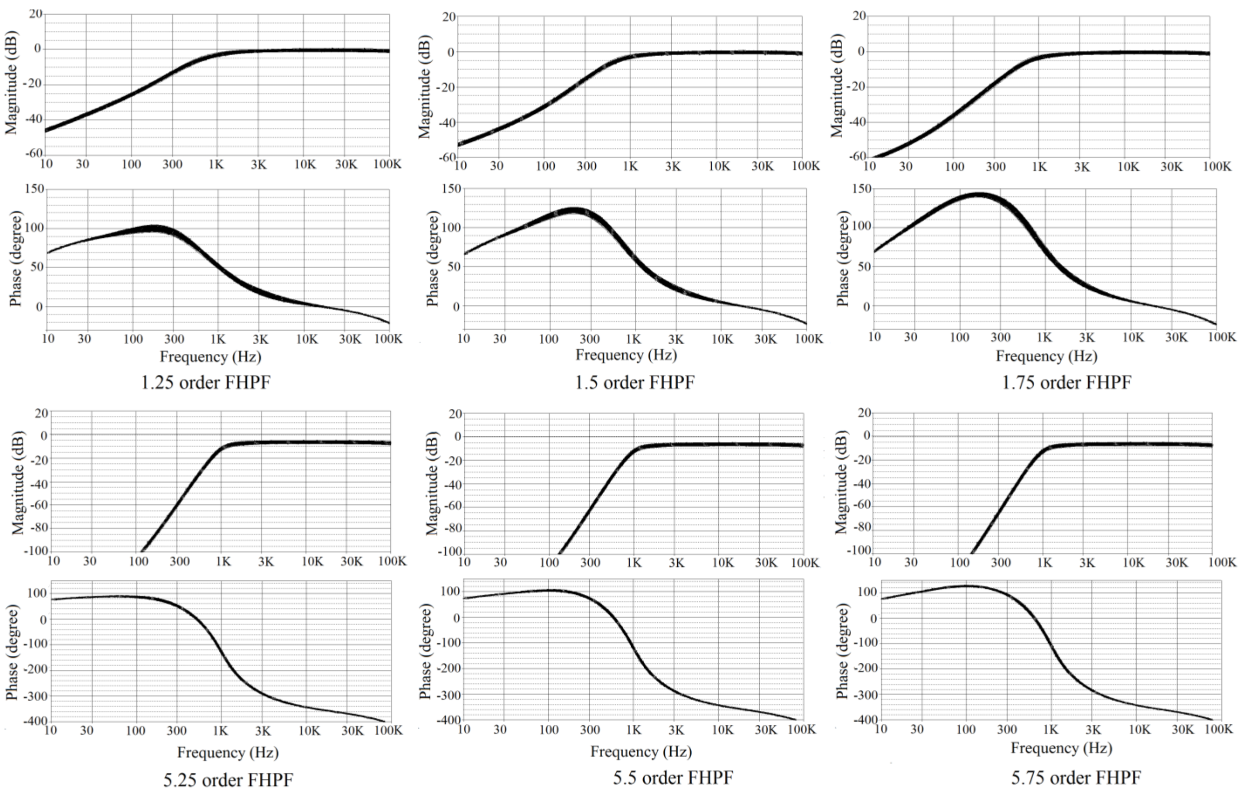

Fig. 6.15: Magnitude and phase responses under Monte Carlo analysis for proposed FHPFs

The effect of parasitics is on FOFs is also studied via simulations using parasitic values. The simulation results for FLPF and FHPF of 1.5 and 5.5 orders are shown in Fig. 6.16 and the observations are enlisted in Table 6.3.

Table 6.3: Effect of parasitics on proposed FOFs

Parasitic Effects	1.5 order FLPF	1.5 order FHPF	5.5 order FLPF	5.5 order FHPF
R_Y (2MΩ)	No effect	No effect	Negligible deviation in frequency response Max deviation of 0.007 dB in magnitude and 0.017° in phase at ω_h	Negligible deviation in frequency response Max deviation of 0.004 dB in magnitude and 0.017° in phase at ω_h
C_Y (2pF)	No effect	No effect	Negligible magnitude deviation Slight increase of phase in stop band (0.11° at 100 kHz)	Negligible magnitude deviation Slight increase of phase in stop band (0.07° at 100 kHz)
R_X (50Ω)	Magnitude deviates by 1.2 dB around 1.5 kHz and then decreases at the rate of 1 dB/decade in stop-band Phase deviation – maximum of 2.2° at 250 Hz	Small magnitude deviation of 0.5 dB in passband, an additional shift of 2 dB/ decade beyond 15 kHz in passband A maximum of 1.22° phase deviation is observed around 400 Hz in stop band. In pass band, phase	Constant magnitude deviation in passband (0.32 dB) which decreases at the rate of 0.5 dB/decade in transition band Max phase shift of 1.5° is observed at ω_h	Magnitude deviation of 2dB at 55 kHz is observed. Maximum phase deviation of 2.6° is observed in the frequency range below 500 Hz. Phase deviation of 5.5° is observed beyond 18 kHz.

	(pass-band), decreases in transition band up to 0.02° at 2.4 kHz, increases at the rate of 6 °/decade afterwards	changes at a rate of 2.2 °/ decade		
R_Z (3MΩ)	Very small deviation (0.02 dB) is observed at ω_h Very small change in phase (max=0.02° at 2.4 kHz)	Magnitude deviation of 0.01 dB/decade and phase deviation of 1.4°/decade are prevalent in transition band.	Maximum magnitude deviation is 0.3 dB at ω_h Phase deviation of 0.3°/decade exists in transition band	Magnitude deviation is higher in stopband (1.5 dB at 10 Hz) than passband deviation (0.009 dB at 10 kHz) Phase deviation is large in stopband e.g. 6.8° at 10 Hz
C_Z (4.5pF)	Very small magnitude deviation i.e. max 0.016 dB at 1.4 kHz Phase deviation slightly increases at the rate of 0.06	Negligible magnitude deviation of 0.001dB exists below 300 kHz Max phase deviation of 0.1° below 20 kHz	Very small magnitude deviation i.e. 0.08 dB below 100 kHz Phase deviation increases at the rate of 0.4 °/decade-during transition of bands and 1.8 °/decade below 70 kHz in the stopband (phase deviation is	Below 15 kHz magnitude deviation is negligible Phase deviation slightly increases at the rate of 0.12 °/decade in HF passband and found 0.4° below 80 kHz

	°/decade during transition from passband to stopband (0.09° at ω_h)		0.17° at ω_h)	
Overall parasitic effects	Magnitude response slightly differs in the transition band (0.3 dB at ω_h). Slightly shifts (around 0.25°) in passband (below 250 Hz) and transition band at the rate of 0.2 °/decade but major influence is due to approximation form of $(s\tau)^{\alpha}$	Considerable amount of magnitude is present in very LF and HF band (1.18 dB at 5 Hz and 200 kHz) Phase deviation is large in passband e.g. 4.8° at 30 kHz	Small deviation in magnitude response (0.63 dB in frequency band of 10 Hz-100 kHz) Phase deviation increases in passband (around 4° upto 100 kHz frequency band)	Maximum magnitude deviation of 0.37 dB exist in stopband and 0.28 dB in passband Maximum phase deviation of 5.4° exists in both stop and pass bands

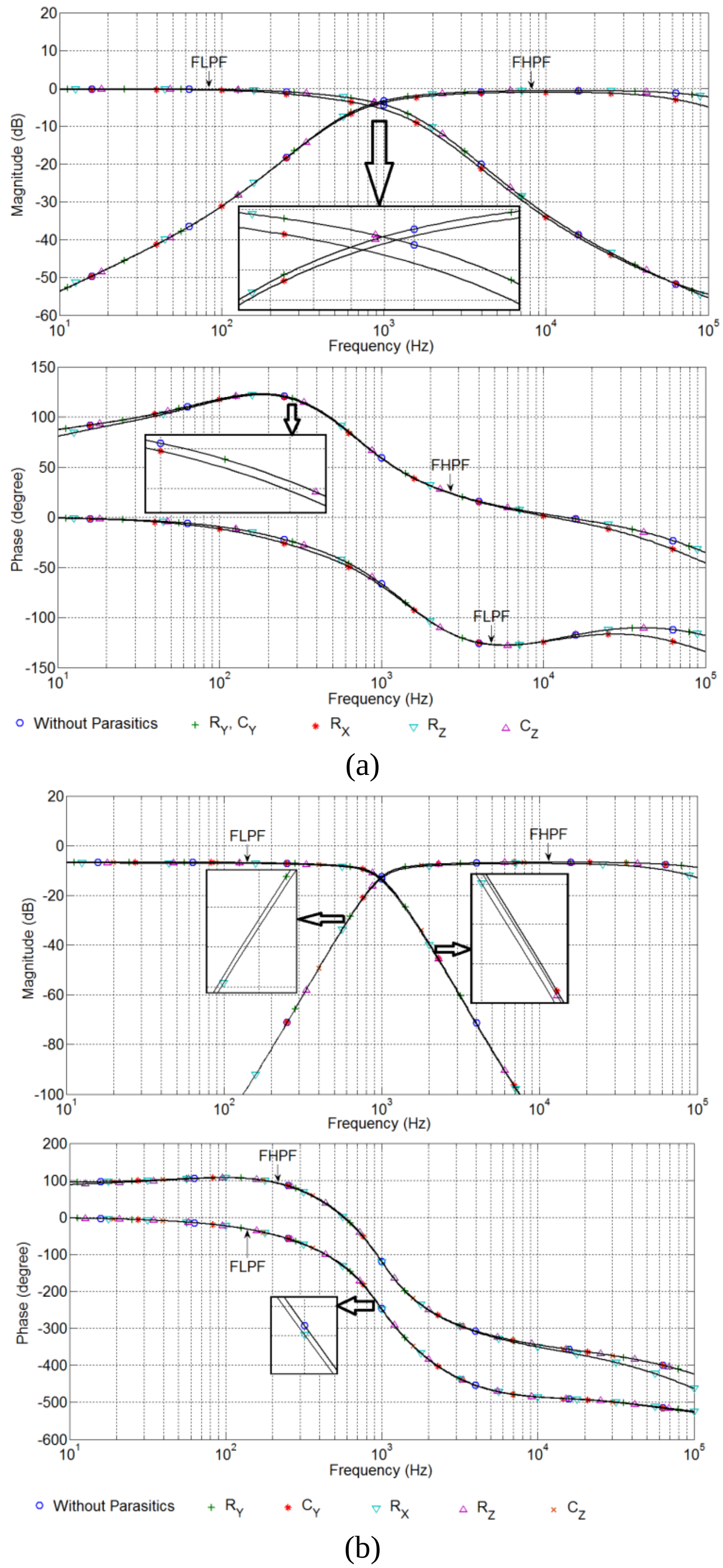

Fig. 6.16: Simulation results of FLPF and FHPF with parasitics **(a)** 1.5 order and **(b)** 5.5 order

6.5.2 Experimental Results

The operation of proposed filters is also examined experimentally using commercially available CFOA IC (AD844AN). The theoretical component values used for proposed filters and those used for experimental verification are placed in Table 6.4. The transient responses of proposed LP filters are studied by applying 100 Hz sinusoidal input having peak to peak voltage of 2V. The transient responses for LP filters of 1.5, 4 and 5.5 order are shown in Figs. 6.17 (a), (b) and (c) respectively. Fig. 6.17 (d) shows transient response of 1.5 order FHPF for 2.5 kHz sinusoidal input. The measured values of output amplitude (in volts) and phase for LP filters of 1.5, 4, 5.5 order and 1.5 order FHPF are found to be (1.02, 0.5, 0.55, 1.022) and (-7°, -12°, -23°, 28°) respectively which are in close agreement with corresponding theoretical values of (1, 0.5, 0.5, 1) and (-10°, -15°, -25°, 26°).

Table 6.4: Component values for different filters

Filter	Components	R_1 (kΩ)	R_2 (kΩ)	R_3 (kΩ)	R_4 (kΩ)	R_5 (kΩ)	R_6 (kΩ)	R_7 (kΩ)	R_8 (kΩ)	C_1 (nF)	C_2 (nF)	C_3 (nF)	C_4 (nF)
1.5 order FLPF	Theory	56	56	100	56	255.692	29.89	17.823	46	0.97	2.473	5.243	None
	Experiment	56	56	100	56	255.68	30	17.8	46	0.94	2.4	5.2	None
1.5 order FHPF	Theory	4.829	18.22	45	4.829	7.955	69.209	None	5.22	10	10.04	10.08	None
	Experiment	4.82	18.2	45	4.82	8	69.2	None	5.22	10	10	10	None
4^{th} order LP	Theory	1.2184	1.2184	2.9417	2.9417	1.4709	1.2184	1.2184	None	100	100	100	100
	Experiment	1.2	1.2	2.88	2.88	1.47	1.2	1.2	None	100	100	100	100

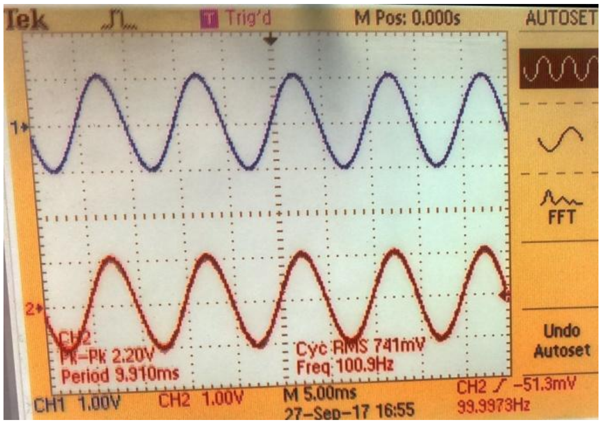

(a)

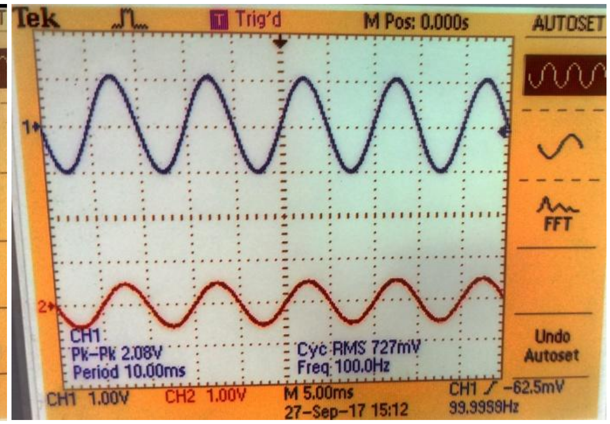

(b)

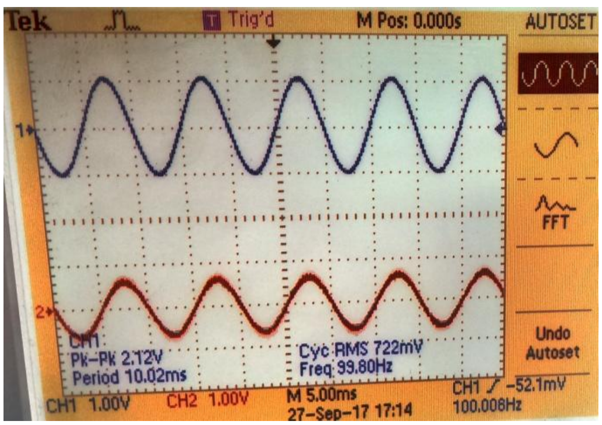

(c)

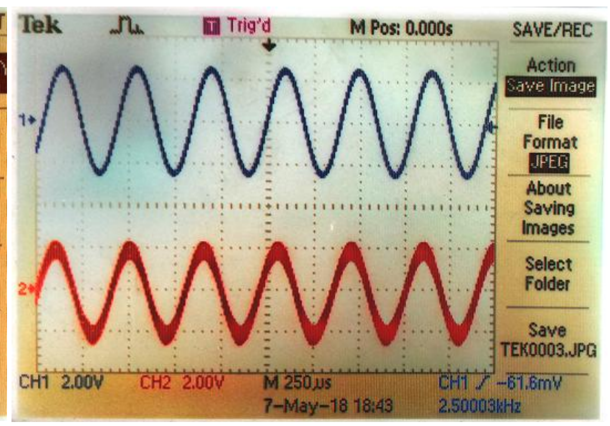

(d)

Fig. 6.17: Input (Channel 1) and Output (Channel 2) waveforms of LP filters of order **(a)** 1.5 **(b)** 4 **(c)** 5.5; and **(d)** 1.5 order FHPF

Figs. 6.18 (a) - (c) show comparison of experimental/ simulation (using AD844 SPICE model)/ theoretical magnitude frequency responses for FLPFs of order 1.5 and 5.5; and 1.5 order FHPF respectively. The half power frequencies for 1.5 and 5.5 order FLPFs; and 1.5 order FHPF are observed respectively as 1.19 kHz, 1.1 kHz, and 1.2 kHz. The corresponding slopes of stop band attenuation are -10.5 dB/octave (or -35 dB/decade), -32 dB/octave (or -106.67 dB/decade), and 9.9

dB/octave (or 33 dB/decade). The theoretical frequencies for 90° phase shifts for 1.5 and 5.5 order FLPFs; and 1.5 order FHPF are computed respectively as 1.73 kHz, 450 Hz and 612 Hz. Experimentally the frequency of input signal is varied and Lissajous patterns are observed. Figures Figs. 6.18 (d) - (f) shows Lissajous patterns for phase shift ±90° for 1.5 and 5.5 order FLPFs; and 1.5 order FHPF and their respective frequencies are 1.8 kHz, 510 Hz and 600 Hz. The order of the filters is computed from experimental response and the values are 1.67 and 5.33 for corresponding 1.5 and 5.5 order FLPFs; and 1.45 for 1.5 order FHPF.

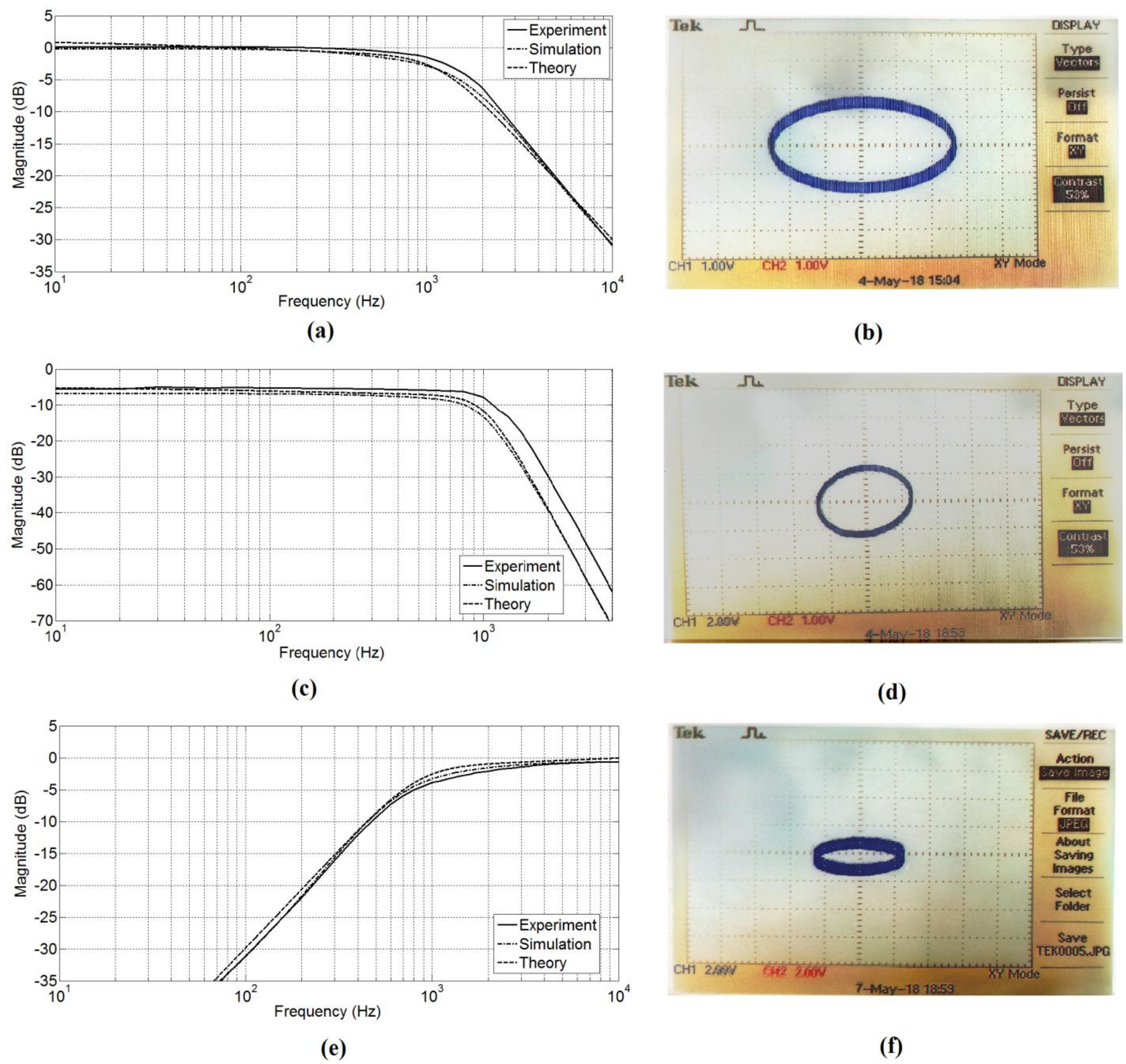

Fig. 6.18: Magnitude responses **(a)-(c)** for 1.5 order FLPF, 5.5 order FLPFs, and 1.5 order FHPF; **(d)-(f)** corresponding Lissajous patterns

6.6 Comparison

This section first compares the proposed CFOA based FLPF design with the available CFOA based FLPF [62] followed by comparison with other available structures.

Following are the key points of comparison with CFOA based FLPF [62]:

- Though both use FBD approach for (1+α) order FLPF implementation, FLF topology of [62] uses three lossless integrators whereas proposal employs two lossless and one lossy integrator which reduces feedback connections by one, therefore one passive component is less.
- Both employ FLF topology and suggest use of cascading of (1+α) order FLPF with (n-1) integer order filter for realization of higher order FLPF. However, the difference lies in integer order filter realization. The FLF method is used in [62] while proposal employs leapfrog topology.
- To compare performance of proposal with [62], 1.5 and 5.5 order FLPFs given in [62] are realized. Simulation results for Monte Carlo analysis of 1.5 order FLPF topology [62] by taking 5% resistance and capacitance tolerances with 150 samples is shown in Figs. 6.19(a) – 6.19(b). Maximum spread in pass band (stop band) magnitude and phase are 2.8 dB (3.718 dB) and 12.71° (11.341°) in comparison to 1.79 dB (2.188 dB) and 10.03° (10.678°) for the proposed FLPFs. Therefore, proposal performs better than [62] in presence of component variation. Further, the frequency response of 5.5 order FLPF [62] is plotted in Figs. 6.19(c) –

6.19(d) which includes theoretical and proposed 5.5 order FLPF responses also. It is observed that magnitude lies within 1.4 dB magnitude error for frequency ranges of 7.21 kHz and 17.5 kHz for topology of [62] and the proposed one respectively. Corresponding phase responses show frequency ranges of 2.6 kHz and 8.35 kHz that lie within 4° phase errors. Thus, the proposed method demonstrates superior performance in terms of accuracy and sensitivity as compared to structure of [62].

Additionally, the performance of proposed design is also compared with other reported implementations and following observations are made-

- Like [54 - 55, 60 - 62], the proposed designs perform voltage mode (VM) FOF operation while [56 - 59, 63 - 66] are current mode (CM) FOFs. The CM FOFs also provide electronic tuning feature but at the cost of more active elements. The proposed designs lack in electronic tuning feature for order and frequency adjustment.
- For higher order FOF, the proposal recommends use of $(1+\alpha)$ order FLF topology followed by leapfrog topology of (n-1) order which reduces the component sensitivity in comparison to higher order filters realized through fully FBD based approach [61, 62].

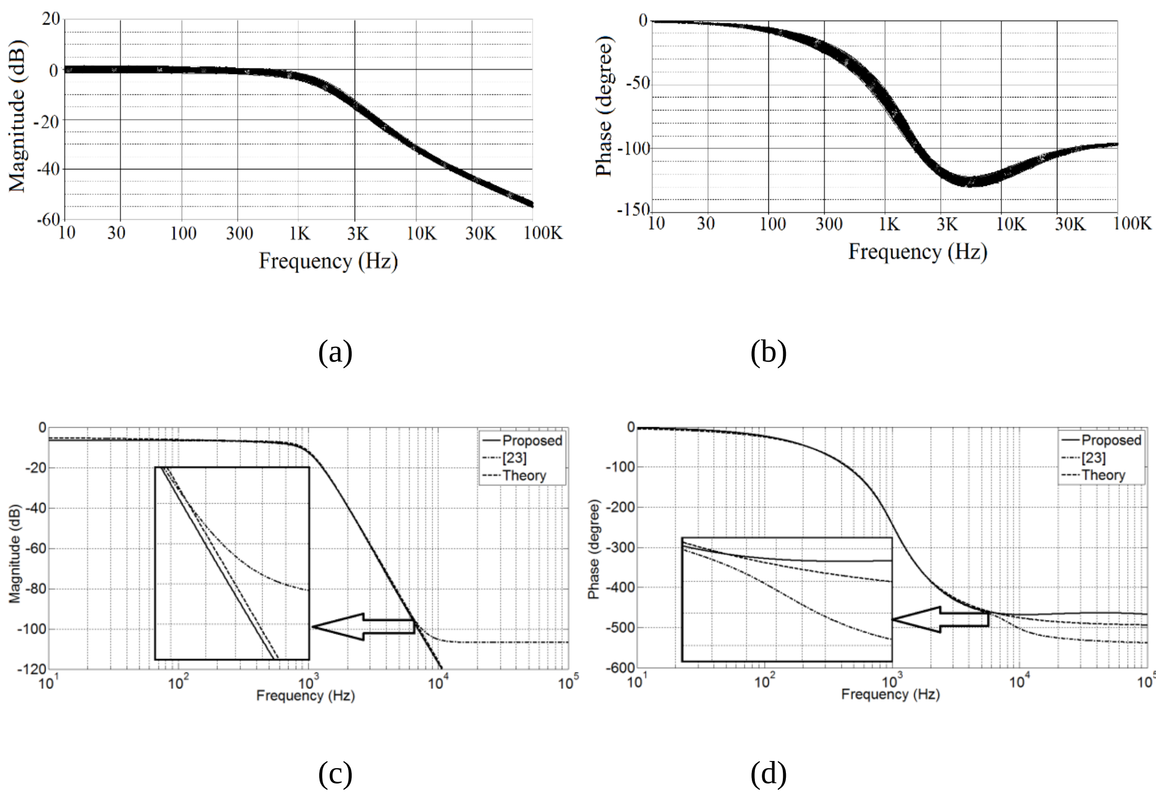

Fig. 6.19: Monte Carlo simulation results for 1.5 order FLPF [62] **(a)** Magnitude **(b)** phase; 5.5 order FLPF frequency response **(c)** Magnitude **(d)** Phase

6.7 Conclusion

New realizations of CFOA based (1+α) order FOFs (FLPF/FHPF), based on 2nd order CFE approximation form of the FO Laplacian operator, are presented in this chapter. These filters are cascaded with (n-1) integer order filters is used to realize higher order (n+α) FOFs. To illustrate this, CFOA based LP (HP) FOFs of order (5+α) are obtained by cascading LP (HP) FOFs of order (1+α) with proposed leapfrog realization of 4th order LP (HP) filter. The functionality of the proposed filters is verified through realization of 5.25, 5.5 and 5.75 order FSFs by cascading

1.25, 1.5 and 1.75 order FSFs with 4th order leapfrog filter topology. The proposed work is verified through SPICE simulations and experimentation. The CFOA IC (AD844AN) and its macro model are used for experiment and SPICE simulation works. These results are found in close agreement with theoretical values. The performance of proposed circuits is examined at 1 kHz half power frequency

CHAPTER 7

CONCLUSION

The processes in nature and real objects can be modeled more precisely by using fractional calculus as fractional order dynamics offer extra degree of freedom to express the control mechanism of the physical phenomena. Fractional approach has been used in modeling of various physical processes and systems. In this thesis various fractional order current mode signal processing circuits, using integer order design equations generalized in fractional domain, are presented. In this chapter a summary of major work done as reported in various chapters of the thesis is presented.

7.1 Summary of Work Presented in this Thesis

The introduction chapter presents literature review on fractional order elements and analog signal processing circuits realized using fractional order dynamics. Literature review helped in identifying the significant research gaps and hence forming objectives. The organization of thesis is also presented in this chapter.

The fundamental concepts of fractional order circuits are presented in chapter 2. The chapter reviews the CFE approximation method for realizing FOE. The 4^{th} order CFE approximation is then used to realize an FC using 4^{th} order RC domino ladder network. The behavior of three FCs (i) $C_\alpha = 1\ \mu\mho/s^\alpha$, $\alpha = 0.1$, (ii) $C_\alpha = 1\ \mu\mho/s^\alpha$, $\alpha = 0.5$ and (iii) $C_\alpha = 1\ \mu\mho/s^\alpha$, $\alpha = 0.9$; scaled to 1 kHz frequency is demonstrated using SPICE simulation. The simulation results are found in close agreement with theoretical results in the frequency range of few tens of Hz to hundreds kHz for magnitude responses whereas constant phase behavior is observed within few tens Hz to few kHz. The stability analysis of fractional order circuits and systems may be investigated from the transformation of s plane into fractional domain F or W plane with mapping of pole locations. The circuits proposed in this thesis are designed using either CFOA or OTA therefore in this chapter CFOA and OTA are characterized using SPICE simulations. The AC and DC responses are shown and important observations about their functional limitations are presented.

CFOA based integer and fractional order capacitance scaling circuits are presented in chapter 3. First a new integer order capacitance scaling circuit with smaller component spread having multiplication factor K=1/(1-P) is proposed. This type of circuit can provide very high multiplication factor by selecting P close to unity. The impedance of proposed configuration gets affected due to non-idealities of CFOA. Thus a compensation technique is also proposed. Further, four fractional order capacitance scaling circuits are presented out of which one is generalization of proposed integer order capacitance multiplier and the rest are generalization of existing integer order C-multipliers. The functionality of all the propositions is verified through SPICE simulations and MATLAB simulations are also presented for FC multipliers to study effect of variation of FO and resistor ratios simultaneously. Close match between theoretical and simulation results is observed. Further, the integer order C-multiplier is verified experimentally as well using CFOA IC AD844AN IC and results corroborate with theory.

The chapter 4 is devoted to realization of FOE with order α >1. The proposed structure is based on the concept of impedance inverter designed using

OTA. A new structure, termed as IIMC, using n OTAs based modular structures is proposed first which provides an input impedance of the form $\frac{s^n {C_1}^n}{{g_m}^{n+1}}$. The proposed IIMC is then generalized in fractional domain to obtain a fractional inductor and capacitors of (n-1+α) order. Thus by increasing the number of OTA based modules the order of FOE can be enhanced. The proposed theory is verified through SPICE simulations by designing 1+α order (where α =0.2, 0.5) FI and FC for illustration. The experimental results are obtained for order 1+α = 1.5 ing ICs LM 13600N (dual OTAs). For simulation and experimental purpose the FCs (α =0.2, 0.5)) are realized with 12^{th} order parallel RC domino ladder network. The frequency range of such FCs is observed to be around few Hz to few MHz. The realized (1+α) order FC and FI are used in a current driven parallel resonator to design a current mode 2(1+α) order filter providing FLPF, FHPF and FBPF responses simultaneously. This filter structure is further verified through SPICE simulation for two different fractional orders to verify the propositions. The stability of the proposed FOF for different orders is examined and root locations are also plotted.

Chapter 5 deals with realization of electronically tunable fractional order filters (FOFs) using OTAs. These FOFs are obtained through (i) generalization of first order multi input single output structure leading to Topology I (ii) generalization of second order single input multi output filter resulting in Topology II. In topology I, one FC of order α is used for realization of CM electronically tunable FOFs of order α and provides FAPF and FLPF responses through appropriate input selection. Topology II uses two identical FCs of order α to obtain CM electronically tunable FLPF and FBPF responses simultaneously of order 2α. Mathematical formulations for critical frequencies of theses FOFs such as maximum/minimum, half power and right phase frequencies are presented. Furthermore sensitivities analysis of these FOFs with respect to order α, value of C_α and g_m of OTA are formulated and plots for the same are obtained through MATLAB simulations. Further, magnitude and phase responses are obtained through SPICE simulation and various critical frequency points are measured. These results are found in close agreement with theoretically computed values. Electronic tuning of critical frequencies is shown through variations on transconductance gains of OTAs. In these works, The time domain responses along with Lissajous patterns for FAPF are also demonstrated for ±90° phase shift between input and output signals. Their stability conditions for both the structures are also derived.

Chapter 6 puts forward a new proposal for CFOA based Low pass (LP) and High Pass (HP) FOFs. The proposed filters are designed by approximating the fractional Laplacian operator by an appropriate integer order transfer function. Subsequently, FBD approach is used for CFOA based realization of LP and HP FOFs of order (1+α). Higher order FOFs are realized by cascading FOF of order (1+α) with higher integer order filters. To illustrate this, CFOA based FLPF and FHPF structures of order (5+α) are obtained by cascading respective FOFs of order (1+α) with proposed leapfrog realization of 4th order integer order LP and HP filters respectively. The proposal is verified through SPICE simulations and experimentation (using AD844AN IC). These results are compared with approximated and ideal values. The performance of proposed circuits is examined at 1 kHz cut off frequency. The proposed (1+α) FOF is tested for orders (1.25, 1.5 and 1.75) leading to (n+ α) order as 5.25, 5.5 and 5.75 respectively. Stability, sensitivity and non-ideal analyses are also included. The root-locus technique for FO linear system is used to plot the location of roots for characteristic equation of (1+α) and (5+α) order FOFs.

7.2 Future Scope

The fractional domain is primarily interdisciplinary in nature and has unlimited research opportunities that can be investigated. During the course of thesis candidate has explored scaling and order alterations of FOE; electronically tunable fractional order filters using OTA and CFOA based higher order filters. There are possibilities to extend the work in several directions. Some of the aspects which may be addressed are

1. As the FOEs are integral part of fractional order circuits, alternate FOE emulations may be investigated which improve their performance in terms of extended frequency range of operation.
2. CFE approximation based emulation of FC is used to validate the concepts proposed in this work. The effect of other approximation methods on the designing FO circuits may be explored.
3. Most of the research effort has been verified through emulated FOEs in literature. To develop real time applications it is essential to have

miniaturized FOEs. Thus FOE fabrication is another area which may be investigated.

4. In integrated circuit environment, electronically tunable filters are useful for adjusting performance parameters. Two circuit realizations are presented here. This work may be extended to new circuit realizations for electronically tunable FOFs.
5. The FOEs presented in this work may be used to design different applications.

REFERENCES

[1] L. Debnath, “Recent applications of fractional calculus to science and engineering”, *International Journal of Mathematics and Mathematical Sciences,* vol. 54, pp. 3413–3442, 2003.

[2] A. S. Elwakil, “Fractional-order circuits and systems: an emerging interdisciplinary research area”, *IEEE Circuits and Systems Magazine*, vol. 10, no. 4, pp. 40–50, 2010.

[3] Y. Q. Chen, I. Petras and D. Xue, “Fractional order control—a tutorial”, in *Proceeding American Control Conference (ACC),* pp. 1397–1411, 2009.

[4] S. Das and I. Pan, “Fractional order signal processing—introductory concepts and applications”, in *Springer Briefs in Applied Sciences and Technology*, 2012.

[5] L. Dorcak, J. Valsa, E. Gonzalez, J. Terpak, I. Petras and L. Pivka, “Analogue realization of fractional-order dynamical systems”, *Entropy*, vol. 15, no. 10, pp. 4199–4214, 2013.

[6] I. Podlubny, I. Petras, B. M. Vinagre, P. O. Leary and L. Dorcak, “Analogue realizations of fractional-order controllers”, *Nonlinear Dynamics*, vol. 29, no. 4, pp. 281–296, 2012.

[7] T. Suksang, W. Loedhammacakra and V. Pirajnanchai, “Implement the fractional-order, half integrator and differentiator on the OTA based $PI^{\lambda}D^{\mu}$ controller circuit”, in *IEEE Conference on ECTICON*, 2012. doi:10.1109/ECTICON.2012.6254136.

[8] L. A. Geddes and L. E. Baker, “Principles of applied biomedical instrumentation”, *Wiely*, 3rd edition, New York, 1989.

[9] A. C. Faria, J. Veiga, A. J. Lopes and P. L. Melo, “Forced oscillation, integer and fractional-order modeling in asthma”, *Computer Methods and Programs in Biomedicine*, vol. 128, pp. 12–26, 2016.

[10] H. Sheng, Y. Q. Chen and T. S. Qiu. “Fractional processes and fractional-order signal processing: techniques and applications”, *Springer*, New York, 2011.

[11] A. G. Radwan, A. M. Soliman, A. S. Elwakil and A. Sedeek, “On the stability of linear systems with fractional-order elements”, *Chaos, Solitons and Fractals*, vol. 40, no. 5, pp. 2317-2328, 2009.

[12] A. G. Radwan, “Stability analysis of the fractional-order $RL_{\beta}C_{\alpha}$ circuit”, *Journal of Fractional Calculus and Applications*, vol. 3, no. 1, pp. 1-5, 2012.

[13] R. Mansouri, M. Bettayeb and S. Djennoune, "Approximation of high order integer systems by fractional order reduced parameters models," *Mathematical and Computer Modelling*, vol. 51, pp. 53-62, 2010.

[14] M. Nakagava and K. Sorimachi, “Basic characteristics of a fractance device”, *IEICE Transactions on Fundamentals*, vol. E75-A, no. 12, pp. 1814–1818, 1992.

[15] A. Adhikary S. Sen and K. Biswas, “Practical realization of tunable fractional order parallel resonator and fractional order filters”, *IEEE Transactions on Circuits and Systems I*, vol. 63, no. 8, pp. 1142-1151, 2016.

[16] T. J. Freeborn, B. Maundy and A. S. Elwakil, “Fractional-step tow-thomas biquad filters”, *Nonlinear Theory and Its Applications, IEICE (NOLTA)*, vol. 3, no. 3, pp. 357–374, 2012.

[17] K. Biswas, S. Sen, and P. K. Dutta, “Realization of a constant phase element and its performance study in a differentiator circuit”, *IEEE Transactions on Circuits and Systems*, vol. 53, no. 9, pp. 802–806, 2006.

[18] M. C. Tripathy, K. Biswas and S. Sen, “A design example of a fractional-order Kerwin-Huelsman-Newcomb biquad filter with two fractional capacitors of different order”, *Circuits, Systems, and Signal Processing*, vol. 32, pp. 1523–1536, 2013.

[19] G. Tsirimokou, C. Psychalinos, A. S. Elwakil and K.N. Salama, “Experimental behavior evaluation of series and parallel connected constant phase elements”, *AEU - International Journal of Electronics and Communications*, vol. 14, pp. 5-12, 2017.

[20] T. Suksang, V. Pirajnanchai, C. Suppitaksakul and W. Loedhammacakra, “Design and improve the performance of OTA low pass filter with

fractional-order step”, *IEEE Conference on Electron Devices and Solid State Circuit (EDSSC)*, 2012.

[21] B. T. Krishna, "Studies on fractional order differentiators and integrators: a survey," *Signal Processing*, vol. 91, no. 3, pp. 386-426, 2011.

[22] M. Sugi, Y. Hirano, Y. F. Miura and K. Saito, “Frequency behavior of self-similar ladder circuits”, *Colloids and Surfaces A: Physicochemical and Engineering Aspects*, vol. 198, pp. 683–688, 2002. doi:10.1016/S0927-7757(01)00988-8

[23] K. B. Oldham and C. G. Zoski, “Analogue instrumentation for processing polarographic data”, *Journal of Electroanalytical Chemistry and Interfacial Electrochemistry*, vol. 157, no. 1, pp. 27–51, 1983. doi:10.1016/S0022-0728(83)80374-X.

[24] G. Tsirimokou, "A systematic procedure for deriving RC networks of fractional-order elements emulators using MATLAB," *AEU-International Journal of Electronics and Communications*, vol. 78, pp 7-14, 2017.

[25] A. Adhikary, P. Sen, S. Sen and K. Biswas, “Design and performance study of dynamic fractors in any of the four quadrants,” *Circuits, Systems and Signal Processing*, vol. 35, no. 6, pp. 1909-1932, 2016. ISSN: 1531-5878. doi:10.1007/s00034-015-0213-3.

[26] B. M. Vinagre, I. Podlubny, A. Hernandez and V. Feliu, “Some approximations of fractional order operators used in control theory and applications”, *Fractional Calculus & Applied Analysis*, vol. 3, no. 3, pp. 945-950, 2000.

[27] D. Y. Xue, C. Zhao and Y. Q. Chen, “A modified approximation method of fractional order system”, in *IEEE Conference on Mechatronics and Automation*, pp. 1043–1048, 2006.

[28] R. El-Khazali, “On the biquadratic approximation of fractional order laplacian operators”, *Analog Integrated Circuits and Signal Processing*, vol. 82, no. 3, pp. 503-517, 2015.

[29] D. Biolek, R. Senani, V. Biolkova and Z. Kolka, “Active elements for analog signal processing: classification, review, and new proposals,” *Radioengineering*, vol. 17, no. 4, pp. 15-32, 2008.

[30] K. K. Abdalla, D. R. Bhaskar and R. Senani, “A review of the evolution of current-mode circuits and techniques and various modern analog circuit building blocks”, *Nature and Science*, vol.10, no. 10, pp. 1-13, 2012.

[31] P. Ahmadi, B. Maundy, A. S. Elwakil and L. Belostostski, “High-quality factor asymmetric-slope bandpass filters: a fractional-order capacitor approach”, *IET Circuits, Devices & Systems*, vol. 6, no. 3, pp. 187–197, 2012.

[32] T. J. Freeborn, B. Maundy and A. Elwakil, “Fractional resonance-based $RL_{ß}C_{a}$ filters”, *Mathematical Problems in Engineering*, pp. 1–10, 2013.

[33] M. C. Tripathy, D. Mondal, K. Biswas and S. Sen, “Experimental studies on realization of fractional inductors and fractional-order bandpass filters”, *International Journal of Circuit Theory and Applications*, vol. 43, no. 9, pp. 1183–1196, 2014. doi: 10.1002/cta.2004.

[34] T. J. Freeborn, “Comparison of (1+α) fractional-order transfer functions to approximate lowpass butterworth magnitude responses”, *Circuits, Systems, and Signal Processing*, vol. 35, no. 6, pp. 1983–2002, 2016. doi:10.1007/s00034-015-0226-y.

[35] T. J. Freebom, B. Maundy and A. S. Elwakil, “Approximated fractional-order Chebyshev lowpass filters”, *Hindawi-Mathematical Problems in Engineering*, 2015. doi:10.1155/2015/832468.

[36] T. J. Freeborn, A. S. Elwakil and B. Maundy, “Approximated fractional-order inverse Chebyshev lowpass filters”, *Circuits, Systems, and Signal Processing*, vol. 35, no. 6, pp. 1973–1982, 2016.

[37] E. M. Hamed, A. M. AbdelAty, L. A. Said and A. G. Radwan, “Effect of different approximation techniques on fractional-order KHN filter design”, *Circuits, Systems, and Signal Processing*, pp.1-31, 2018. doi:10.1007/s00034-018-0833-5.

[38] A. Radwan, A. Elwakil, A. Soliman, “On the generalization of second-order filters to the fractional order domain”, *Journal of Circuits, Systems and Computers*, vol. 18, no. 2, pp. 361–386, 2009.

[39] A. S. Ali, A. G. Radwan and A. M. Soliman, “Fractional order butterworth filter: active and passive realization”, *IEEE Journal on Emerging and Selected Topics in Circuits and Systems*, vol. 3, no. 3, pp. 346–354, 2013.

[40] A. Soltan, A. G. Radwan and A. M. Soliman, “Fractional order sallen-key and KHN filters stability and poles allocation”, *Circuits, Systems, and Signal Processing*, vol. 34, no. 5, pp. 1461–1480, 2014.

[41] A. Soltan, A. G. Radwan and A. M. Soliman, “CCII based fractional filters of different orders”, *Journal of Advanced Research*, vol. 5, no. 2, pp. 157–164, 2014.

[42] A. Soltan, A. G. Radwan and A. M. Soliman, “CCII based KHN fractional order filter”, in *IEEE-Midwest Symposium on Circuits and Systems (MWSCAS)*, pp. 197–200, 2013.

[43] A. Soltan, A. G. Radwan and A. M. Soliman, “Fractional order filter with two fractional elements of dependant orders”, *Microelectronics Journal*, vol., 43, no. 11, pp. 818–827, 2012.

[44] L. A. Said, S. M. Ismail, A. G. Radwan, A. H. Median, M. F. A. El Yazeed and A. M. Soliman, “On the optimization of fractional order low pass filter”, *Circuits, Systems, and Signal Processing*, vol. 35, no. 6, pp. 2017-2039, 2016.

[45] N. Herencsar, R. Sotner, A. Kartci and K. Vrba, “A novel pseudo-differential integer/ fractional-order voltage-mode all-pass filter”, *IEEE International Symposium on Circuits and Systems (ISCAS)*, Florence, Italy, pp. 1-5, 2018.

[46] G. Kaur, A. Q. Ansari and M. S. Hashmi, “Fractional order multifunction filter with 3 degrees of freedom”, *AEU - International Journal of Electronics and Communications*, vol. 82, pp. 127-135, 2017.

[47] A. G. Radwan, A. M. Soliman and A. S. Elwakil, “First-order filters generalized to the fractional domain”, *Journal of Circuits, Systems and Computers*, vol. 17, no. 1, pp. 55–66, 2008.

[48] A. Soltan, A. G. Radwan and A. M. Soliman, “Butterworth passive filter in the fractional-order”, *ICM 2011 Proceeding*, pp. 1–5, 2011.

[49] D. R. Bhaskar, M. Kumar and P. Kumar, “Fractional order inverse filters using operational amplifier”, *Analog Integrated Circuits and Signal Processing*, vol. 97, no. 1, pp.149–158, 2018.

[50] D. V. Kamath, S. Navya and N. Soubhagyaseetha, "Fractional order OTA-C current-mode all-pass filter," in *Second International Conference on Inventive Communication and Computational Technologies (ICICCT)*, Coimbatore, pp. 383-387, 2018.

[51] J. Dvorak, J. Jerabek, L. Langhammer, S. Kapoulea and C. Psychalinos, “Design of fully-differential frequency filter with fractional-order elements”, in *proceedings of 41st international conference on telecommunications and signal processing (TSP)* 2018, pp. 1–7, 2018. doi:10.1109/TSP.2018.8441259.

[52] J. Dvorak, J. Jerabek, Z. Polesakova, L. Langhammer and P. Blazek, “Multifunctional electronically reconfigurable and tunable fractional-order filter”, *Elektronika IR Elektrotechnika*, vol. 25, no 1, 2018.

[53] N. A. Khalil, L. A. Said, A. G. Radwan and A. M. Soliman, “Generalized two port network based fractional order filters”, *AEU - International Journal of Electronics and Communications*, vol. 104, pp. 128–146, 2019.

[54] B. Maundy, A. S. Elwakil and T. J. Freeborn, “On the practical realization of higher order filters with fractional stepping”, *Signal Processing*, vol. 91, no. 3, pp. 484-491, 2011. doi:10.1016/j.sigpro.2010.06.018.

[55] S. Mahata, S. K. Saha, R. Kar and D. Mandal, “Optimal design of fractional order low pass butterworth filter with accurate magnitude response”, *Digital Signal Processing*, vol. 72, pp. 96–114, 2018. doi:10.1016/j.dsp.2017.10.001.

[56] J. Jerabek, R. Sotnar, J. Dvorak, L. Langhammer and J. Kotton, “Fractional-order high pass filter with electronically adjustable parameters”, in *IEEE International Conference on Applied Electronics*, pp. 111-116, 2016. doi:10.1109/AE.2016.7577253.

[57] L. Langhammer, J. Dvorak, R. Sotner and J. Jerabek, “Electronically tunable fully-differential fractional-order low-pass filter”, *Elektronika IR Elektrotechnika*, vol. 23, no. 3, 2017. doi:10.5755/j01.eie.23.3.18332.

[58] L. Langhammer, J. Dvorak, J. Jerabek, J. Koton and R. Sotner, “Fractional-order low-pass filter with electronic tunability of its order and pole frequency”, *Journal of Electrical Engineering*, Slovak, vol. 69, no. 1, pp. 3-13, 2018. doi:10.1515/jee-2018-0001.

[59] J. Jerabek, R. Sotner, J. Dvorak, J. Polak, D. Kubanek, N. Herencsar and J. Koton, “Reconfigurable fractional-order filter with electronically controllable slope of attenuation, pole frequency and type of approximation”, *Journal of Circuits, Systems and Computers*, vol. 26, no. 10, pp. 1-21, 2017. doi:10.1142/S0218126617501572.

[60] J. Koton, D. Kubanek, O. Sladok and K. Vrba, “Fractional-order low- and high-pass filters using UVCs”, *Journal of Circuits, Systems and*

Computers, vol. 26, no. 12, pp. 1-23, 2017. doi:10.1142/S0218126617501924.

[61] F. Khateb, D. Kubanek, G. Tsirimokou and C. Psychalinos, "Fractional-order filter based on low-voltage DDCCs", *Microelectronics Journal*, vol. 50, pp. 50-59, 2016. doi:10.1016/j.mejo.2016.02.002.

[62] G. Tsirimokou, S. Koumousi and C. Psychalinos, "Design of fractional-order filters using current feedback operational amplifiers", *Journal of Engineering Science and Technology Review*, vol. 9, no. 4, pp. 77-81, 2016.

[63] J. Dvorak, L. Langhammer, J. Jerabek, J. Koton, R. Sotner and J. Polak, "Electronically tunable fractional-order low-pass filter with current followers", *39th International Conference on Telecommunications and Signal Processing (TSP)*, pp. 587-592, 2016.

[64] L. Langhammer, R. Sotner, J. Dvorak, J. Jerabek and J. Polak, "Fully-differential tunable fractional-order filter with current followers and current amplifiers", *27th International Conference Radioelektronika (Radioelektronika)*, 2017. doi:10.1109/RADIOELEK.2017.7937576.

[65] J. Dvorak, L. Langhammer, J. Jerabek, J. Koton, R. Sotner and J. Polak, "Synthesis and analysis of electronically adjustable fractional-order low-pass filter", *Journal of Circuits, Systems and Computers*, vol. 27, no. 2, 2018.

[66] J. Dvorak, Z. Polesakova, J. Jerabek, L. Langhammer, A. Kartci and J. Koton, "Non-integer-order low-pass filter with electronically controllable

parameters", *IEEE International Symposium on Circuits and Systems (ISCAS)*, Florence, Italy, pp. 1-5, 2018.

[67] L. Langhammer, R. Sotner, J. Dvorak and T. Dostal, "Fully-differential multifunctional electronically configurable fractional-order filter with electronically adjustable parameters", *Elektronika IR Elektrotechnika*, vol. 24, no. 5, pp 42-45, 2018. ISSN 1392-1215.

[68] D. Kubanek, T. Freeborn, J. Koton and N. Herencsar, "Evaluation of (1 + α) fractional-order approximated butterworth high-pass and band-pass filter transfer functions", *Elektronika IR Elektrotechnika*, vol. 24, no. 2, pp. 37-41, 2018.

[69] G. Tsirimokou, C. Laoudias and C. Psychalinos, "0.5-V fractional-order companding filters", *International Journal of Circuit Theory and Applications*, vol. 43, no. 9, pp. 1105-1126, 2015. doi:10.1002/cta.1995.

[70] T. J. Freeborn, B. Maundy and A. S. Elwakil, "Field programmable analogue array implementations of fractional step filters", *IET Circuits, Devices & Systems*, vol. 4, no. 6, pp. 514–524, 2010. http://dx.doi.org/10.1049/iet-cds.2010.0141.

[71] A. Soltan, A. M. Soliman and A. G. Radwan, "Fractional-order impedance transformation based on three port mutators", *AEU - International Journal of Electronics and Communications*, vol. 81, pp. 12-22, 2017. doi:10.1016/j.aeue.2017.06.012.

[72] L. DorCak, I. Petras and J. Terpak, "Design of the fractional-order $PI^{\lambda}D^{\mu}$ controller," in *Proceedings of 7th International Carpathian Control Conference (ICCC)*, Czech Republic, pp. 121-124, 2006.

[73] L. Dorcak, V. Lesko and I. Kostial, "Identification of fractional order dynamical systems", in *12th International Conference on Process Control and Simulation ASRTP'96*, Slovak Republic, vol. 1, pp. 62-68, 1996.

[74] I. Podlubny, "On identification of fractional order dynamic systems," *Proceeding of the 3rd Scientific-Technical Conference, Process Control*, Czech Republic, vol. 1, pp. 328-331, 1998.

[75] J. Dorcak, J. Terpak, I. Petras and F. Dorcakova, "Electronic realization of the fractional order systems," *Acta Montanistica Slovaca-International Scientific Journal*, vol. 12, no. 3, pp. 231-237, 2007.

[76] I. Podlubny, "Fractional order systems and fractional order controllers," *UEF-03-94, The Academy of Sciences Institute of Experimental Physics*, Kosice, Slovak Republic, pp. 32, 1994.

[77] I. Podlubny, "Fractional-order systems and $PI^{\lambda}D^{\mu}$ –controllers," *IEEE Transactions on Automatic Control*, vol. 44, no. 1, pp. 208–213, 1999.

[78] A. Oustaloop, "CRONE control principle, synthesis, performances with non-linearities and robustness input immunity dilemma," *Lecture Notes in Control and Information Sciences*, vol. 144, pp. 767-777, 1990.

[79] L. Dorcak, "Numerical models for the simulation of the fractional order control systems," *The Academy of Sciences, Institute of Experimental Physics UEF-04-94*, Kosice, Slovak Republic, 1994.

[80] O. Domansky, R Sotner, L. Langhammer, J. Jerabek, C. Psychalinos and G. Tsirimokou , "Practical design of RC approximants of constant phase elements and their implementation in fractional-order PID regulators using CMOS voltage differencing current conveyors", *Circuits, Systems, and Signal Processing*, vol. 38, pp. 1520-1546, 2019.

[81] C. Muniz-Montero, L.V. Garcia-Jimenez, L. A. Sanchez-Gaspariano, C. Sanchez-Lopez, V. R. Gonzalez-Diaz and E. Tlelo-Cuautle, "New alternatives for analog implementation of fractional-order integrators, differentiators and PID controllers based on integer order integrators", *Nonlinear Dynamics*, vol. 90, no. 1, pp. 241–256, 2017.

[82] J. Petrzela, "New network structures of reconfigurable fractional-order PID regulators with DVCC", in *Proceedings of 2017 24th International Conference of Mixed Design of Integrated Circuits and Systems (MIXDES)*, pp. 527–531, 2017.

[83] L. Said, A. Madian, A. G. Radwan and A. M. Soliman, "Fractional order oscillator with independent control of phase and frequency," in *2nd International Conference on Electronic Design (ICED)*, Malaysia, 2014.

[84] L. A. Said, A. G. Radwan, A. H. Madian and A. M. Soliman, "Fractional order oscillators based on operational transresistance amplifiers," *AEU-International Journal of Electronics and Communications*, vol. 69, no. 7, pp. 988–1003, 2015.

[85] [82] A. G. Radwan, A. S. Elwakil and A. M. Soliman, "Fractional-order sinusoidal oscillators: design procedure and practical examples," *IEEE Transactions on Circuits and Systems*, vol. 55, no. 7, pp. 2051-2063, 2008.

[86] A. G. Radwan, A. M. Soliman and A. S. Elwakil, “Design equations for fractional-order sinusoidal oscillators: four practical design examples,” *International Journal of Circuit Theory and Applications*, vol. 36, pp. 473–492, 2008.

[87] L. A. Said, A. H. Madian, A. G. Radwan and A. M. Soliman, "Current feedback operational amplifier (CFOA) based fractional order oscillators," *IEEE-ICECS, International Conference*, Marseille, France, 2014.

[88] A. Kartci, N. Herencsar, J. Koton, and C. Psychalinos, “Compact MOS-RC voltage-mode fractional-order oscillator design”, *European Conference on Circuit Theory and Design (ECCTD)*, 2017. doi:10.1109/ECCTD.2017.8093281.

[89] L. A. Said, A. G. Radwan, A. H. Madian and A. M. Soliman, “Survey on two-port network-based fractional-order oscillators”, in *Fractional Order Systems, Elsevier*, pp. 305–327, 2018.

[90] L. A. Said, A. G. Radwan, A. H. Madian and A. M. Soliman, “Three fractional-order-capacitors-based oscillators with controllable phase and frequency”, *Journal of Circuits, Systems and Computers*, vol. 26, no. 10, 2017.

[91] B. Maundy, S. J. G. Gift and A. S. Elwakil, "On a multivibrator that employs a fractional capacitor," *Analog Integrated Circuits and Signal Processing*, vol. 62, no. 1, pp. 99-103, 2010.

[92] K. Biswas, S. Sen and P. K. Dutta, “Realization of a constant phase element and its performance study in a differentiator circuit,” *IEEE Transactions on Circuits and Systems*, vol. 53, no. 9, pp. 802–806, 2006.

[93] M. S. Krishna, S. Das, K. Biswas and B. Goswami, “Fabrication of a fractional order capacitor with desired specifications: a study on process identification and characterization”, *IEEE Transactions on Electron Devices*, vol. 58, no. 11, pp. 4067-4073, 2011.

[94] I. S. Jesus and J. A. T. Machado, “Development of fractional order capacitors based on electrolyte processes”, *Nonlinear Dynamics*, vol. 56, pp. 45-55, 2009.

[95] K. Biswas, S. Sen and P. K. Dutta, “Modeling of a capacitive probe in a polarizable medium”, *Sensor Actuators A: Physical*, vol. 120, pp. 115-122, 2005.

[96] D. Mondal and K. Biswas, “Packaging of single-component fractional order element”, *IEEE Transactions on Device and Materials Reliability*, vol. 13, no. 1, pp. 73–80, 2013.

[97] A. Adhikary, M. Khanra, S. Sen, and K. Biswas, “Realization of a carbon nanotubes based electrochemical fractor. *IEEE International Symposium on Circuits and Systems (ISCAS)*, 2015.

[98] G. Tsirimokou, C. Psychalinos, A. S. Elwakil and K. N. Salama, "Experimental verification of on-chip CMOS fractional-order capacitor emulators", *Electronics Letters*, vol. 52, pp. 1298-1300, 2016.

[99] G. Tsirimokou, C. Psychalinos and A. S. Elwakil, "Emulation of a constant phase element using operational transconductance amplifiers", *Analog Integrated Circuits and Signal Processing*, vol. 85, pp. 413-423, 2015.

[100] A. M. Elshurafa, M. N. Almadhoun, K. N. Salama and H. Alshareef, "Microscale electrostatic fractional capacitors using reduced graphene oxide percolated polymer composites" *Applied Physics Letters*, vol. 102, no. 23, 2013. doi:10.1063/1.4809817.

[101] A. Agambayev, S. P. Patole, M. Farhat, A. Elwakil, H. Bagci and K. N. Salama, "Ferroelectric fractional-order capacitors", *Chem Electro Chem*, vol. 4, no. 11, pp. 2807-2813, 2017.

[102] D. A. John and K. Biswas, "Electrical equivalent circuit modelling of solid state fractional capacitor", *AEU - International Journal of Electronics and Communications*, vol. 78, pp. 258–264, 2017.

[103] M. Sugi, Y. Hirano, Y. F. Miura and K. Saito, "Simulation of fractal immittance by analog circuits: an approach to the optimized circuits," *IEICE Transactions on Fundamentals*, vol. E82-A, no. 8, pp.205-209, 1999.

[104] M. E. Fouda, A. AboBakr, A. S. Elwakil, A. G. Radwan and A. M. Eltawil, "Simple MOS transistor-based realization of fractional-order

capacitors", in *IEEE International Symposium on Circuits and Systems (ISCAS)*, pp. 1-4, 2019.

[105] P. Bertsias, C. Psychalinos, A. S. Elwakil and A. G. Radwan, "Low-voltage and low-power fractional-order parallel tunable resonator", *Microelectronics Journal*, vol. 88, pp. 108–116, 2019. doi:10.1016/j.mejo.2019.05.002.

[106] P. Bertsias, C. Psychalinos, A. G. Radwan and A. S. Elwakil, "High-frequency capacitorless fractional-order CPE and FI emulator", *Circuits, Systems, and Signal Processing*, vol. 37, no. 7, pp. 2694–2713, 2018.

[107] P. Bertsias, C. Psychalinos, A. Elwakil and B. Maundy, "Current-mode capacitorless integrators and differentiators for implementing emulators of fractional-order elements", *AEU - International Journal of Electronics and Communications*, vol. 80, pp. 94–103, 2017.

[108] P. Bertsias, C. Psychalinos, A. Elwakil, L. Safari and S. Minaei, "Design and application examples of CMOS fractional-order differentiators and integrators', *Microelectronics Journal*, vol. 83, pp. 155–167, 2019. doi:10.1016/j.mejo.2018.11.013.

[109] G. Tsirimokou, C. Psychalinos and A. Elwakil, "Design of CMOS analog integrated fractional-order circuits: applications in medicine and biology", *Springer* 2017. doi:10.1007/978-3-319-55633-8.

[110] G. Tsirimokou, C. Psychalinos, A. S. Elwakil and K. N. Salama, "Electronically tunable fully integrated fractional-order resonator", *IEEE*

Transactions on Circuits and Systems II: Express Briefs, vol. 65, no. 2, pp. 166–170, 2018.

[111] S. Kapoulea, C. Psychalinos, A. S. Elwakil and A. G. Radwan, "One-terminal electronically controlled fractional-order capacitor and inductor emulator", *AEU - International Journal of Electronics and Communications*, vol. 103, pp. 32-45, 2019. doi:10.1016/j.aeue.2019.03.002.

[112] R. Sotner,J. Jerabek, J. Petrzela, O. Domansky, G. Tsirimokou and C. Psychalinos, "Synthesis and design of constant phase elements based on the multiplication of electronically controllable bilinear immittances in practice, *AEU - International Journal of Electronics and Communications*, vol. 78, pp. 98–113, 2017.

[113] R. Sotner, L. Polak, J. Jerabek and J. Petrzela, "Simple two operational transconductance amplifiers-based electronically controllable bilinear two port for fractional-order synthesis", *Electronics Letters,* vol. 54, no. 20, pp. 1164–1166, 2018.

[114] G. Tsirimokou, C. Psychalinos, T. J. Freeborn and A. S. Elwakil, "Emulation of current excited fractional-order capacitors and inductors using OTA topologies," *Microelectronics Journal*, vol. 55, pp.70–81, 2016.

[115] A. Soltan, A. G. Radwan and A. M. Soliman, "Fractional-order mutual inductance: analysis and design," *Wiley-International Journal of Circuit Theory and Applications*, vol. 12, no. 3, pp. 231-237, 2015.

[116] A. Soltan, A. M. Soliman and A. G. Radwan, "Fractional-order impedance transformation based on three port mutators", *AEU - International Journal of Electronics and Communications*, vol. 81, pp. 12-22, 2017. doi:10.1016/j.aeue.2017.06.012.

[117] G. Tsirimokou, C. Psychalinos, and A. S. Elwakil, "Fractional-order electronically controlled generalized filters", *International Journal of Circuit Theory and Applications*, vol. 45, no. 5, pp. 595–612, 2017.

[118] A. Oustaloup, F. Levron, B. Mathieu and F. M. Nanot, "Frequency-band complex noninteger differentiator: characterization and synthesis", *IEEE Transactions on Circuits and Systems I: Fundamental Theory and Applications*, vol. 47, no. 1, pp. 25–39, 2000.

[119] J. Valsa, P. Dvorak and M. Friedl, "Network model of the CPE", *Radioengineering*, vol. 20, no. 3, pp. 619–626, 2011.

[120] J. Baranowski, M. Pauluk and A. Tutaj, "Analog realization of fractional filters: Laguerre approximation approach", *AEU - International Journal of Electronics and Communications*, vol. 81, pp. 1-11, 2017. doi:10.1016/j.aeue.2017.06.011.

[121] AD 844 Datasheet and SPICE macro models, Analog Devices Inc.

[122] R. Senani, D. R. Bhaskar, M. Gupta and A. K. Singh, "Canonic OTA-C sinusoidal oscillators: generation of new grounded-capacitor versions", *American Journal of Electrical and Electronic Engineering*, vol. 3, no. 6, pp. 137–146, 2015.

[123] A. D. Marcellis, G. Ferri and V. Stornelli, “NIC-based capacitance multipliers for low-frequency integrated active Filter applications”, in *IEEE Research in Microelectronics and Electronics Conference*, pp. 225-228, 2007. ISBN: 978-1-4244-1000-2. doi:10.1109/RME.2007.4401853.

[124] Y. A. LI, “A series of new circuits based on CFTAs”, *AEU-International Journal of Electronics and Communication*, vol. 66, pp. 587-592, 2012. ISSN: 1434-8411. doi: 10.1016/j.aeue.2011.11.011.

[125] U. E. Ayten, M. Sagbas, N. Herencsar and J. Koton, “Novel floating general element simulators using CBTA”, *Radioengineering*, vol. 21, no. 1, pp. 11–19, 2012. ISSN: 1210-2512. ISSN: 1210-2512.

[126] I. Myderrizi and A. Zeki, “Electronically tunable DXCCII-based grounded capacitance multiplier”, *AEU - International Journal of Electronics and Communications*. vol. 68, pp. 899–906, 2014. ISSN: 1434-8411. doi:10.1016/j.aeue.2014.04.013

[127] H. Alpaslan, “DVCC-based floating capacitance multiplier design”, *Turkish Journal of Electrical Engineering and Computer Sciences*, vol. 25, pp. 1334–1345, 2017. ISSN: 1303-6203. doi:10.3906/elk-1509-112.

[128] H. Alpaslan and E. Yuce, “Bandwidth expansion methods of inductance simulator circuits and voltage-mode biquads”, *Journal of Circuits, Systems and Computers*, vol. 20, no. 3, pp. 557–572, 2011. ISSN (online): 1793-6454. doi:10.1142/S0218126611007451.

[129] S. Unhavanich, O. Onjan and W. Tangsrirat, “Tunable capacitance multiplier with a single voltage differencing buffered amplifier”, in

Proceedings of the International MultiConference of Engineers and Computer Scientists, vol. 2, pp. 1–4, 2016. ISBN: 978-988-14047-6-3.

[130] P. Silapan, C. Tanaphatsiri and M. Siripruchyanun, "Current controlled CCTA based-novel grounded capacitance multiplier with temperature compensation", in *APCCAS 2008 IEEE Asia Pacific Conference on Circuits and Systems*, pp. 1490–1493, 2008. ISBN: 978-1-4244-2342-2. doi:10.1109/APCCAS.2008.4746314.

[131] E. Yuce, "On the realization of the floating simulators using only grounded passive components", *Analog Integrated Circuits and Signal Processing*, vol. 49, pp. 161-166, 2006. ISSN: 1573-1979. doi:10.1007/s10470-006-9351-7.

[132] A. Jantakun, N. Pisutthipong and M. Siripruchyanun, "Single element based-novel temperature insensitive/electronically controllable floating capacitance multiplier and its application", in *International Conference on Electrical Engineering/Electronics, Computer, Telecommunications and Information Technology (ECTI-CON 2010)*, pp. 37–41, 2010. ISBN: 978-1-4244-5606-2.

[133] E. Yuce, "A novel floating simulation topology composed of only grounded passive components", *International Journal of Electronics*, vol. 97, pp. 249–262, 2010. ISSN 1362-3060. doi:10.1080/00207210903061907.

[134] P. Prommee and M. Somdunyakanok, "CMOS-based current-controlled DDCC and its applications to capacitance multiplier and universal filter",

AEU - International Journal of Electronics and Communications, vol. 65, pp. 1–8, 2011. ISSN: 1434-8411. doi:10.1016/j.aeue.2009.12.002.

[135] A. Kartci, U. E. Ayten, N. Herencsar, R. Sotner, J. Jerabek and K. Vrba, "Application possibilities of VDCC in general floating element simulator circuit", in *European Conference on Circuit Theory and Design*, pp. 1-4, 2015. ISBN: 978-1-4799-9876- 0. doi:10.1109/ECCTD.2015.7300064.

[136] M. A. Al-Absi, E. S. Al-Suhaibani and M. T. Abuelma'atti, "A new compact CMOS C-multiplier", *Analog Integrated Circuits and Signal Processing*, vol. 90, no. 3, pp. 653–658, 2017. ISSN: 1573-1979. doi:10.1007/s10470-016-0822-1.

[137] Y. Tang, M. Ismail and S. Bibyk, "Adaptive Miller capacitor multiplier for compact on-chip PLL filter", *Electronics Letters*, vol. 39, no. 1, pp. 43-45, 2003. ISSN: 0013-5194. doi:10.1049/el: 20030086.

[138] E. Yuce, "Floating inductance, FDNR and capacitance simulation circuit employing only grounded passive elements", *International Journal of Electronics*, vol. 93, no. 10, pp. 679–688, 2006. ISSN: 1362-3060. doi:10.1080/00207210600750208.

[139] W. Jaikla and M. Siripruchyanan, "An electronically controllable capacitance multiplier with temperature compensation", in *International Symposium on Communications and Information Technologies*, pp. 356–359, 2006. ISSN: 2643-6175. doi:10.1109/ISCIT.2006.340064.

[140] I. A. KHAN and M. T. Ahmed, “OTA-based integrable voltage/current-controlled ideal C-multiplier”, *Electronics Letters*, vol. 22, no. 7, pp. 365-366, 1986. ISSN: 0013-5194. doi:10.1049/el:19860248.

[141] M. T. Ahmed, I. A. Khan and N. Minhaj, “Novel electronically tunable C-multipliers”, *Electronics Letters*, vol. 31, no. 1, pp. 9–11, 1995. ISSN: 0013-5194. doi:10.1049/el:19950018.

[142] E. Yuce and S. Minaei, “A modified CFOA and its applications to simulated inductors, capacitance multipliers, and analog filters”, *IEEE Transactions on Circuits and Systems I*, vol. 55, no. 1, pp. 266–275, 2008. ISSN: 1558-0806. doi:10.1109/TCSI.2007.913689.

[143] M. T. Abuelma’atti, S. K. Dhar and Z. J. Khalifa, “New two-CFOA-based floating immittance simulators”, *Analog Integrated Circuits and Signal Processing*, vol. 91, no. 3, pp. 479-489, 2017. ISSN: 0925-1030. doi:10.1007/s10470-017-0956-9.

[144] M. T. Abuelma'atti and S. K. Dhar, “New CFOA-based floating lossless negative immittance function emulators”, in *TENCON 2015-IEEE Region 10 Conference*, pp. 1-4, 2015. ISSN: 2159-3450. doi:10.1109/TENCON.2015.7372799.

[145] A. A. Khan, S. Bimal, K. K. Dey and S. S. Roy, “Current conveyor based R- and C- multiplier circuits”, *AEU - International Journal of Electronics and Communications*, vol. 56, pp. 312–316, 2002. ISSN: 1434-8411. doi:10.1078/1434-8411-54100121.

[146] M. T. Abuelma'atti, "New grounded immittance function simulators using single current feedback operational amplifier", *Analog Integrated Circuits and Signal Processing*, vol. 71, no. 1, pp. 95–100, 2012. doi:10.1007/s10470-011-9742-2.

[147] M. T. Abuelma'atti and S. K. Dhar, "CFOA-based floating negative inductance, positive frequency dependent resistance and resistance-controlled capacitance and resistance emulator", in *IEEE International Conference on Electronics, Information and Communications (ICEIC)*, Da Nang, pp. 1–3, 2016.

[148] A. Lahiri and M. Gupta, "Realizations of grounded negative capacitance using CFOAs", *Circuits, Systems, and Signal Processing*, vol. 30, no. 1, pp. 143–55, 2011. doi:10.1007/s00034-010-9215-3.

[149] A. Fabre, "Gyrator implementation from commercially available operational transimpedance operational amplifiers", *Electronics Letters*, vol. 28, pp. 263–264, 1992.

[150] R. Senani, "Realization of a class of analog signal processing/signal generation circuits: novel configurations using current feedback op-amps", *Frequenz*, vol. 52, no. 9–10, pp. 196–206, 1998.

[151] R. Senani, D. R. Bhaskar, A. K. Singh and V. K. Singh, "Current feedback operational amplifiers and their applications", *Springer Science + Business Media*, New York, pp. 54-56, 2013.

[152] C. Psychalinos, K. Pal and S. Vlassis, "A floating generalized impedance converter with current feedback operational amplifiers", *AEU* -

International Journal of Electronics and Communications, vol. 62, pp. 81–85, 2008.

[153] G. Komanapalli, R. Pandey and N. Pandey, “New sinusoidal oscillator configurations using operational transresistance amplifier”, *International Journal of Circuit Theory and Applications*, pp. 1–20, 2019.

[154] A. M. Soliman, “Applications of the current feedback operational amplifiers”, *Analog Integrated Circuits and Signal Processing*, vol. 11, no. 3, pp. 265–302, 1996.

[155] A. H. Madian, S. A. Mahmoud and A. M. Soliman, “New 1.5-V CMOS current feedback operational amplifier”, in *13th IEEE International Conference On Electronics, Circuits And Systems*, pp. 600–603, Dec 10–13, 2006.

[156] A. Adhikary, S. Sen and K. Biswas, “Design and hardware realization of a tunable fractional-order series resonator with high quality factor,” *Circuits, Systems, and Signal Processing*, vol. 36, no. 9, pp. 3457–3476, 2017.

[157] G. Tsirimokou, C. Psychalinos, and A. S. Elwakil, “Fractional-order electronically controlled generalized filters”, *International Journal of Circuit Theory and Applications*, vol. 45, no. 5, pp. 595–612, 2017.

[158] G. Tsirimokou, C. Psychalinos, T. J. Freeborn and A. S. Elwakil, “Emulation of current excited fractional-order capacitors and inductors using OTA topologies,” *Microelectronics Journal*, vol. 55, pp.70–81, 2016.

[159] R. L. Geiger and E. Sanchez-Sinecio, "Active filter design using operational transconductance amplifiers: a tutorial", *IEEE Circuits and Devices Magazine*, vol. 1, pp. 30–31, 1985.

[160] M. D. Patil, V. A. Vyawahare and M. K. Bhole, "A new and simple method to construct root locus of general fractional-order systems," *ISA Transaction*, vol. 53, no. 2, pp. 380–390.

[161] Y. Sumi, T. Tsukutani, H. Tsunetsugu and N. Yabuki, "Electrical tunable multiple-mode universal biquadratic circuits", in *International Conference on Computer Application and Industrial Electronics*, 2010. doi:10.1109/ICCAIE.2010.5735109.

[162] D. Kubanek and T. Freeborn, "(1+α) Fractional-Order transfer functions to approximate low-pass magnitude responses with arbitrary quality factor", *AEU - International Journal of Electronics and Communications*, vol. 83, pp. 570-578, 2018.

[163] D. E. Goldberg, "Genetic algorithms in search optimization and machine learning", *Addison-Wesley*, 1989.

[164] J. Kennedy and R. Eberhart, "Particle swarm optimization", in *Proceedings of the 4th International Conference on Neural Network-IEEE, Australia*, pp. 1942–1948, 1995.

[165] R. Schaumann R and M. E. V. Valkenberg, "Design of analog filters", *Oxford University Press*, New York, 2001.

[166] V. Katopodis and C. Psychalinos, "Multiple-loop feedback filters using current feedback amplifiers", *AEU - International Journal of Electronics*

and Communications, vol. 98, pp. 7, pp. 833-846, 2011. doi:10.1080/00207217.2011.582445.

[167] P. K. Sinha, A. Saini, P. Kumar and S. Mishra, “CFOA based low pass and high pass ladder filter -a new configuration”, *Circuits and Systems*, vol. 5, no. 12, pp. 293-300, 2014. doi:10.4236/cs.2014.512030.

[168] Y. Sun, “Synthesis of leap-frog multiple-loop feedback OTA-C filters”, *IEEE Transactions on Circuits and Systems*, vol. 53, no. 9, pp. 961-965, 2006. doi.10.1109/TCSII.2006.879095.

[169] Li Z. Fractional order root locus; 2015. [Online] (Matlab Central) http://www.mathworks.com/matlabcentral/fileexchange/50458.

PUBLICATIONS

Papers in International Journals

[1] **R. Verma,** N. Pandey, R. Pandey, "Novel CFOA based Capacitance Multiplier and Its Application", AEU- International Journal of Electronics and Communications, vol. 107, pp. 192-198, 2019. (Elsevier) **Indexing: SCI, SCIE, SCOPUS; IF: 2.115**

[2] **R. Verma,** N. Pandey, R. Pandey, "CFOA based Low Pass and High Pass Fractional Step Filter Realizations", AEU- International Journal of Electronics and Communications, vol. 99, pp. 161-76, 2019. https://doi.org/10.1016/j.aeue.2018.11.032. (Elsevier) **Indexing: SCI, SCIE, SCOPUS; IF: 2.115**

[3] **R. Verma,** N. Pandey, R. Pandey, "Realization of a Higher Fractional Order Element based on Novel OTA based IIMC and Its Application in Filter. Analog Integrated Circuits and Signal Processing, vol. 97, no. 1, pp. 177–191, 2018. https://doi.org/10.1007/s10470-018-1315-1. (Springer) **Indexing: SCI, SCIE, SCOPUS; IF: 0.8**

[4] **R. Verma,** N. Pandey, R. Pandey, "Electronically Tunable Fractional Order Filter", Arabian Journal for Science and Engineering, vol. 42, no. 8, pp 3409–22, 2017. https://doi.org/10.1007/s13369-017-2500-8. (Springer) **Indexing: SCIE, SCOPUS; IF: 1.092**

Papers in International Conferences

[5] **R. Verma,** N. Pandey, R. Pandey, "Electronically Tunable Fractional Order All Pass Filter", IOP: Materials Science and Engineering, vol. 225: 012229, 2017. **(SCOPUS).** https://doi:10.1088/1757-899X/225/1/012229